Optimization of the GluCl/IVM Neuronal Silencing Tool via Protein Engineering

Thesis by

Shawnalea J. Frazier

In Partial Fulfillment of the Requirements for the Degree of

Doctor of Philosophy

California Institute of Technology

Pasadena, California

2012

(Defended June 6, 2012)

The following work is dedicated to Professor JM Tomich.

Thank you for my foundation.

Thank you for my fortitude.

Thank you for my future.

ACKNOWLEDGEMENTS

I would like to thank my Ph.D. advisor, Professor Henry Lester, for his support throughout this endeavor and co-advisor, Professor Dennis Dougherty, for his genuine interest in seeing me succeed. Thanks to my additional committee members, Professor David Anderson and Professor Shu-ou Shan, for perceptive scientific discussions. I would especially like to thank my first-year post-doc mentor, Dr. Fraser Moss, for providing me with extensive electrophysiology training and sage advice about everything from graduate school to life in general. And, I would like to thank Dr. Bruce Cohen for his electrophysiology expertise and worthwhile mentorship, as well as his tolerant company and daily chatter about food and travel. I would also like to acknowledge Dr. Chris Richards and Weston Nichols for their patience and friendly assistance with imaging experiments. Thanks to lab manager Purnima Deshpande for the supply ordering and equipment maintenance that kept my experiments going, to Sheri McKinney for providing my weekly neuronal cultures, and to other current and former Lester lab members for their constructive criticisms and lively conference room conversations. To our wonderful 'lab Momma' Eloisa Imel, thank you for fostering an enjoyable work environment and for your obliging resourcefulness with day-to-day tasks and formalities, but more importantly for being a great friend, keeping me encouraged, well-fed and caffeinated. Finally, I would like to give special thanks to fellow lab members Dr. Ying Wang, Crystal Dilworth, and Rell Parker for their friendship, tremendous support and counsel through the rollercoaster ride we call graduate school.

ABSTRACT

A variety of genetically encoded tools have been developed for deciphering the neural circuitry of the brain. Such tools allow physical manipulation of neuronal excitability in a reversible, cell-specific manner, enabling researchers to establish how electrical activity and connectivity facilitate the information processing that mediates perception and drives behavior. An expanding toolkit of engineered neuroreceptors, particularly those actuated by orthogonal pharmacological ligands, provide noninvasive manipulation of regional or disperse neuronal populations with adequate spatiotemporal precision and great potential for multiplexing. We previously engineered an invertebrate glutamate-gated chloride channel (GluCl αβ) that enabled pharmacologically induced silencing of electrical activity in targeted CNS neurons *in vivo* by the anthelmintic drug compound ivermectin (IVM; Lerchner et al., 2007). With this receptor, GluCl opt α-CFP + opt β-YFP Y182F, the concentration of IVM necessary to elicit a consistent silencing phenotype was higher than expected, raising concern about its potential side effects. Considerable variability in the extent of spike suppression was also apparent and was attributed to variable co-expression levels of α and β subunits. Thus, a rational protein engineering strategy was employed to optimize the GluCl/IVM tool. To increase agonist sensitivity, a gain-of-function gating mutation involving the highly conserved leucine 9' residue of the α pore-lining M2 transmembrane domain was introduced. Various mutations at this position facilitate channel opening in the absence and presence of ligand. Analysis of side chain properties revealed that helix-destabilizing energy correlated with increases in agonist sensitivity. One mutation, L9'F, enhances β subunit incorporation to substantially

increase IVM sensitivity without permitting unliganded channel opening. Removal of an arginine-based ER retention motif (RSR_AAA) from the intracellular loop of β promoted plasma membrane expression of heteromeric GluCl αβ by preventing ER-associated degradation of the β subunit. An additional monomeric XFP mutation complements these effects. The newly engineered GluCl opt α-mXFP L9'F + opt β-mXFP Y182F RSR_AAA receptor significantly increases conductance and reduces variability in evoked spike generation *in vitro* using a lower concentration of IVM. This receptor, dubbed 'GluClv2.0', is an improved tool for IVM-induced silencing.

TABLE OF CONTENTS

LIST OF FIGURES

LIST OF TABLES

Chapter 1

Introduction to Neuroscience and Neuronal Manipulation Tools

The brain is the most complex and highly adaptable organ in the human body. Every thought, sensation, perception, movement, motivation, emotion, mood, and memory we experience is produced as a continuous stream of information. This information exists as an encoded array of complex and simultaneous physical, chemical, and biological events all accomplished in the brain by individual nerve cells and the connections between them.

Neurons are the Excitatory Cells of the Brain

The human brain is composed of approximately 86 billion neurons (nerve cells) and 85 billion nonneuronal (glial) cells organized into distinct anatomical regions[1]. Neurons are the functional unit of the brain. They are electrically excitable and their activity affects the electrical state of adjacent neurons. In contrast, glial cells are not directly involved in electrical signaling. Rather, they are deemed support cells, providing structure, regulation, and protection to the neurons. Glial cells also insulate the nerve cell axons and synaptic connections necessary for the conduction of electrical signals.

At rest, all cells including neurons maintain a separation of positive and negative ions on either side of the plasma membrane. A resting nerve cell has an excess of positive

charge on the outside of the membrane and an excess of negative charge on the inside. This separation of charge creates an electrical potential difference, or voltage, across the membrane called the resting membrane potential. A typical quiescent neuron has a resting membrane potential of -65 mV. As excitable cells, neurons differ from other cells in their ability to rapidly and dramatically change their membrane potential.

Rapid changes in membrane potential are mediated by ion channels. Ion channels are integral membrane proteins found in all cells of the body, however, those present in nerve cells are optimally tuned for rapid information processing. Ion channels of nerve cells open in response to specific electrical, mechanical, or chemical stimuli to conduct charge-specific ionic current at rates up to 10^8 ions/channel/second. Some channels are selective for a particular ion over others with the same charge. The most abundant, permeable ions in biological systems include the positively charged cations potassium (K^+), sodium (Na^+), and calcium (Ca^{2+}), and the negatively charged anion chloride (Cl^-). These ions are not distributed equally across the membrane; the concentration of K^+ ions is higher inside the cell, while the concentrations of Na^+, Cl^-, and Ca^{2+} are higher outside the cell. This unequal distribution generates a concentration gradient. Thus, the direction of passive ion flow is subject to both chemical and electrical driving forces due to concentration and ionic charge differentials. Passive diffusion of ions down their electrochemical gradient will proceed until reaching the point at which the electrical driving force in one direction exactly opposes the chemical driving force in the opposite direction and there is no longer a net flow. The membrane voltage at which this occurs is called the equilibrium potential (or Nernst potential) for that particular ion. The equilibrium potential of an ion is dependent on the valence charge of that ion, z, and the

concentrations of that ion inside, $[X]_i$, and outside, $[X]_o$, of the cell, and can be calculated using the Nernst Equation, defined as

$$E_X = \frac{RT}{zF} \ln \frac{[X]_o}{[X]_i}$$

where R is the universal gas constant (8.314 J K^{-1} mol^{-1}), T is the temperature (in Kelvin), and F is the Faraday constant (9.65×10^{-4} C mol^{-1}).

At rest, a nerve cell membrane is mostly permeable to K^+ ions, therefore the membrane voltage (resting membrane potential) is close to the potassium equilibrium potential, E_K. A net flow of cations or anions into or out of the cell disturbs the charge separation across the membrane, altering the voltage. A reduction of charge separation, or depolarization, leads to a less negative membrane potential (e.g., from -65 mV to -55 mV). An increase in charge separation, or hyperpolarization, results in a more negative membrane potential (e.g., from -65mV to -75mV).

Neuronal Communication

When depolarization approaches a critical membrane potential, called the threshold voltage, it triggers the opening of voltage-gated Na^+ channels present in the cell membrane. This allows Na^+ ions to flow into the cell (i.e., down their electrochemical gradient), causing further depolarization, which facilitates the opening of even more voltage-gated Na^+ channels, rapidly driving the membrane potential toward E_{Na}. In this

depolarized state, the Na^+ channels begin to inactivate, while voltage-gated K^+ channels, which opened more slowly in response to the initial depolarization, remain open. Slow, outward K^+ current repolarizes the membrane back its resting membrane potential. The entire depolarization-repolarization process occurs within a millisecond. This rapid, transient, all-or-nothing voltage impulse is called an action potential.

The morphology of a typical neuron consists of (1) the cell body (soma), which contains the nucleus including the genes of the cell, (2) dendrites, processes which branch out to receive incoming signals from other neurons, (3) the axon, a single tubular extension which transmits the electrical signal over some distance, and (4) presynaptic terminals, fine branches extending from the axon that communicate the electrical signal at a site called the synapse to the dendrites or soma of receiving (postsynaptic) neurons (Figure 1-1A). The presynaptic terminal and postsynaptic cell are physically separated by a space known as the synaptic cleft (Figure 1-1B). At a synapse, the electrical signal is converted to a chemical signal, in which chemical neurotransmitter molecules are released from the presynaptic cell and diffuse across the synaptic cleft to activate receptors present on the postsynaptic membrane, where the signal is then converted back to an electrical potential. The sign of the signal, inhibitory or excitatory, depends on the type of receptors in the postsynaptic cell, not the identity of the neurotransmitter. All synaptic input of the receiving neuron is integrated at the axon hillock, the initial segment of the axon. This region of the cell membrane contains the highest density of voltage-gated Na^+ channels in the cell, and thus has the lowest threshold for spike initiation. If the summation of input signals reaches the threshold voltage, an action potential will be generated (Figure 1-1C).

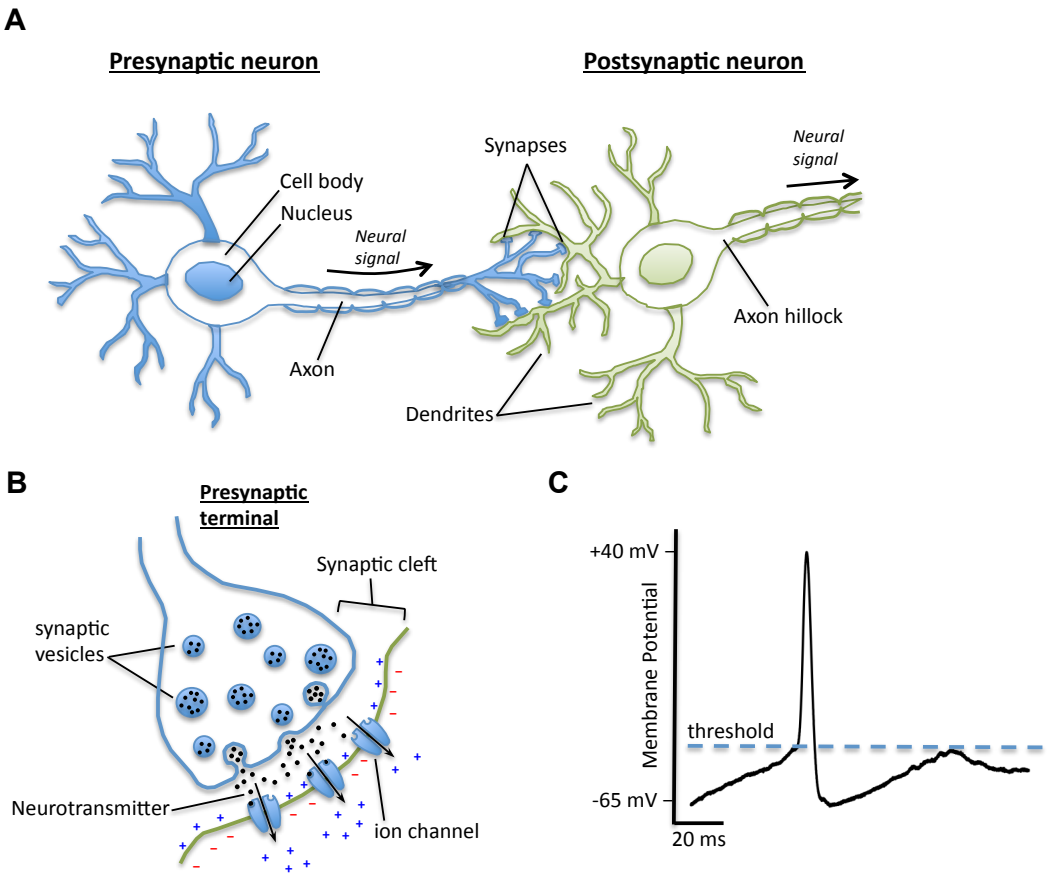

Figure 1-1. Neuronal communication. *A*. Typical neuron morphology consists of the cell body, dendrites, the axon, and presynaptic terminals. The presynaptic neuron communicates the neural signal to the postsynaptic neuron at synapses. *B*. Chemical neurotransmitter molecules packaged in synaptic vesicles are released from the presynaptic cell and diffuse across the synaptic cleft to activate ion channel receptors on the postsynaptic membrane. *C*. Synaptic input of the receiving neuron is integrated at the axon hillock. If the summation of input signals reaches the threshold voltage, an action potential will be generated.

Neural Circuits Convey Information

An action potential initiated at the axon hillock is actively propagated along the axon, regenerating with constant amplitude at regular intervals, until it reaches the presynaptic terminals where the signal is transmitted to other cells. Input signals below threshold voltage will not initiate an action potential, whereas all signals above the threshold will

produce the same all-or-nothing action potentials in succession in a "spike firing" pattern. All spikes fired are the same size and shape, but they differ in frequency (i.e., the number of action potentials and the time intervals between them). Thus, information in the brain is conveyed through neuronal firing patterns and the specific pathways in which they travel.

Nerve cells in the brain are highly organized into signaling pathways and have the same gross anatomical arrangement in every individual. Neurons are clustered into discrete groups that are functionally specialized for processing specific types of information. These regions are projected and interconnected to form extensive neural networks, generating sensory and motor functions, and facilitating learning, memory, and language abilities. The neural pathways for certain higher functions have been precisely mapped in the brain, though exactly how they produce complex cognition and behavior is still poorly understood. The majority of neurological and psychiatric disorders are believed to result from disruption of neural circuits caused by cellular abnormalities and/or molecular imbalance. Therefore, a detailed understanding of neural circuitry will aid in proper diagnoses and treatment strategies for such conditions.

The Study of Neuroscience: A Brief Chronology

The original notion that individual brain regions have distinct functions associated with different behaviors has been around since 1796 with the creation of phrenology by the German physician, Franz Joseph Gall. Phrenologists believed that the brain was the organ of the mind and that one's personality could be determined by the variation of bumps on

their skull. Now considered a pseudoscience, phrenological thinking was an important historical advancement toward the discipline of modern neuroscience. In 1861, the French neurologist Pierre Paul Broca extended the idea of phrenology, arguing that localization of brain function should be based on examining behavior that results from clinical lesion of internal brain regions rather than external inspection of bumps on the head. A short fifteen years later, German neurologist Karl Wernicke proposed that only the most basic mental functions such as perception and movement were localized to single areas of the brain, but more complex cognitive functions resulted from interconnections between several anatomical sites, advancing the idea of 'distributed processing' (i.e., various components of a single behavior are processed in different regions of the brain). At the beginning of the twentieth century, German anatomist Korbinian Brodmann used a staining technique to divide the human cerebral cortex into 52 discrete functional areas based on distinctive structural variation and characteristic organization of the cells. The cytoarchitectonic scheme of Brodmann areas is still widely used and continually updated today.

In the days of Broca and Wernicke, everything known about brain function had come from studying the behavior of brain-damaged patients and determining the site of damage in a postmortem analysis. If a patient had a deficit in some behavior, then execution of that behavior must depend on the lesioned area. In the 1920s, American psychologist Karl Lashley performed intentional lesion studies on laboratory animals by assessing the ability of a rat to complete a maze task after lesioning separate regions of brain cortex. A variety of animal lesion models and behavioral assays have since been created to associate specific brain regions with brain function. When establishing such

correlations, lesion models can be useful for demonstrating the necessity of an anatomical region, but they cannot resolve its particular role within a neural pathway. Disruption of adjacent brain regions during surgery or adaptive rewiring postsurgery may also complicate functional interpretations. Hence, lesion studies often produce confounding results and are not sufficient for investigating neural circuitry.

Need to Manipulate Neuronal Activity

The basic principles of brain organization, and to some extent information processing, have been pieced together using functional data from both brain slices (*in vitro*) and brains of awake, behaving animals (*in vivo*). Functional data can be obtained by various imaging and electrophysiology techniques, while additional pharmacological application and electrical stimulation can be used to directly probe neuronal function and connectivity. However, these methods are also limited in their ability to elucidate neural circuitry. Pharmacology often lacks specificity for particular cell types. Microstimulation excites both excitatory and inhibitory neurons and the precise region or number of stimulated cells is in many cases unknown.

Absolute resolution of intact neural circuits requires the direct manipulation of defined neuronal populations[2,3]. Such manipulation entails the ability to selectively and reversibly turn neuronal activity on and off in a tunable way on a relevant timescale. This can be approached in two different ways: controlling neurotransmitter availability to manipulate signal transmission, or controlling neuronal membrane potential to manipulate signal transduction. Both strategies have been used to induce or inhibit

neuronal activity. Manipulation is achieved via chemical, physical or genetic influences on transcription or protein activation.

Neurotransmitter availability can be restricted by preventing release into the synaptic cleft. For example, cleavage of vesicle-associated membrane protein 2 (VAMP2, also known as synaptobrevin) by inducible transcription of tetanus neurotoxin light chain (TeNT) can be used to inhibit synaptic vesicle fusion and subsequent neurotransmitter release[4,5]. An alternative approach called 'Molecules for Inactivation of Synaptic Transmission' (MISTs), utilizes a small molecule dimerizer to induce cross-linking of genetically modified forms of vesicular proteins including VAMP2 and synaptophysin to interfere with the protein-protein interactions necessary for vesicle fusion[6]. Induced neurotransmitter availability can be achieved with the use of caged neurotransmitters. With this technique, neurotransmitters are rendered biologically inactive, or caged, by chemical modifications with a photocleavable protecting group. A flash of light liberates the active form, imitating neurotransmitter release and permitting photostimulation of synaptic activity. Glutamate uncaging has been used extensively to study circuitry *in vitro*[7], however, most mammalian neurons express glutamate receptors so the technique lacks cellular specificity. The usefulness of TeNT and MISTs methods for *in vivo* studies is also limited due to a slow onset (14 days) of transcriptional induction and issues with delivery of chemical dimerizers. Furthermore, these methods alter the activity of neurotransmitter molecules rather than the neuron itself, so the postsynaptic targets must already be known in order to confirm the manipulated effect by electrophysiology.

Manipulation of neuronal membrane potential to control signal transduction is possible through modification of membrane ion channels or receptors. Rapid current flow

of selective ions into or out of the cell provides the dramatic changes in membrane potential necessary for versatile neuronal signaling. Direct alteration of the membrane potential can enhance the cell's ability to generate an action potential through depolarization, or inhibit the cell's ability to generate an action potential by hyperpolarization or shunting (clamp the $V_m \approx E_K$). Thus, neuronal activity can be induced by cation influx or silenced by K^+ efflux or Cl^- influx. Neurons have successfully been silenced by overexpression of various K^+ channels[8-10]. Since many of these channels are constitutively active, induction and reversal can only be accomplished through transcriptional control. Overexpression of K^+ channels can also yield undesirable effects such as disruption of native potassium channel expression or cell death[11,12]. Another effective silencing strategy uses membrane-tethered toxins to inhibit endogenous sodium channel or nicotinic receptor function[13]. Since toxins are peptides tethered to the membrane by a GPI anchor, they also require regulated gene expression for temporal control. Tethering of the ligand to the receptor with a photoisomerizable moiety addressed the need for controlled initiation and termination of modulating effects. Photoswitchable tethered ligands allow exogenously engineered channels or native channels to become 'light-gated', as light-induced isomerization presents or removes the ligand from its binding site[14,15].

Other strategies have involved chemically induced inhibition of neuronal activity. One study administered the allosteric modulator zolpidem to activate selectively expressed $GABA_A$ chloride channels using a transgenic mouse model in which endogenous $GABA_A$ channels were engineered to abolish sensitivity to zolpidem[16]. A related technique used a serotonin receptor 1A ($5\text{-}HT_{1A}$) knockout mouse and targeted

restoration of 5-HT_{1A} receptor expression with administration of selective serotonergic agonists[17]. Though successful, these methods unfortunately require animals with specialized genetic backgrounds and implement native receptors that can still be activated by endogenous neurotransmitters.

Expression of Foreign Receptor Tools

Many of these methods lack cell specificity, have slow temporal control, limited reversibility, constitutive activity, or interfere with native protein expression. Such issues have clarified the need for more refined control over neuronal activity.

Detailed circuit analysis requires the ability to manipulate and monitor a specific cell type. Cell types may be defined by anatomical characteristics including cell body location, dendritic morphology, axonal projection as well as electrophysiological characteristics and gene expression patterns. Molecular and genetic technology has been used to target gene expression of foreign receptor proteins to specific neuron types that, when activated, can inhibit or enhance neuronal activity within complicated neuronal circuits.

Genetically targeted manipulation must be precisely controlled in space and in time. The expression of an exogenous protein by itself should be innocuous, but when activated should enhance or silence neuronal firing in a selectively inducible and reversible manner. Many successful applications of targeted neuronal manipulation have involved the use of light to activate exogenous ion channels and receptor proteins. These include opsin proteins which are naturally light-sensitive ion channels and pumps

activated by photoisomerization of the chromophore retinal, a native compound of vertebrate nervous systems, to directly photoregulate membrane potential. Light activation of channelrhodopsin, an ion channel from the unicellular green algae *Chlamydomonas reinhardtii*, produces cationic currents to enable action potential firing that is time-locked to pulsed light[18,19]. Conversely, halorhodopsin, a chloride pump from the microorganism *Natronomonas pharaonis,* hyperpolarizes neurons to inhibit the production of action potentials[20]. Such optical control over neuronal activity allows millisecond timescale modulation. However, optical approaches require specialized equipment and are invasive, as light sources must be applied directly to the brain region of interest. Poor light penetration and heat generation also limit its applications to anatomically defined regions and short-termed modulations.

Alternative approaches use small molecule agonists for activation of exogenous receptors and ion channels, extending manipulation capabilities to deep and disperse neuronal populations with virtually limitless opportunities for simultaneous applications. These pharmacologically induced methods come with their own advantages, limitations, and requirements for specificity and are described in the next chapter. One such pharmacological tool, GluCl/IVM, is the subject of experimentation in this thesis.

References

1. Azevedo FA, Carvalho LR, Grinberg LT, Farfel JM, Ferretti RE, Leite RE, Jacob Filho W, Lent R, Herculano-Houzel S. (2009) Equal numbers of neuronal and nonneuronal cells make the human brain an isometrically scaled-up primate brain. *J Comp Neurol* **513**:532–541.

2. Crick F. *What Mad Pursuit: A Personal View of Scientific Discovery*. Basic Books, New York, 1988.

3. Wulff P, Wisden W. (2005) Dissecting neural circuitry by combining genetics and pharmacology. *Trends Neurosci* **28**:44–50.

4. Kobayashi T, Kai N, Kobayashi K, Fujiwara T, Akagawa K, Onda M, Kobayashi K. (2008) Transient silencing of synaptic transmitter release from specific neuronal types by recombinant tetanus toxin light chain fused to antibody variable region. *J Neurosci Methods* **175**:125–132.

5. Yamamoto M, Wada N, Kitabatake Y, Watanabe D, Anzai M, Yokoyama M, Teranishi Y, Nakanishi S. (2003) Reversible suppression of glutamatergic neurotransmission of cerebellar granule cells in vivo by genetically manipulated expression of tetanus neurotoxin light chain. *J Neurosci* **23**:6759–6767.

6. Karpova AY, Tervo DG, Gray NW, Svoboda K. (2005) Rapid and reversible chemical inactivation of synaptic transmission in genetically targeted neurons. *Neuron* **48**:727–735.

7. Callaway EM, Katz LC. (1993) Photostimulation using caged glutamate reveals functional circuitry in living brain slices. *Proc Natl Acad Sci U S A* **90**:7661–7665.

8. Ehrengruber MU, Doupnik CA, Xu Y, Garvey J, Jasek MC, Lester HA, Davidson N. (1997) Activation of heteromeric G protein-gated inward rectifier K+ channels overexpressed by adenovirus gene transfer inhibits the excitability of hippocampal neurons. *Proc Natl Acad Sci U S A* **94**:7070–7075.

9. Heron-Milhavet L, Xue-Jun Y, Vannucci SJ, Wood TL, Willing LB, Stannard B, Hernandez-Sanchez C, Mobbs C, Virsolvy A, LeRoith D. (2004) Protection against hypoxic-ischemic injury in transgenic mice overexpressing Kir6.2 channel pore in forebrain. *Mol Cell Neurosci* **25**:585–593.

10. Johns DC, Marx R, Mains RE, O'Rourke B, Marban E. (1999) Inducible genetic suppression of neuronal excitability. *J Neurosci* **19**:1691–1697.

11. Nadeau H, McKinney S, Anderson DJ, Lester HA. (2000) ROMK1 (Kir1.1) causes apoptosis and chronic silencing of hippocampal neurons. *J Neurophysiol* **84**:1062–1075.

12. Sutherland ML, Williams SH, Abedi R, Overbeek PA, Pfaffinger PJ, Noebels JL. (1999) Overexpression of a Shaker-type potassium channel in mammalian central nervous system dysregulates native potassium channel gene expression. *Proc Natl Acad Sci U S A* **96**:2451–2455.

13. Ibanez-Tallon I, Wen H, Miwa JM, Xing J, Tekinay AB, Ono F, Brehm P, Heintz N. (2004) Tethering naturally occurring peptide toxins for cell-autonomous modulation of ion channels and receptors in vivo. *Neuron* **43**:305–311.

14. Banghart M, Borges K, Isacoff E, Trauner D, Kramer RH. (2004) Light-activated ion channels for remote control of neuronal firing. *Nat Neurosci* **7**:1381–1386.

15. Fortin DL, Banghart MR, Dunn TW, Borges K, Wagenaar DA, Gaudry Q, Karakossian MH, Otis TS, Kristan WB, Trauner D, Kramer RH. (2008) Photochemical control of endogenous ion channels and cellular excitability. *Nat Methods* **5**:331–338.

16. Wulff P, Goetz T, Leppa E, Linden AM, Renzi M, Swinny JD, Vekovischeva OY, Sieghart W, Somogyi P, Korpi ER, Farrant M, Wisden W. (2007) From synapse to behavior: rapid modulation of defined neuronal types with engineered GABAA receptors. *Nat Neurosci* **10**:923–929.

17. Tsetsenis T, Ma XH, Lo Iacono L, Beck SG, Gross C. (2007) Suppression of conditioning to ambiguous cues by pharmacogenetic inhibition of the dentate gyrus. *Nat Neurosci* **10**:896–902.

18. Boyden ES, Zhang F, Bamberg E, Nagel G, Deisseroth K. (2005) Millisecond-timescale, genetically targeted optical control of neural activity. *Nat Neurosci* **8**:1263–1268.

19. Nagel G, Brauner M, Liewald JF, Adeishvili N, Bamberg E, Gottschalk A. (2005) Light activation of channelrhodopsin-2 in excitable cells of Caenorhabditis elegans triggers rapid behavioral responses. *Curr Biol* **15**:2279–2284.

20. Zhang F, Wang LP, Brauner M, Liewald JF, Kay K, Watzke N, Wood PG, Bamberg E, Nagel G, Gottschalk A, Deisseroth K. (2007) Multimodal fast optical interrogation of neural circuitry. *Nature* **446**:633–639.

Chapter 2

Orthogonal Pharmacological Control of Neuronal Activity

The following text is a reproduced excerpt, with minor editing, from:

Mikhail G. Shapiro[1,2,3], Shawnalea J. Frazier[4,5], Henry A. Lester[5]. Unparalleled control of neural activity using orthogonal pharmacogenetics. Review. American Chemical Society Chemical Neuroscience. *submitted 05-04-2012*

[1]Miller Research Institute,
[2]Department of Bioengineering,
[3]Department of Molecular and Cell Biology,
University of California at Berkeley
Berkeley, CA 94720

[4]Biochemistry and Molecular Biophysics
[5]Division of Biology
California Institute of Technology
Pasadena, CA 91125

Abstract

Studying the functional architecture of the brain requires technologies to precisely measure and perturb the activity of specific neural cells and circuits in live animals. Substantial progress has been made in recent years to develop and apply such tools. In particular, technologies that provide precise control of activity in genetically defined populations of neurons have enabled the study of causal relationships between and among neural circuit elements and behavioral outputs. Here, we review an important subset of such technologies, in which neurons are genetically engineered to respond to specific chemical ligands that have no other pharmacological effect in the central nervous system. A rapidly expanding set of these "orthogonal pharmacogenetic" tools provides a unique combination of genetic specificity, functional diversity, spatiotemporal precision and potential for multiplexing. We review the main orthogonal pharmacogenetic technologies that utilize engineered neuroreceptors to control neuronal excitability. We describe the key performance characteristics informing the use of these technologies in the brain, and potential directions for improvement and expansion of the orthogonal pharmacogenetics toolkit to enable more sophisticated systems neuroscience.

Introduction

The brain is a complex system comprising billions of interconnected, specialized cells whose collective function gives rise to mental states and observable behavior, while malfunction leads to neurological and psychiatric disease. Studying this system requires technologies to precisely sense and control the activity of specific neural cells and circuits in model organisms. An important focus of technical development in recent years has been technologies that provide precise control of activity in genetically defined populations of neurons. Such technologies have enabled the study of causal relationships between the functioning of neural circuits and behavior, yielding novel insights into processes such as aggression[1], anxiety[2] and appetite[3]. Here, we review an important subset of such technologies, in which exogenous genes introduced into neurons enable them to respond to specific chemical ligands that have no other pharmacological effect in the central nervous system (CNS). An expanding repertoire of such tools provides a powerful combination of genetic specificity, functional diversity, spatiotemporal precision and potential for multiplexing that will be critical in obtaining a systems-level understanding of brain function.

In the past, neuroscientists have modulated neural activity using pharmacology or electrical stimulation, obtaining either molecular or spatial specificity (Table 2-1). Each method is incomplete, since both location and molecular identity are needed to define the functional circuit roles of neurons. Recently, novel technologies have been developed that are capable of controlling neural activity with both spatial and molecular precision. These technologies take advantage of advances in understanding of cell type-specific gene expression in neurons[4] and methods of targeting transgenes to cells based on their

	Conventional Pharmacology	Electrical Stimulation	Optogenetics	Orthogonal Pharmacogenetics
Cell type specificity	Medium	None	High	High
Temporal precision	Medium	High	High	Medium
Spatial precision	None	High	High	Medium
Multiplexing	Low	Low	Medium	High
Signaling variety	Low	Low	Medium	High
Spatial Coverage	High	Low	Low	High
Requires gene delivery	No	No	Yes	Yes
Requires device	No	Yes	Yes	No

Table 2-1. Capabilities of neural control technologies

genetic properties, location and circuit connectivity[5]. Control is achieved by expressing exogenous actuator proteins that make specific neurons responsive to "orthogonal" stimuli that normally have no effect on nervous system function.

One successful instantiation of this concept, "optogenetics", uses actuator proteins that are sensitive to visible light, including ion channels, transporters, G-protein coupled receptors (GPCRs) and protein-protein binding domains. Expressing these proteins in neurons makes it possible to control various aspects of their activity with light[6-8]. In addition to the molecular, spatial and circuit specificity achievable through genetic targeting, optical stimulation provides a high degree of temporal precision, in some cases on millisecond timescales enabling control of neuronal spike timing and frequency[9] (Table 2-1). Multiplexing is possible with up to 3–4 channels using actuator proteins that respond to different wavelengths. A drawback of optogenetic brain stimulation in mammals is the need for implanted optical fibers to deliver light. In addition to being

burdensome experimentally, the resulting localized illumination makes it difficult to control diffuse signaling networks.

Another approach to orthogonal control of genetically specified neurons uses actuator proteins that respond to unique chemical ligands that have no other pharmacological activity in the CNS. This approach, to which we refer as orthogonal pharmacogenetics (OP), has been used for some time to control gene expression (e.g. using tetracycline-dependent transcriptional promoters). Recently, novel actuator proteins have been developed that enable chemical control of neuronal firing, second-messenger signaling and synaptic function. Like optogenetics, OP can use genetic targeting to achieve molecular, spatial and circuit specificity. In addition, ligands with different pharmacokinetic properties can be used to specify the timescale of neural control, ranging from minutes to days. This temporal resolution is not so high as with optogenetics. However, it is fully satisfactory in many cases where circuits play modulatory roles or the objective of the perturbation is long-term inhibition. Unlike optogenetics, OP does not require invasive implants, and both local and diffuse groups of neurons can be controlled depending on where the actuator gene is expressed (Table 2-1). In theory, OP also has the capacity for virtually unlimited multiplexing, as long as a sufficient number of unique ligand-receptor pairs can be developed. Importantly, such multiplexing can be both within a cell type (e.g., by expressing inhibitory and excitatory ion channels controlled by different ligands) and between multiple cell types (Figure 2-1).

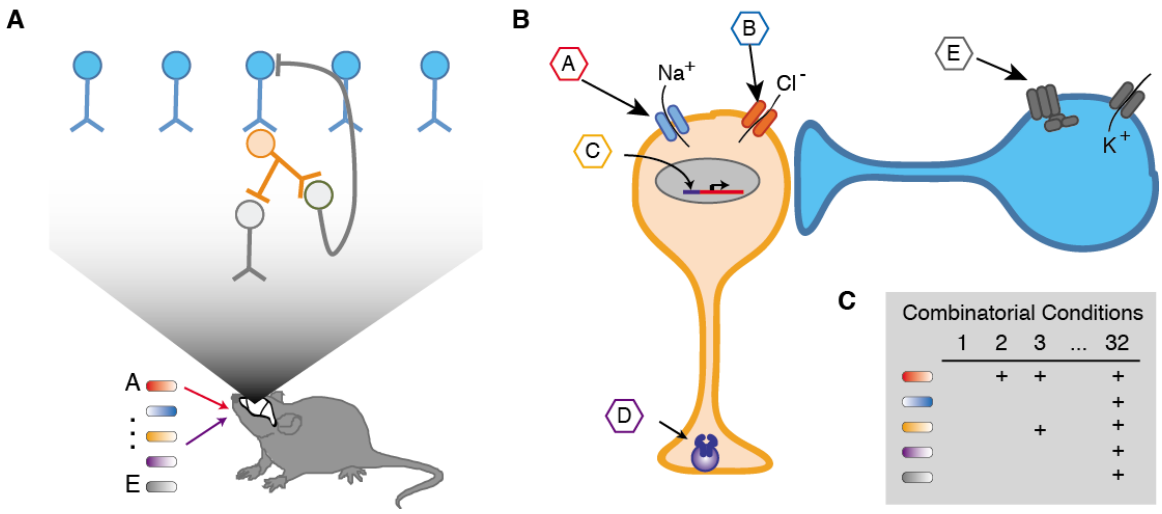

Figure 2-1. Illustrated example of multiplexed orthogonal pharmacogenetics. *A*. Two cell types (blue and orange) involved in a particular neural circuit (top) are genetically modified to express orthogonal actuators responding to several distinct ligands that can be administered orally to the model organism (bottom). *B*. One neuron (orange) expresses four distinct OP constructs, enabling temporally specific, multiplexed control of excitation (ion channel controlled by ligand A), inhibition (ion channel controlled by ligand B), gene transcription (transcriptional transactivator controlled by ligand C) and decreased presynaptic transmitter release (vesicle protein multimerization controlled by ligand D). A second neuron (blue) has an orthogonal GPCR coupled to an endogenous potassium channel, enabling orthogonal inhibition under control of ligand E. *C*. Using the five ligands corresponding to different orthogonal actuators, it is possible to test 32 binary (ligand on or off) experimental conditions in this system.

OP systems have been engineered to provide chemical control over various aspects of neural activity, including ion channel and GPCR signaling, gene transcription and synaptic function. In addition, OP actuators have been developed providing control over gene translation and enzymatic activity that could be adapted to neurons. Below, we highlight the major categories of recently developed OP systems and their applications in neuroscience. We evaluate them with reference to a common set of performance characteristics applicable to functional actuators (orthogonality, compatibility, modularity and deliverability) their chemical effector ligands (molecular specificity and

deliverability), and the combination of ligand and actuator (temporal response, dose response), as defined in Table 2-2.

Actuator characteristics	
Orthogonality	Actuator is insensitive to endogenous ligands or other signaling elements. Actuator inactive until triggered by ligand (or inactive in presence of ligand in a switch-off system).
Compatibility	Endogenous machinery needed for actuator performance is present in target cells. Actuator does not interfere with normal cell function unless it is activated by ligand.
Modularity	Actuator can be modified to produce different signaling effects upon ligand binding.
Deliverability	Actuator can be delivered to target cells by viral vectors and through transgenesis. Ideally, the essential genetic payload should be a single gene smaller than 1.5kb to enable single AAV construct delivery.
Effector ligand characteristics	
Molecular specificity	At the effective dose, ligand acts only on its corresponding actuator.
Deliverability	Ligand is bioavailable, preferably *per orum*, and penetrates CNS.
System characteristics	
Temporal response	On and off kinetics for cellular and behavioral response after administration as determined by ligand pharmacokinetics and receptor activation, inactivation and second-messenger signaling.
Dose response	Dependence of cellular and behavioral response on ligand dose.

Table 2-2. Performance characteristics of orthogonal pharmacogenetic systems

Orthogonal neuroreceptors: LGICs and GPCRs

The most active recent area of development in OP has focused on neuroreceptors. Both ligand-gated ion channels (LGICs) and GPCRs have been developed as orthogonal actuators by identifying or engineering receptors with minimal sensitivity to endogenous neurotransmitter agonists and strong activation by specific exogenous ligands that have no other significant pharmacological effect in the CNS. Targeted expression of these orthogonal receptors permits temporally controlled excitation or inhibition of neurons through the administration of their cognate ligands.

The first orthogonal GPCR and LGIC systems for use in neuroscience were based on receptors from nonmammalian organisms. The Callaway group developed a system based on the *Drosophila* allatostatin receptor (AlstR) and its cognate neuropeptide ligand allatostatin (AL), neither of which is expressed in mammals[10]. AL does not cross-activate endogenous mammalian GPCRs, nor is AlstR activated by mammalian GPCR ligands[11]. Activation of heterologously expressed AlstR by AL leads to Gi-coupled activation of endogenous mammalian G protein-gated inward rectifier K^+ (GIRK) channels, leading to a reduction in cell excitability (Figure 2-2). Virally targeted expression of AlstR in cortical and thalamic neurons and intracranial administration of AL produce neuronal silencing on a timescale of minutes in several species[12].

Around the same time, the Lester group adapted the *C. elegans* glutamate-gated chloride channel (GluCl) for silencing of mammalian neurons by administration of the anthelmintic GluCl agonist ivermectin (IVM). GluCl was rendered insensitive to its native ligand glutamate by a single point mutation and codon-optimized to achieve

greater expression in mammalian cells[13,14]. IVM activation of GluCl α and β subunits expressed in neurons elicits a Cl^- conductance across the membrane that effectively shunts action potential generation[15] (Figure 2-2). The GluCl/IVM system later became the first to be used for neuronal silencing with a systemically administered ligand in awake, behaving animals[16].

More recently, versatile orthogonal neuroreceptor systems have been established by modifying mammalian GPCRs and LGICs. A collection of modified GPCRs called DREADDs, "designer receptors exclusively activated by designer drugs", were developed using a combination of directed evolution and rational protein engineering[17]. Building on previous efforts to engineer the ligand selectivity of GPCRs[18], the first DREADDs were generated from the human M3 muscarinic receptors (hM3). Survival screens based on the yeast pheromone response[19] were used to evolve this receptor for activation by the small molecule clozapine-*N*-oxide (CNO) and lack of activation by the native ligand acetylcholine. CNO is a normally inactive metabolite of the atypical antipsychotic clozapine. CNO activation of the mutant hM3D triggers Gq-coupled signaling leading to membrane depolarization through phospholipase Cβ (PLCβ)/PIP_2 mediated inhibition of KCNQ channels[20] (Figure 2-2). Following a similar design scheme, a second CNO-activated DREADD, hM4D, was generated that couples to Gi, leading to activation of GIRK channels and neuronal silencing similar to that elicited by AlstR/AL (Figure 2-2).

Recently, a systematic engineering approach was also taken to the development of a modular system of orthogonally controlled Cys-loop ion channels with distinct ligand sensitivity and ion conductance properties[3]. The modularity of this system is based on

fusing the α7 nicotinic acetylcholine receptor (nAChR) ligand-binding domain onto the ion pore domain of either a cation-selective serotonin 5-HT3 receptor (α7-5HT3) or anion-selective glycine receptor (α7-GlyR) to produce functional channels with the same pharmacological profile but different ion permeability[21,22]. Novel ligand recognition properties were engineered through a "bump-hole" approach, which uses structural models to generate libraries of predicted ligand-receptor pairs that are then synthesized and screened for selective functional activity. Structural analogs of the α7-specific synthetic agonist PNU-282987 were tested for selective activation of mutant, but not wild-type, channels. At the same time, mutant channels were screened for lack of activation by acetylcholine and nicotine. The resulting mutant ligand binding domains are dubbed 'pharmacologically selective actuator modules' (PSAMs). Each PSAM is exclusively activated by a cognate synthetic agonist, called a "pharmacologically selective effector molecule" (PSEM). Three specific PSAM/PSEM tools have been designed, each with different ion conductance properties for controlling neuronal excitability[3]. These include the cation-selective activator, $PSAM^{Q79G,Q139G}$-5HT3HC/$PSEM^{22S}$, the anion-selective silencer, $PSAM^{L141F,Y115F}$-GlyR/$PSEM^{89S}$, and a third Ca^{2+}-selective channel, $PSAM^{Q79G,L141S}$-nAChR V13'T/$PSEM^{9S}$.

Another orthogonal LGIC system is based on the transient receptor potential ion channel TRPV1, an endogenous mammalian receptor predominantly expressed in the peripheral nervous system. TRPV1 is a nonselective cation channel activated by noxious heat, pH and exogenous ligands including the hot chili pepper compound capsaicin[23]. Targeted neuronal expression of TRPV1 in the mouse brain leads to capsaicin-activated currents and action potentials[24]. To use TRPV1 for orthogonal control of specific

neurons, the host organism can be modified to knock out endogenous TRPV1 expression. On this TRPV1$^{-/-}$ background one can reintroduce TRPV1 into target cells as an exogenous OP actuator[25].

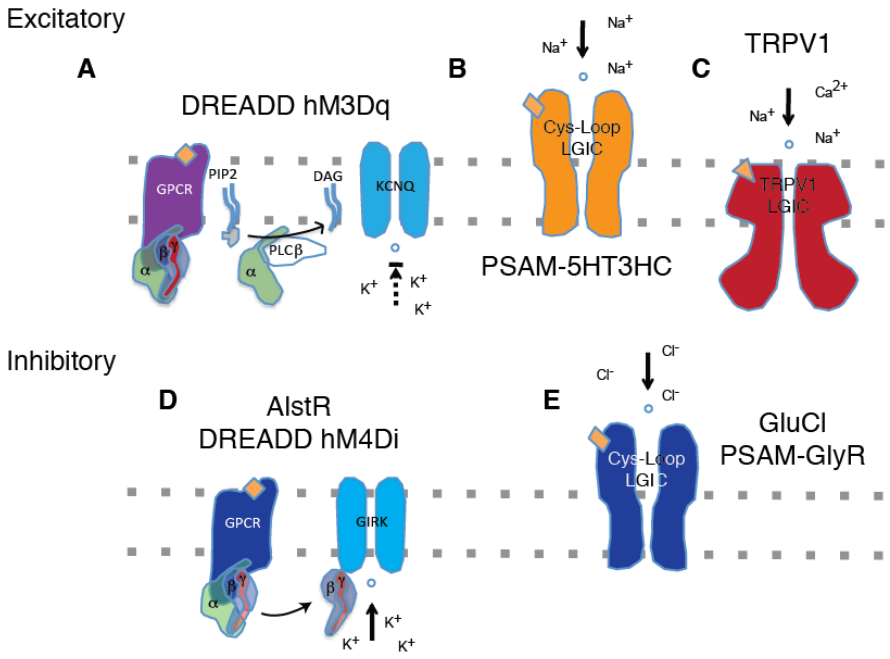

Figure 2-2. Mechanisms of orthogonal neuroreceptors. GPCRs form the basis for both excitatory and inhibitory OP systems (*A, D*) based on interactions with different endogenous G proteins. GPCR signaling cascades leading to excitation and inhibition are described in the text. Cys-loop LGICs (*B, E*) are also used to effect inhibition and excitation based on pore domain ion selectivity. TRPV1 (*C*) excites cells through a nonselective cation conductance.

Performance Characteristics

The set of available OP neuroreceptor tools is summarized in Table 2-3. Their specific performance characteristics inform their ability to fulfill the unique objectives of a neuroscience study. As defined in Table 2-2, key performance characteristics depend on the properties of actuators, effectors, or both.

Actuator orthogonality, compatibility, modularity and deliverability

GPCR and LGIC architectures of orthogonal receptors confer distinct functional properties. Neural control using GPCR-based systems depends on second messenger signaling cascades. Although these secondary effectors are generally present in neurons, their precise quantity and subcellular localization could impose limits on actuator function. Conversely, expression of heterologous receptors could sequester second messenger molecules, disrupting endogenous receptor activity[26]. G-protein-mediated cascades may also have undesirable effects beyond altering neuronal firing (e.g., affecting gene expression), especially with sustained activation[27,28]. In contrast to GPCRs, LGIC actuators are self-contained membrane proteins with ligand-dependent ionic conduction directly affecting membrane excitability. They require no intermediary molecules. However, close attention must be paid to their ionic selectivity. The high Ca^{2+} permeability of TRPV1, for example, is likely to trigger Ca^{2+}-mediated cell signaling events in addition to exciting cells.

Both LGICs and GPCRs are functionally modular. The PSAM/PSEM system described above illustrates the relative ease of generating new chimeric channels based

on the modularity of Cys-loop receptors. Ligand-binding domains developed and tested while connected to one transmembrane domain were transplanted onto other transmembrane domains, resulting in constructs with completely different ionic conductance. Structure-function studies support further potential for altering ion selectivity, single-channel conductance, and open channel duration (reviewed in[29-31]). When modifying Cys-loop receptors, one must ensure that mutant channels have minimal leak current in the resting state. GPCRs are modular with regard to their second messenger coupling. Domain swapping and point mutations of intracellular loops can alter G-protein specificity, allowing modulation of Gi-, Gs-, and Gq-coupled signaling pathways[32].

Engineered receptors can be delivered into the CNS via transgenic modification or viral vectors. With coding sequences of approximately 1.7 kb for the M3 muscarinic receptor, 1.2 kb for AlstR, 1.4 kb for GluCl, 1.5 kb for PSAMs and 2.5 kb for TRPV1, each receptor construct can be accommodated by lentiviral vectors; in addition, GluCl, AlstR and PSAMs can be delivered by adeno-associated virus (AAV). Most of these tools require the delivery of only one genetic construct, except GluCl, which requires α and β subunits. The requirement for two constructs permitted GluCl to be used with intersectional genetic targeting[33]. Codon optimization and signal peptide fusions can improve translation and membrane trafficking of nonnative receptors[14,34-36]. Receptors can also be regionally targeted to somato-dendritic, axonal, or postsynaptic sites[37-39].

Class	Actuator	Effector	Effect on neurons	Signaling and Endogenous Partners	Design & Proof-of-concept Refs.	Application Refs.
GPCR	AlstR *drosophila*	AL	Inhibition	G_i-coupled; activates GIRK K^+ channel	10, 12, 46	56-58
GPCR	DREADD hM4Di *human*	CNO	Inhibition	G_i-coupled; activates GIRK K^+ channel	17	59, 61-62
GPCR	DREADD hM3Dq *human*	CNO	Excitation	G_q-coupled; inhibits KCNQ K^+ channel	17, 20	60-62
LGIC	GluCl α & β *C. elegans*	IVM	Inhibition	Cl^- channel	13-16	1, 33
LGIC	PSAM-5HT3HC *human-mouse*	$PSEM^{22S}$	Excitation	Cation channel ($Na^+ \approx K^+ > Ca^{2+}$)	3	
LGIC	PSAM-GlyR *human*	$PSEM^{89S}$	Inhibition	Cl^- channel	3	3
LGIC	PSAM-nAChR V13'T *human-rat*	$PSEM^{9S}$	Not shown	Ca^{2+} channel	3	
LGIC	TRPV1 *rat*	Capsaicin	Excitation	Cation channel ($Ca^{2+} > Na^+ \approx K^+$)	24-25	

Table 2-3. Orthogonal neuroreceptors. Far-right columns indicate corresponding references.

Ligand deliverability and specificity

Ligands with good pharmacokinetics, including oral bioavailability and brain penetration, allow manipulation of deep brain structures and dispersed neuronal populations. The ability to conveniently deliver effector ligands is a key advantage of the DREADD/CNO, GluCl/IVM, and the PSAM/PSEM systems (Table 2-4). No specialized equipment is necessary, as the exogenous activating ligands of these tools allow convenient systemic administration of rapidly diffusible agonists orally or by intraperitoneal or intravenous injection. The bioavailability (i.e., degree to which the drug becomes available to the target tissue after administration) depends on its ability to cross the BBB. On the other hand, neuronal manipulation using AlstR/AL or TRPV1/capsaicin (in a wild-type background) requires localized application of their effector ligands via parenchymal or

Ligand	Origins	Specificity	CNS penetration	Bioavailability	Kinetics	Refs.
Clozapine-N-oxide (CNO)	Inactive metabolite of clozapine	No known activity at effective dose	Yes	Oral	On: 5-10m Clearance: 2h	20
Allatostatin (AL)	Natural neuropeptide	No known activity in mammals	No	Injection only	On: 1-3m Clearance: 40-60m* (ICV)	12, 46, 56
Ivermectin (IVM)	Anthelmintic	Specific up to 10X effective dose	Yes	Oral	On: 4-12h* Clearance: 2-4d*	16, 33
PSEM^{89s}	Synthetic derivative of nAChR agonist PNU-282987	Minimal binding to endogenous nAChRs	Yes	Oral	On: 15m Clearance: 1-2h	3
Capsaicin	Pepper ingredient, natural TRPV1 agonist	Acts on native TRPV1 receptors unless they are knocked out	Yes	Oral	On: 2-5min Clearance: <15min	25

Table 2-4. Key effector ligands used in orthogonal pharmacogenetic systems. The * indicates timescales inferred from behavioral or signaling response. Far-right column indicates corresponding references.

intracerebroventricular administration. AL is a neuropeptide that cannot cross the BBB. In wild-type background, systemically administered capsaicin would elicit unwanted effects via endogenous TRPV1 receptors.

To achieve truly orthogonal control, effector ligands must have no significant activity in cells not expressing their partner actuator at doses used for actuation. IVM is known to activate or potentiate other Cys-loop receptors present in the CNS, but with much lower sensitivity[40-43]. PSEMs were screened for ligand binding by radioligand displacement against a number of other LGICs, GPCRs and transporters[3], revealing weak to moderate binding of PSEM89^{S} to the α4β2 neuronal nAChR receptor; off-target functional activation remains to be assayed. Conversely, undesired on-target effects can result from agonism by endogenous ligands. For example, endogenous TRPV1 ligands including the endocannabinoid anandamide and N-arachidonoyl-dopamine are expressed

in the CNS[44,45] and could possibly allow capsaicin-independent enhancement of neuronal activity. For each system it is important to determine an effective dosage range for optimal control with minimal side effects.

Temporal resolution and dose response

The activation and deactivation kinetics of *in vivo* neuronal manipulation using OP systems can range from minutes to hours and depend on the pharmacokinetic properties of the ligand such as absorption, distribution, metabolism and excretion, as well as receptor properties including affinity for agonist, desensitization and internalization. The TRPV1/capsaicin tool allows the most rapid, transient neuronal activation, with excitatory responses occurring within minutes of administration and lasting approximately 10 minutes, attributed to rapid capsaicin metabolism[25]. Activation of DREADDs by CNO can also be observed within 5-10 minutes of drug administration, with induced behavior lasting from minutes to many hours. GPCRs are especially sensitive to desensitization and/or internalization with prolonged ligand exposure. These processes can either terminate a pharmacologically induced signal prematurely or facilitate sustained signaling or hyperexcitability[46] as endocytosis of GPCRs does not always terminate the signal[47]. CNO itself is cleared after approximately 2 hours[20]. IVM-induced GluCl currents activate over several hours and remain open for times on the order of 8 hours, presumably because neither desensitization nor ligand dissociation occur. Silencing effects by GluCl/IVM can last for 2–4 days; postsilencing recovery may actually require receptor turnover[16]. Long periods of enhanced or silenced activity can be

beneficial in some experiments, but present the risk of adaptive, compensatory, or plastic changes at the cellular or network levels. PSAMs are activated by their ligands within 15 minutes and recovery is observed after 24 hours.

Where temporal response depends on desensitization kinetics, it may be possible to modify it at the actuator level. Mutations in the ligand binding domain, transmembrane domains and the large cytoplasmic domain of Cys-loop receptors have all been shown to affect desensitization[48-51]. For TRPV1, a point mutation that reduces Ca^{2+} permeability also abolishes desensitization[52]. Phosphorylation is also known to effect desensitization of many membrane receptors[52-54]. The removal of phosphorylation sites in the C-terminus of a heterologously expressed GPCR produced receptors that were resistant to internalization and less prone to desensitization, resulting in prolonged signaling[55]. For applications requiring more defined endpoints, it may be possible to design synthetic antagonists or selective pore blockers for controlled termination of manipulated activity. Thus, there would be both an "on" ligand and an "off" ligand.

Dose-dependence of behavioral responses has been reported for Alst/AL[56] and GluCl/IVM[16] and dose-dependent increases in neuronal activity have been demonstrated with hM3Dq/CNO[20] and TRPV1/capsaicin[24,25]. There is no *in vivo* dose-response info for the PSAM/PSEMs.

Applications of Orthogonal Neuroreceptors

Several orthogonal neuroreceptor systems have been used *in vivo* to study neural circuitry (Table 2-3). Viral-mediated expression of AlstR has been targeted to somatostatin-expressing neurons of the ventrolateral medulla to study pathological breathing patterns of adult rats[56]. Transgenic mouse lines expressing AlstR have been used to examine locomotor activity in V1 and V3 spinal cord neurons[57,58].

GluCl/IVM-induced silencing has been used in conjunction with channelrhodopsin-2 (ChR2) mediated activation to define an inhibitory microcircuit within the amygdala involved in mouse fear conditioning[33]. Because the GluCl channel requires co-expression of α and β subunits, an intersectional approach was used to restrict the expression of GluCl to specific GABAergic neurons within an anatomically defined amygdala subregion.

Viral vectors bearing different gene promoters have been used for targeted expression of the hM4Di/CNO DREADD silencer in striatonigral vs striatopallidal neurons to study the opposing roles of direct and indirect pathways in regulating adaptations from repeated psychostimulant drug exposure[59]. Recently, the hM3Dq/CNO activator was expressed in an activity-dependent manner to examine how artificial reactivation of a stimulated network affects the encoding of contextual fear memory in mice[60]. The hM4Di/CNO silencer and hM3Dq/CNO activator tools have also been used in parallel experiments to study the opposing impact of activation and silencing of agouti-related protein (AgRP) neurons of the hypothalamus on feeding patterns and energy expenditure[61]. Controlled activation and inhibition of orexinergic neurons in the

hypothalamus elucidated their role in controlling sleep and wakefulness[62]. Because CNO activates both excitatory and inhibitory DREADD actuators, opposite effects had to be studied in separate cohorts of animals.

Simultaneous bidirectional control of neuronal activity has been demonstrated by OP and optogenetic actuators in the same set of cells. A bicistronic Cre-dependent AAV was used to co-express the PSAM^{L141F,Y115F}-GlyR silencer and the light-activated channel ChR2 in AgRP neurons. Voracious feeding behavior evoked from continuous photostimulation was strongly suppressed by intraperitoneal administration of PSEM^{89S3}. Such bidirectional modulation will be most informative for deciphering neuronal networks and their role in behavior.

Prospects for Further Engineering of Orthogonal Neuroreceptors

The systems described above represent a promising start for the use of OP to control neural activity, demonstrating actuation of various aspects of neuronal signaling over a range of timescales, triggered conveniently by peripheral ligand administration. Substantial further work is needed to enact the vision presented in Figure 2-1. Multiplexed control over a significant number of cell types will require a larger set of orthogonal ligand-receptor pairs. Investigators should be able to choose among OP systems with various of temporal profiles to meet experimental requirements. More precise control over cellular signaling also necessitates greater "cassette" modularity of ligand interaction and signaling domains.

Further development of OP neuroreceptor systems will be aided by increasing knowledge about receptor structure. The three-dimensional structures of a number of GPCRs and Cys-loop receptors have now been resolved, including the M3 muscarinic receptor[63] and the GluCl channel[64]. Structures have also been solved for various conformational states, mutant forms and ligand complexes[65]. Growing availability of structural data along with homology modeling and docking programs will be useful in optimizing current tools and in rational construction of new ones. Already the PSAM/PSEM system has demonstrated the utility of homology-based structural information.

A major goal of future OP receptor engineering efforts should be to expand the repertoire of ligand-receptor pairs. Most ligands used to date are either active on the native receptor or are close relatives of known agonists (Table 2-4). Many molecules with

desirable properties (lack of activity on endogenous targets, high CNS penetration, rapid PK) exist outside of this constrained chemical space. Antimicrobial medications and inactive drug metabolites, for example, are sizeable categories of compounds with characterized pharmacokinetics and lack of activity in mammals. An even larger repository of potential effector ligands may be found among inactive analogs of drug candidates synthesized and characterized by pharmaceutical firms during lead compound optimization.

Engineering receptors that respond to effectors dissimilar from their native ligands could build on previous accomplishments using directed evolution[17] and structure-guided modification[3]. Directed evolution, in particular, has been successful in altering the chemical substrate and ligand specificity of enzymes and allosteric switches[66,67]. Directed evolution requires efficient high-throughput screens, which are available for both GPCR signaling[17] and ion channel conductance[68]. Furthermore, directed evolution libraries based on structure-guided recombination between homologous proteins (or domains) have been shown to enhance evolution efficiency[69]. The substantial homology of receptors and ligand-binding domains within and among organisms could enable the use of homologous recombination in OP receptor engineering.

Conclusions

Systems neuroscience research is now more tractable than ever thanks in part to molecular technologies enabling precise sensing and control of neural activity. We have reviewed an important class of such technologies, which provides a chemically addressable orthogonal dimension for neural control, and whose development is a highly active area of research. While a number of orthogonal pharmacogenetic tools have been used in neuroscience to great effect, many more (including those originally developed for use outside the brain) are ready for application. Future engineering efforts are expected to increase the variety of neuronal signaling pathways that can be manipulated. In addition, we believe it is particularly important to expand the repertoire of CNS-compatible ligands used in OP to enable multiplexed interrogation within and across cell types. Here, we have focused on the use of OP tools in neurons, but other relevant cell types in the brain such as glia and endothelial cells may also be targets for application.

A key feature of this class of technologies is the ability of many OP tools to be triggered noninvasively through peripheral ligand administration. The use of these tools together with new technologies for high-resolution noninvasive molecular imaging will make it possible to create complete noninvasive neural input/output systems to study brain-wide neural circuits, complementing more localized research using optical techniques. Furthermore, as gene and cell therapy make progress towards clinical acceptance, it may be possible for genetically encoded OP and noninvasive imaging technologies to help diagnose and treat neurological disease. Thus, orthogonal approaches for interfacing with the brain point in an exciting direction for both basic and clinical neuroscience.

References

1. Lin D, Boyle MP, Dollar P, Lee H, Lein ES, Perona P, Anderson DJ. (2011) Functional identification of an aggression locus in the mouse hypothalamus. *Nature* **470**:221–226.

2. Tye KM, Prakash R, Kim SY, Fenno LE, Grosenick L, Zarabi H, Thompson KR, Gradinaru V, Ramakrishnan C, Deisseroth K. (2011) Amygdala circuitry mediating reversible and bidirectional control of anxiety. *Nature* **471**:358–362.

3. Magnus CJ, Lee PH, Atasoy D, Su HH, Looger LL, Sternson SM. (2011) Chemical and genetic engineering of selective ion channel-ligand interactions. *Science* **333**:1292–1296.

4. Hatten ME, Heintz N. (2005) Large-scale genomic approaches to brain development and circuitry. *Annu Rev Neurosci* **28**:89–108.

5. Luo L, Callaway EM, Svoboda K. (2008) Genetic dissection of neural circuits. *Neuron* **57**:634–660.

6. Bernstein JG, Boyden ES. (2011) Optogenetic tools for analyzing the neural circuits of behavior. *Trends Cogn Sci* **15**:592–600.

7. Fenno L, Yizhar O, Deisseroth K. (2011) The development and application of optogenetics. *Annu Rev Neurosci* **34**:389–412.

8. Moglich A, Moffat K. (2010) Engineered photoreceptors as novel optogenetic tools. *Photochem Photobiol Sci* **9**:1286–1300.

9. Boyden ES, Zhang F, Bamberg E, Nagel G, Deisseroth K. (2005) Millisecond-timescale, genetically targeted optical control of neural activity. *Nat Neurosci* **8**:1263–1268.

10. Lechner HA, Lein ES, Callaway EM. (2002) A genetic method for selective and quickly reversible silencing of Mammalian neurons. *J Neurosci* **22**:5287–5290.

11. Birgul N, Weise C, Kreienkamp HJ, Richter D. (1999) Reverse physiology in drosophila: identification of a novel allatostatin-like neuropeptide and its cognate receptor structurally related to the mammalian somatostatin/galanin/opioid receptor family. *EMBO J* **18**:5892–5900.

12. Tan EM, Yamaguchi Y, Horwitz GD, Gosgnach S, Lein ES, Goulding M, Albright TD, Callaway EM. (2006) Selective and quickly reversible inactivation of mammalian neurons in vivo using the Drosophila allatostatin receptor. *Neuron* **51**:157–170.

13. Li P, Slimko EM, Lester HA. (2002) Selective elimination of glutamate activation and introduction of fluorescent proteins into a Caenorhabditis elegans chloride channel. *FEBS Lett* **528**:77–82.

14. Slimko EM, Lester HA. (2003) Codon optimization of Caenorhabditis elegans GluCl ion channel genes for mammalian cells dramatically improves expression levels. *J Neurosci Methods* **124**:75–81.

15. Slimko EM, McKinney S, Anderson DJ, Davidson N, Lester HA. (2002) Selective electrical silencing of mammalian neurons in vitro by the use of invertebrate ligand-gated chloride channels. *J Neurosci* **22**:7373–7379.

16. Lerchner W, Xiao C, Nashmi R, Slimko EM, van Trigt L, Lester HA, Anderson DJ. (2007) Reversible silencing of neuronal excitability in behaving mice by a genetically targeted, ivermectin-gated Cl- channel. *Neuron* **54**:35–49.

17. Armbruster BN, Li X, Pausch MH, Herlitze S, Roth BL. (2007) Evolving the lock to fit the key to create a family of G protein-coupled receptors potently activated by an inert ligand. *Proc Natl Acad Sci U S A* **104**:5163–5168.

18. Coward P, Wada HG, Falk MS, Chan SD, Meng F, Akil H, Conklin BR. (1998) Controlling signaling with a specifically designed Gi-coupled receptor. *Proc Natl Acad Sci U S A* **95**:352–357.

19. Dong S, Rogan SC, Roth BL. (2010) Directed molecular evolution of DREADDs: a generic approach to creating next-generation RASSLs. *Nat Protoc* **5**:561–573.

20. Alexander GM, Rogan SC, Abbas AI, Armbruster BN, Pei Y, Allen JA, Nonneman RJ, Hartmann J, Moy SS, Nicolelis MA, McNamara JO, Roth BL. (2009) Remote control of neuronal activity in transgenic mice expressing evolved G protein-coupled receptors. *Neuron* **63**:27–39.

21. Eisele JL, Bertrand S, Galzi JL, Devillers-Thiery A, Changeux JP, Bertrand D. (1993) Chimaeric nicotinic-serotonergic receptor combines distinct ligand binding and channel specificities. *Nature* **366**:479–483.

22. Grutter T, de Carvalho LP, Dufresne V, Taly A, Edelstein SJ, Changeux JP. (2005) Molecular tuning of fast gating in pentameric ligand-gated ion channels. *Proc Natl Acad Sci U S A* **102**:18207–18212.

23. Caterina MJ, Schumacher MA, Tominaga M, Rosen TA, Levine JD, Julius D. (1997) The capsaicin receptor: a heat-activated ion channel in the pain pathway. *Nature* **389**:816–824.

24. Arenkiel BR, Klein ME, Davison IG, Katz LC, Ehlers MD. (2008) Genetic control of neuronal activity in mice conditionally expressing TRPV1. *Nat Methods* **5**:299–302.

25. Guler AD, Rainwater A, Parker JG, Jones GL, Argilli E, Arenkiel BR, Ehlers MD, Bonci A, Zweifel LS, Palmiter RD. (2012) Transient activation of specific neurons in mice by selective expression of the capsaicin receptor. *Nat Commun* **3**:746.

26. Nichols CD, Roth BL. (2009) Engineered G-protein Coupled Receptors are Powerful Tools to Investigate Biological Processes and Behaviors. *Front Mol Neurosci* **2**:16.

27. Ma'ayan A, Jenkins SL, Barash A, Iyengar R. (2009) Neuro2A differentiation by Galphai/o pathway. *Sci Signal* **2**:cm1.

28. Redfern CH, Degtyarev MY, Kwa AT, Salomonis N, Cotte N, Nanevicz T, Fidelman N, Desai K, Vranizan K, Lee EK, Coward P, Shah N, Warrington JA, Fishman GI, Bernstein D, Baker AJ, Conklin BR. (2000) Conditional expression of a Gi-coupled receptor causes ventricular conduction delay and a lethal cardiomyopathy. *Proc Natl Acad Sci U S A* **97**:4826–4831.

29. Jensen ML, Schousboe A, Ahring PK. (2005) Charge selectivity of the Cys-loop family of ligand-gated ion channels. *J Neurochem* **92**:217–225.

30. Keramidas A, Moorhouse AJ, Schofield PR, Barry PH. (2004) Ligand-gated ion channels: mechanisms underlying ion selectivity. *Prog Biophys Mol Biol* **86**:161–204.

31. Thompson AJ, Lester HA, Lummis SC. (2010) The structural basis of function in Cys-loop receptors. *Q Rev Biophys* **43**:449–499.

32. Pei Y, Rogan SC, Yan F, Roth BL. (2008) Engineered GPCRs as tools to modulate signal transduction. *Physiology (Bethesda)* **23**:313–321.

33. Haubensak W, Kunwar PS, Cai H, Ciocchi S, Wall NR, Ponnusamy R, Biag J, Dong HW, Deisseroth K, Callaway EM, Fanselow MS, Luthi A, Anderson DJ. (2010) Genetic dissection of an amygdala microcircuit that gates conditioned fear. *Nature* **468**:270–276.

34. Gradinaru V, Thompson KR, Deisseroth K. (2008) eNpHR: a Natronomonas halorhodopsin enhanced for optogenetic applications. *Brain Cell Biol* **36**:129–139.

35. Ma D, Zerangue N, Lin YF, Collins A, Yu M, Jan YN, Jan LY. (2001) Role of ER export signals in controlling surface potassium channel numbers. *Science* **291**:316–319.

36. Srinivasan R, Pantoja R, Moss FJ, Mackey ED, Son CD, Miwa J, Lester HA. (2011) Nicotine up-regulates α4β2 nicotinic receptors and ER exit sites via stoichiometry-dependent chaperoning. *J Gen Physiol* **137**:59–79.

37. Dong S, Allen JA, Farrell M, Roth BL. (2010) A chemical-genetic approach for precise spatio-temporal control of cellular signaling. *Mol Biosyst* **6**:1376–1380.

38. Gradinaru V, Thompson KR, Zhang F, Mogri M, Kay K, Schneider MB, Deisseroth K. (2007) Targeting and readout strategies for fast optical neural control in vitro and in vivo. *J Neurosci* **27**:14231–14238.

39. Xu J, Zhu Y, Heinemann SF. (2006) Identification of sequence motifs that target neuronal nicotinic receptors to dendrites and axons. *J Neurosci* **26**:9780–9793.

40. Adelsberger H, Lepier A, Dudel J. (2000) Activation of rat recombinant α(1)β(2)γ(2S) GABA(A) receptor by the insecticide ivermectin. *Eur J Pharmacol* **394**:163–170.

41. Khakh BS, Proctor WR, Dunwiddie TV, Labarca C, Lester HA. (1999) Allosteric control of gating and kinetics at P2X(4) receptor channels. *J Neurosci* **19**:7289–7299.

42. Krause RM, Buisson B, Bertrand S, Corringer PJ, Galzi JL, Changeux JP, Bertrand D. (1998) Ivermectin: a positive allosteric effector of the α7 neuronal nicotinic acetylcholine receptor. *Mol Pharmacol* **53**:283–294.

43. Shan Q, Haddrill JL, Lynch JW. (2001) Ivermectin, an unconventional agonist of the glycine receptor chloride channel. *J Biol Chem* **276**:12556–12564.

44. Huang SM, Bisogno T, Trevisani M, Al-Hayani A, De Petrocellis L, Fezza F, Tognetto M, Petros TJ, Krey JF, Chu CJ, Miller JD, Davies SN, Geppetti P, Walker JM, Di Marzo V. (2002) An endogenous capsaicin-like substance with high potency at recombinant and native vanilloid VR1 receptors. *Proc Natl Acad Sci U S A* **99**:8400–8405.

45. Smart D, Gunthorpe MJ, Jerman JC, Nasir S, Gray J, Muir AI, Chambers JK, Randall AD, Davis JB. (2000) The endogenous lipid anandamide is a full agonist at the human vanilloid receptor (hVR1). *Br J Pharmacol* **129**:227–230.

46. Wehr M, Hostick U, Kyweriga M, Tan A, Weible AP, Wu H, Wu W, Callaway EM, Kentros C. (2009) Transgenic silencing of neurons in the mammalian brain by expression of the allatostatin receptor (AlstR). *J Neurophysiol* **102**:2554–2562.

47. Jalink K, Moolenaar WH. (2010) G protein-coupled receptors: the inside story. *Bioessays* **32**:13–16.

48. Bouzat C, Bartos M, Corradi J, Sine SM. (2008) The interface between extracellular and transmembrane domains of homomeric Cys-loop receptors governs open-channel lifetime and rate of desensitization. *J Neurosci* **28**:7808–7819.

49. Giniatullin R, Nistri A, Yakel JL. (2005) Desensitization of nicotinic ACh receptors: shaping cholinergic signaling. *Trends Neurosci* **28**:371–378.

50. Gunthorpe MJ, Peters JA, Gill CH, Lambert JJ, Lummis SC. (2000) The 4'lysine in the putative channel lining domain affects desensitization but not the single-channel conductance of recombinant homomeric 5-HT3A receptors. *J Physiol* **522 Pt 2**:187–198.

51. Hu XQ, Sun H, Peoples RW, Hong R, Zhang L. (2006) An interaction involving an arginine residue in the cytoplasmic domain of the 5-HT3A receptor contributes to receptor desensitization mechanism. *J Biol Chem* **281**:21781–21788.

52. Mohapatra DP, Nau C. (2003) Desensitization of capsaicin-activated currents in the vanilloid receptor TRPV1 is decreased by the cyclic AMP-dependent protein kinase pathway. *J Biol Chem* **278**:50080–50090.

53. Bhave G, Zhu W, Wang H, Brasier DJ, Oxford GS, Gereau RWt. (2002) cAMP-dependent protein kinase regulates desensitization of the capsaicin receptor (VR1) by direct phosphorylation. *Neuron* **35**:721–731.

54. Bunemann M, Hosey MM. (1999) G-protein coupled receptor kinases as modulators of G-protein signalling. *J Physiol* **517 (Pt 1)**:5–23.

55. Scearce-Levie K, Lieberman MD, Elliott HH, Conklin BR. (2005) Engineered G protein coupled receptors reveal independent regulation of internalization, desensitization and acute signaling. *BMC Biol* **3**:3.

56. Tan W, Janczewski WA, Yang P, Shao XM, Callaway EM, Feldman JL. (2008) Silencing preBotzinger complex somatostatin-expressing neurons induces persistent apnea in awake rat. *Nat Neurosci* **11**:538–540.

57. Gosgnach S, Lanuza GM, Butt SJ, Saueressig H, Zhang Y, Velasquez T, Riethmacher D, Callaway EM, Kiehn O, Goulding M. (2006) V1 spinal neurons regulate the speed of vertebrate locomotor outputs. *Nature* **440**:215–219.

58. Zhang Y, Narayan S, Geiman E, Lanuza GM, Velasquez T, Shanks B, Akay T, Dyck J, Pearson K, Gosgnach S, Fan CM, Goulding M. (2008) V3 spinal neurons establish a robust and balanced locomotor rhythm during walking. *Neuron* **60**:84–96.

59. Ferguson SM, Eskenazi D, Ishikawa M, Wanat MJ, Phillips PE, Dong Y, Roth BL, Neumaier JF. (2011) Transient neuronal inhibition reveals opposing roles of indirect and direct pathways in sensitization. *Nat Neurosci* **14**:22–24.

60. Garner AR, Rowland DC, Hwang SY, Baumgaertel K, Roth BL, Kentros C, Mayford M. (2012) Generation of a synthetic memory trace. *Science* **335**:1513–1516.

61. Krashes MJ, Koda S, Ye C, Rogan SC, Adams AC, Cusher DS, Maratos-Flier E, Roth BL, Lowell BB. (2011) Rapid, reversible activation of AgRP neurons drives feeding behavior in mice. *J Clin Invest* **121**:1424–1428.

62. Sasaki K, Suzuki M, Mieda M, Tsujino N, Roth B, Sakurai T. (2011) Pharmacogenetic modulation of orexin neurons alters sleep/wakefulness states in mice. *PLoS One* **6**:e20360.

63. Kruse AC, Hu J, Pan AC, Arlow DH, Rosenbaum DM, Rosemond E, Green HF, Liu T, Chae PS, Dror RO, Shaw DE, Weis WI, Wess J, Kobilka BK. (2012) Structure and dynamics of the M3 muscarinic acetylcholine receptor. *Nature* **482**:552–556.

64. Hibbs RE, Gouaux E. (2011) Principles of activation and permeation in an anion-selective Cys-loop receptor. *Nature* **474**:54–60.

65. White S. (2012) Membrane Proteins of Known 3D Structure. http://blanco.biomol.uci.edu/mpstruc/listAll/list

66. Guntas G, Mansell TJ, Kim JR, Ostermeier M. (2005) Directed evolution of protein switches and their application to the creation of ligand-binding proteins. *Proc Natl Acad Sci U S A* **102**:11224–11229.

67. Romero PA, Arnold FH. (2009) Exploring protein fitness landscapes by directed evolution. *Nat Rev Mol Cell Biol* **10**:866–876.

68. Minor DL, Jr. (2009) Searching for interesting channels: pairing selection and molecular evolution methods to study ion channel structure and function. *Mol Biosyst* **5**:802–810.

69. Carbone MN, Arnold FH. (2007) Engineering by homologous recombination: exploring sequence and function within a conserved fold. *Curr Opin Struct Biol* **17**:454–459.

Chapter 3

Mutation of a Highly Conserved Pore-Lining Leucine Residue Increases Agonist Sensitivity of GluCl

Abstract

The glutamate-gated chloride channel (GluCl) is an invertebrate, ligand-gated anion channel of the Cys-loop receptor family. It is activated by the endogenous neurotransmitter glutamate and by the antiparasitic drug ivermectin (IVM). A crystal structure of the *Caenorhabditis elegans* GluCl α homopentamer shows the location of the glutamate binding site, the separate ivermectin binding site, and the highly conserved leucine residue at the 9' position of the pore-lining M2 transmembrane domain. Mutation of this L9' residue in other Cys-loop receptors dramatically increases agonist sensitivity. Using whole-cell patch clamp, we found that six of seven mutations (L9'S, A, F, I, T, V, but not G) at this position in the α subunit increased the glutamate sensitivity of the heteromeric GluCl αβ channel by factors of 5- to 90-fold. Beta-branched amino acids (Ile, Thr, Val) gave the greatest reductions in EC_{50}. Analysis of side chain properties revealed that helix-destabilizing energy correlated with increased glutamate sensitivity. Many L9' mutations also increased background conductance, suggesting a higher probability of unliganded openings. Only one mutation, L9'F, resulted in increased glutamate sensitivity without increasing spontaneous activity. A fluorescent membrane potential assay confirmed that the L9'F mutation also increased IVM sensitivity. In addition, it was determined that GluCl α homomers indeed form functional, IVM-sensitive channels in mammalian systems. However, GluCl α homomers bearing a L9'F mutation do not show increased sensitivity to IVM, implying incorporation of the β subunit is necessary for the gain-of-function effect. Increasing GluCl sensitivity to ivermectin will benefit its use as a neuronal silencing tool.

Introduction

Ion channel receptors of the Cys-loop superfamily are known to mediate fast-synaptic transmission in vertebrate and invertebrate nervous systems. Vertebrate receptors include the nicotinic acetylcholine (nAChR), serotonin (5-HT_3R), γ-aminobutyric acid type A and C ($GABA_{A/C}$R), glycine (GlyR), and zinc-activated (ZAC) receptors. Invertebrate receptors include a variation of channels gated by these same neurotransmitters in addition to others gated by glutamate (GluCl), histamine (HisCl), tyramine (LGC-55), and pH (pHCl, SsCl). Each class of receptors is comprised of a variety of species-specific subunits, capable of forming receptor subtypes with different functional properties. Each individual Cys-loop receptor is a pentameric complex, with five subunits symmetrically arranged around a central ion-conducting pore. Receptor subtypes are typically heteromeric, however subunits of some receptor classes can form functional and physiologically relevant homomers. All subunits share a common topology composed of a large N-terminal extracellular domain, four helical transmembrane domains (M1–M4), and a variable intracellular loop (M3–M4 loop). The helical M2 domain of each subunit lines the channel pore. Activation of Cys-loop receptors by their respective neurotransmitter gates the entry and/or exit of specific ions through this pore, resulting in a change in membrane potential.

The glutamate-gated chloride (GluCl) channel is an invertebrate Cys-loop receptor with a distinct pharmacological profile. GluCl chloride currents are gated by the traditional neurotransmitter glutamate and the semi-synthetic anthelmintic drug ivermectin (IVM). A 3.3-Å-resolution crystal structure of a modified homomeric GluCl channel reveals the binding site locations for each of these agonists (Figure 3-1A, B)[1].

Glutamate binds at the classical neurotransmitter binding site located in the extracellular domain at the interface of two subunits. Ivermectin binds at a separate, unconventional site, inserting at the upper periphery of the transmembrane helices also at the interface of two adjacent subunits. Structural coordinates of the channel represent an open-pore conformation with the side-chains of pore-lining residues clearly defined (Figure 3-1C, D). One pore-lining residue, leucine 9' (L9'), resides in the middle of the M2 transmembrane domain. L9' is highly conserved among subunits of the Cys-loop receptor family and has been proposed to serve as a hydrophobic channel gate (Figure 3-1E, F)[2-4].

Many studies using various Cys-loop receptors have shown that mutation of L9' to one of several other residues can dramatically increase agonist sensitivity, apparent by a leftward shift in the dose-response curve, allowing channel activation with lower concentrations of agonist[5-13]. Increases in agonist sensitivity have been attributed to effects on channel gating resulting in longer open channel dwell times[5,6,10,11,14]. Other 9' mutational effects have also been described including slowed apparent desensitization[5-8,11,12] and increased spontaneous activity. Spontaneous activity has been indicated by both a large resting conductance that is sensitive to open pore blockers[9,12,14-17] as well as single channel events observed in the absence of agonist[5,14,17]. L9' mutations may also render some partial agonists as full agonists[18] or even convert an antagonist into an agonist[19]. In contrast, some L9' mutant studies have shown no increase in agonist sensitivity[8,16,20,21], no increase in spontaneous activity[16,20], or no blockade of a large resting conductance with specific channel blockers[21] for a selection of L9' mutations. These inconsistencies could be due, in part, to the assortment of amino acids substituted into the L9' position. For example, it has been consistently reported that polarity of the amino acid mutation

influences the gain in agonist sensitivity for several cationic receptors, with more polar amino acids showing a greater reduction in EC_{50} for the muscle type nAChRs[10,11], neuronal α7 nAChRs[7], and 5-HT_3Rs[8]. Aside from this, no other correlations between the functional behavior displayed by L9' mutant receptors, (e.g., cationic versus anionic, heteromeric versus homomeric) and the identity of the amino acid substitution have been determined.

The current study investigates the effect of seven different L9' mutations in the *Caenorhabditis elegans* GluCl receptor. Mutational effects are examined by assaying electrophysiological responses in the presence and absence of agonist as well as changes in membrane potential using a voltage-sensitive fluorescent dye. The L9' gain-of-function effect has been examined exclusively using traditional neurotransmitter agonists. It is unclear whether an L9' mutation would enable a similar increase in sensitivity for an agonist activating the channel at a different binding site location on the receptor, such as IVM. An L9' mutation that allows GluCl to be activated by a lower concentration of IVM would be beneficial toward the application of GluCl/IVM as an electrical silencing tool in mammalian neuronal circuitry studies[22,23].

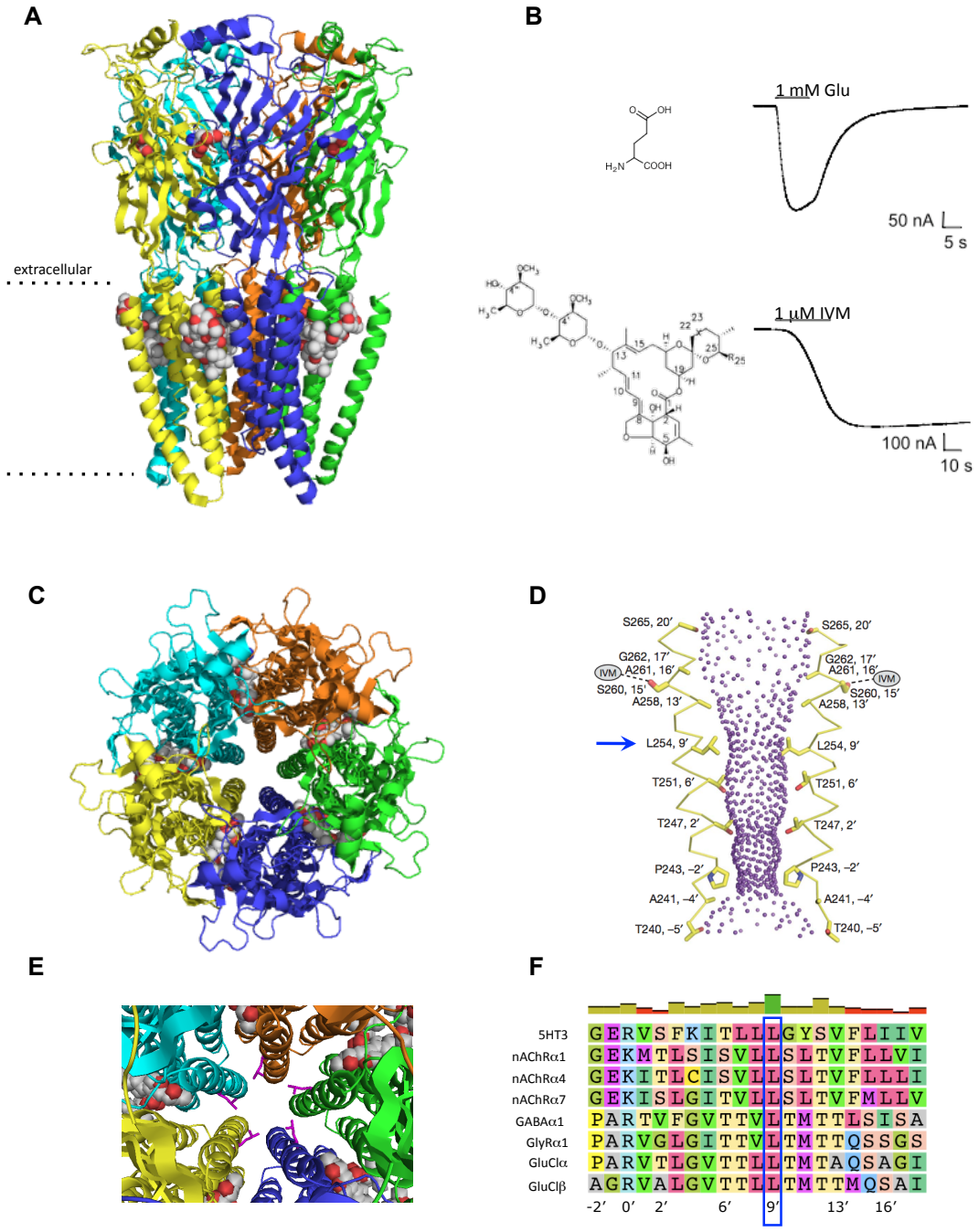

Figure 3-1. The GluCl channel. *A.* Crystal structure (side view) of a modified GluCl α homomeric channel with glutamate and IVM molecules bound (3RIF.pdb). Agonists bind at subunit interfaces; glutamate binds in the extracellular domain, IVM binds at the top half of the transmembrane domain. *B.* GluCl is differentially activated by glutamate and IVM. Electrophysiological traces were obtained from heteromeric GluCl αβ channels expressed in *Xenopus* oocytes (figure adapted from Li et al., 2002[24]). *C.* Top view of the GluCl channel showing symmetrical arrangement of subunits forming the pore. *D, E, & F.* Residues of the helical pore-lining M2 domain. Leucine 9' is a highly conserved pore-lining residue. (Figure *D.* adapted from Hibbs & Gouaux, 2011.)[1]

Results

L9' mutations increase glutamate sensitivity

The highly conserved leucine 9' residue in the M2 domain of the α subunit was mutated to each of seven other residues, L9'I, F, V, A, G, S, T. The heteromeric GluCl αβ wild-type (WT), fluorescently tagged (WT-XFP), and L9' mutant channels (also -XFP tagged) were expressed in HEK293 cells and examined for glutamate sensitivity using the millisecond microperfusion capability of the Dynaflow Pro II chip. Whole-cell concentration-response relations were obtained. Each patched cell was exposed to at least seven glutamate concentrations applied in increasing order. One-second glutamate applications induced fast-activating current responses followed by complete ligand washout upon bath solution postapplication (Figure 3-2A). Currents were activated in a concentration-dependent manner. Normalized concentration-response curves and Hill fit parameters are shown in Figure 3-2B and Table 3-1. A saturating dose was unable to be applied in some cases, as pre-exposure of glutamate, which accumulates in the cell reservoir from the lanes of laminar flow over time, appeared to desensitize receptors leading to reduced or undetected current responses. Response normalization to a less-than-saturating concentration, as is the case for the WT and L9'G mutant receptors, leads to an overestimation of glutamate sensitivity (i.e., a lower, inaccurate estimation of EC_{50}). All other L9' mutations significantly increased glutamate sensitivity by a factor of 5- to 90-fold, as determined by EC_{50}, compared to the WT-XFP receptor (Figures 3-2C; Table 3-1). Maximum current responses for the L9' mutant channels, however, were significantly reduced (Figure 3-2D). In addition, many cells expressing L9' mutant channels revealed a large holding current prior to application of glutamate, which was

often predictable by a lack of capacitive transients in whole-cell configuration. Such observations are characteristic of membrane leakiness, presuming the cells maintained seal resistance and were not sick or dead. Leak currents are likely due to an increased probability of unliganded channel openings resulting from the L9' mutation.

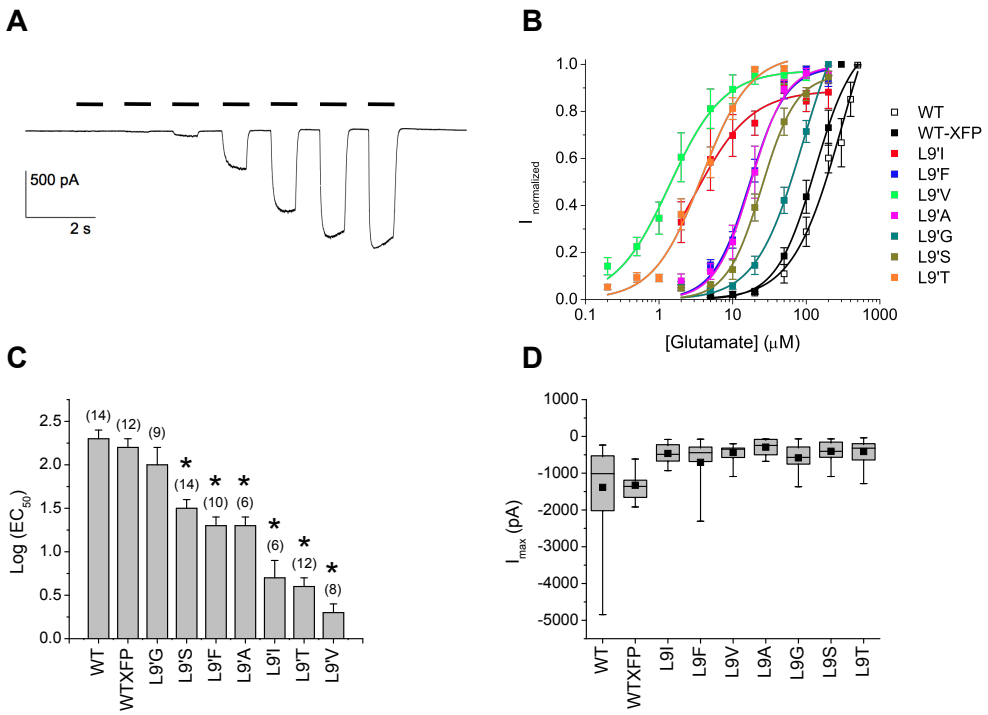

Figure 3-2. Glutamate activation of heteromeric GluCl αβ wild-type (WT), fluorescently tagged (WT-XFP), and L9' mutant channels. *A.* Whole-cell patch clamp recording of glutamate-induced current from the WT receptor expressed in HEK293 cells. Black bars indicate 1-second applications of 5, 10, 20, 50, 100, 200, and 500 μM glutamate. *B.* Glutamate concentration-response curves fit with the Hill equation. *C.* All 9' mutant channels except L9'G significantly increased glutamate sensitivity. *D.* Maximum induced current (I_{max}) from glutamate activation. Current magnitudes are represented as negative values.

GluCl channel	abbr.	EC_{50} (μM)	Hill	n
α(WT) + β(WT)	WT	314 ± 133*	1.28 ± 0.23	14
α-YFP + β-CFP	WT-XFP	132 ± 5	1.64 ± 0.07	12
β(WT) homomer		NR		
α-YFP L9'V homomer		NR		
α-YFP L9'I + β-CFP	L9'I	3.0 ± 0.4	1.13 ± 0.23	6
α-YFP L9'F + β-CFP	L9'F	17.0 ± 1.8	1.75 ± 0.27	10
α-YFP L9'V + β-CFP	L9'V	1.4 ± 0.1	1.18 ± 0.11	8
α-YFP L9'A + β-CFP	L9'A	17.7 ± 1.6	1.79 ± 0.24	6
α-YFP L9'G + β-CFP	L9'G	91.8 ± 17.1*	1.34 ± 0.14	9
α-YFP L9'S + β-CFP	L9'S	24.9 ± 1.7	1.84 ± 0.17	14
α-YFP L9'T + β-CFP	L9'T	3.8 ± 0.6	1.32 ± 0.18	12

Table 3-1. Glutamate activation parameters of GluCl WT, WT-XFP, and L9' mutant channels. Parameters correspond to concentration-response curves in Figure 3-2B. The EC_{50} and Hill coefficient values represent the mean ± SEM for the number of cells (n) recorded. The * indicates response normalization to a less-than-saturating maximum concentration.

Functional studies of GluCl receptors expressed in *Xenopus laevis* oocytes using two-electrode voltage clamp have demonstrated that homomeric channels of both α and β subunits are functional, but they exhibit contrasting agonist activation profiles. Homomeric GluCl α channels are activated directly by IVM, but not glutamate, while homomeric GluCl β channels are activated directly by glutamate, but not IVM[25]. It has since been determined that α homomers do in fact maintain glutamate binding sites, but are deficient in coupling glutamate binding events to channel gating[1,26]. In the present study, no glutamate-induced currents were recorded from HEK293 cells transfected with GluCl β(WT) cDNA only, probably because homomeric GluCl β channels are not expressed at the plasma membrane. Discrepancies in surface expression between mammalian systems and oocytes have been observed for other membrane proteins and are assumed to be the result of different protein trafficking mechanisms[27-30]. The

possibility that presence of an L9' mutation now allowed GluCl α homomers to be gated by glutamate was also considered. No currents were recorded from the L9'V α homomer for the glutamate concentrations applied (≤ 500 μM).

Whole-cell glutamate concentration-response relations for a given receptor were subject to a great deal of cell-to-cell variability. Different cells recorded on the same day, from the same culture dish, using the same glutamate solutions, displayed very different concentration-dependent responses, even for the WT receptor (Figure 3-3A). Desensitization kinetics also varied greatly from cell-to-cell. To examine this variability, concentration-response curves for individual cells were compared. Individual response curves could be separated into distinct categories based on sensitivity (Figure 3-3B, Table 3-2). This wide range in agonist sensitivity was evident with all L9' mutants except for L9'F (Figure 3-3C, Table 3-2). Typically, heteromeric receptor expression that gives rise to multiple agonist sensitivities is due to the presence of different stoichiometric populations which result in biphasic concentration-response relations[31-33]. It is assumed that an individual cell would express some fraction of each receptor stoichiometry. Interestingly, for GluCl, most individual cells display a monophasic concentration-response relationship. It is unclear whether the various glutamate sensitivities are due to stoichiometric preferences or some other inherent inconsistencies (e.g., cross-contamination, phenotypic diversity) within HEK293 cell cultures[34,35].

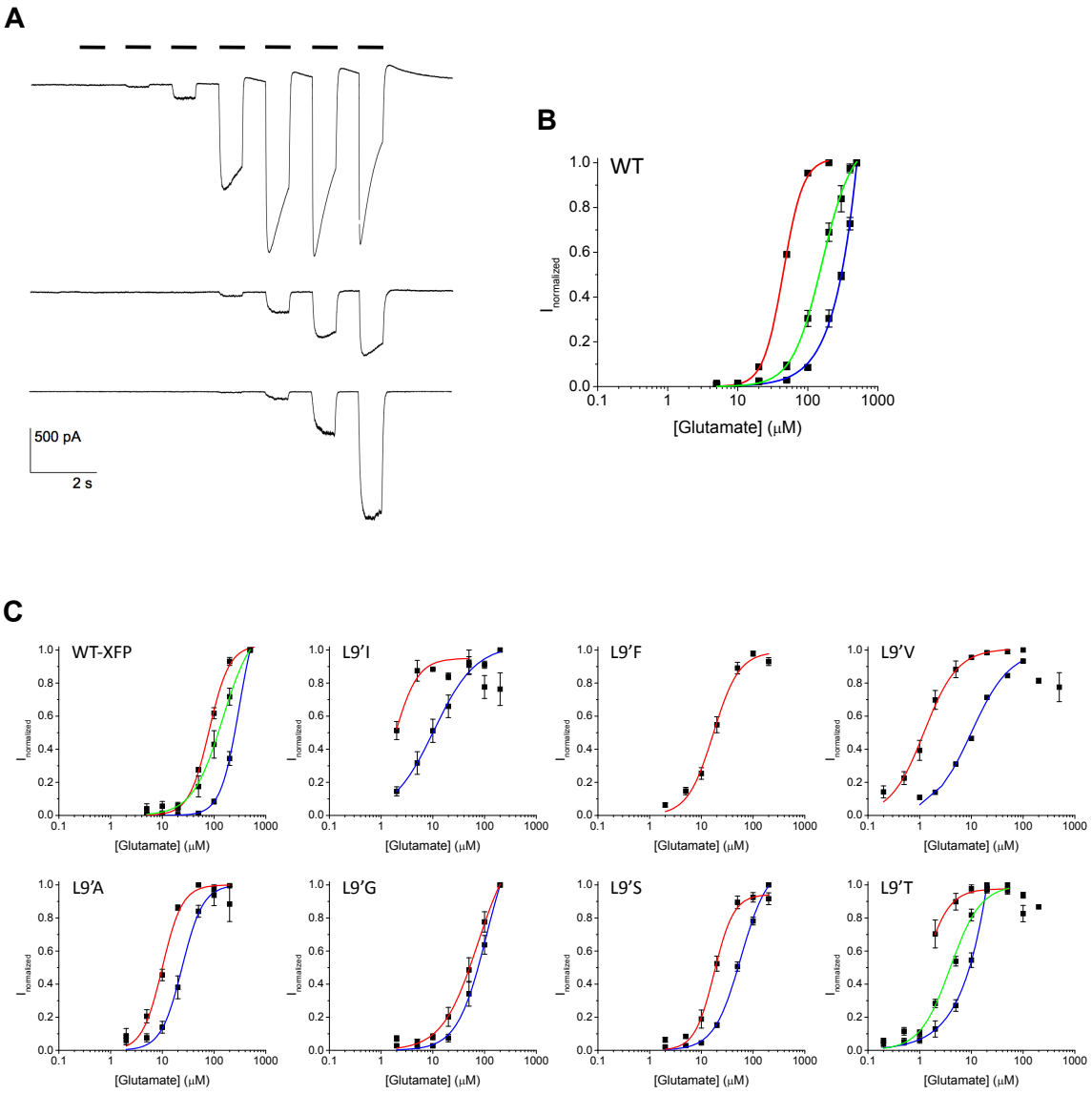

Figure 3-3. Cell-to-cell variability of glutamate concentration-response relations. *A.* Cells expressing GluCl WT receptor recorded on the same day, from the same culture dish, responded differently to application of the same glutamate solutions (see Figure 3-2 for concentrations). *B.* Concentration response curves of individual cells could be separated into three categories: high sensitivity (red line), low sensitivity (blue line), and mixed (green line). *C.* Cell-to-cell variability was observed for nearly all mutant receptors tested.

	High Sensitivity			Mixed			Low Sensitivity		
	EC_{50} (μM)	Hill	n	EC_{50} (μM)	Hill	n	EC_{50} (μM)	Hill	n
WT	44.71 ± 0.00	3.05 ± 0.17	1	159.65 ± 0.01	2.03 ± 0.12	9	2564.9 ± 3.98*	1.45 ± 0.15	4
WT-XFP	80.68 ± 0.00	2.22 ± 0.13	6	145.91 ± 0.02	1.49 ± 0.16	3	306.90 ± 0.01*	2.41 ± 0.09	3
αL9'I	1.80 ± 0.00*	1.91 ± 0.67	3				10.57 ± 0.00	1.08 ± 0.12	3
αL9'F	17.25 ± 0.00	1.75 ± 0.17	10						
αL9'V	1.22 ± 0.00	1.34 ± 0.15	7				9.95 ± 0.00	1.17 ± 0.11	1
αL9'A	9.99 ± 0.00	2.25 ± 0.30	4				24.04 ± 0.00	2.13 ± 0.25	2
αL9'G	74.14 ± 0.02	1.26 ± 0.16	5				108.86 ± 0.02*	1.54 ± 0.16	4
αL9'S	17.76 ± 0.00	2.29 ± 0.34	9				58.13 ± 0.00	1.67 ± 0.11	5
αL9'T	1.19 ± 0.00*	1.81 ± 0.39	3	3.91 ± 0.00	1.48 ± 0.16	7	500.12 ± 2.48*	0.92 ± 0.11	2

Table 3-2. Variability in glutamate activation parameters for heteromeric GluCl αβ WT, WT-XFP, and L9' mutant channels. Parameters correspond to concentration-response curves in Figure 3-3B, C. The EC_{50} and Hill coefficient values represent the mean ± SEM for the number of cells (n) recorded. The * indicates response normalization to a less-than-saturating maximum concentration.

L9' mutational effect on EC_{50} correlates with alpha-helical destabilization

Studies involving the cation-selective Cys-loop receptors suggest the magnitude of increased agonist sensitivity was influenced by the polarity of the L9' mutation[8,10,11]. To check for a correlation between the identity of the amino acid mutation and the magnitude of increased agonist sensitivity, the log(EC_{50}) value of each L9' mutant channel was plotted against several physical properties of the amino acid side-chain, including hydrophobicity[36], surface area[37], and propensity towards α-helix stabilization[38]. GluCl L9' mutations show no functional relationship dependent on side-chain hydrophobicity or side-chain surface area (Figure 3-4A, B). A potential trend in surface area is negated by the fact that Leu and Ile have nearly the same surface area (180 $Å^2$ vs. 182 $Å^2$) but give very different EC_{50} values. There does appear to be a correlation between the identity of the L9' mutant side-chain and its effect on α-helix stabilization (Figure 3-4C). Excluding the two extremes of Ala, the amino acid with the highest helical

propensity[39,40], and Gly, which is given a value of zero on most scales as it lacks a contributing side-chain, the energy values associated with disrupting the stability of the pore-lining α-helix do trend with the shifts in EC_{50}. The less stable the helix (higher energy), the more sensitive the receptor is to glutamate (lower EC_{50}). The three β-branched amino acids, Ile, Val, and Thr, give the largest gain-of-function shifts in EC_{50} for the L9' mutant channels. β-branched amino acids are known to destabilize an α-helix due to a loss of side chain conformational entropy[41-43]. Specifically, the rotational freedom of a β-branched side-chain is restricted by steric hindrance, in that substituents in a γ-position of the side chain interfere with the carbonyl oxygen atoms of the residues *i* – 2 and *i* – 3 in the helix. Overall, destabilization of the M2 pore-lining α-helix at the L9' position may lower the energy barrier for the closed-to-open conformational change making it easier for the channel to open in the presence of agonist.

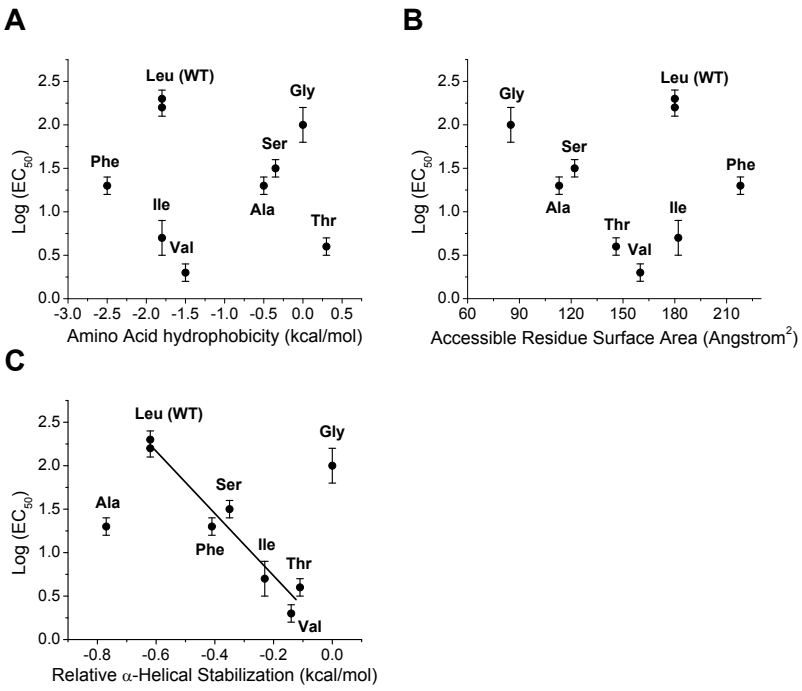

Figure 3-4. Functional relationships of L9' mutant channels with physical properties of amino acid mutation. *A & B.* The L9' gain-of-function effect is not dependent on side-chain hydrophobicity or side-chain surface area. *C.* The L9' gain-of-function effect does correlate with side-chain disruption of an α-helical conformation. Ala and Gly residues are considered outliers. Line represents a linear regression fit of the seven other data points. Two data points for Leu represent those for the WT and WT-XFP receptors.

L9' mutations increase background conductance

Destabilization of the pore-lining helix may also be responsible for the large holding currents and lack of whole-cell transients observed prior to glutamate application. A more flexible gate could increase the probability of spontaneous channel openings which would contribute to the background conductance of a cell at rest. The presence of spontaneous channel activity is often confirmed by the use of open-channel blockers in the absence of agonist. Picrotoxin and fipronil sulfone are known pore blockers of GluCl[44,45]. However, they have both been reported to exhibit differential blocking effects

on the desensitizing and nondesensitizing components of glutamate evoked currents, presumably due to differences in subunit stoichiometry[46-49]. It has also been demonstrated in several studies that the typical blocking mechanism of picrotoxin is impaired with both agonist activated and spontaneously open receptors bearing L9' mutations[9,16,21]. Therefore, the use of pore blockers is not practical for assaying the amount of background conductance for the various GluCl L9' mutant channels. Instead, a voltage ramp protocol was adopted[50].

Cells were voltage clamped in whole-cell configuration with no capacitive compensation. The voltage was ramped continuously from −60 mV to +60 mV over 50 ms in the absence of ligand. An example of a WT current response is shown in Figure 3-5A. The background conductance was measured from the slope of the resistive current ramp and normalized by the mean membrane capacitance of each receptor, which could be calculated from the capacitive current offset. Because it can be difficult to distinguish between cells with a leaky membrane and patches with a poor seal, cells with a seal resistance less than 40 MΩ, corresponding to a chord conductance of > 25 nS, were omitted. GluCl WT and WT-XFP receptors show minimal background conductance that is not different from a mock-transfected control (Figure 3-5B). The two L9' mutations with the smallest side-chains, L9'A and L9'G, had the largest background conductance which was significantly different from WT receptors. Notably, these are the same two L9' mutants that were not in accordance with the disruption of α-helical stability correlation. The three L9' mutants with β-branched side-chains did have a greater background conductance than WT receptors on average, but the increase was not statistically significant for the number of cells sampled.

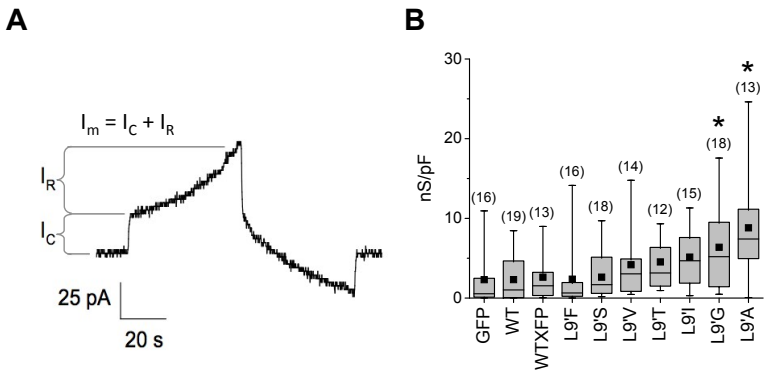

Figure 3-5. Background conductance of GluCl receptors in absence of ligand. *A*. Example of a current response from GluCl WT. Whole-cell voltage-clamped cells with no capacitive compensation were ramped from −60 mV to +60 mV over 50 ms. The total current across the membrane I_m is the sum of the capacitive current I_c, and the resistive current, I_R. *B.* Background conductance normalized by the mean capacitance of each receptor for the number of cells recorded (shown in parentheses). Soluble GFP was used as a mock-transfection control.

The L9' gain-of-function effect is maintained for IVM

It was unknown whether an L9' mutation would maintain a gain-of-function gating effect for an agonist that activates the channel through a different allosteric mechanism (e.g., IVM) than that triggered by a typical neurotransmitter binding event (e.g., glutamate). Assaying channel function with IVM by electrophysiology, however, is challenging. IVM is a lipophilic compound with limited ligand washout, making it difficult to apply successive doses to an individual cell which is necessary for concentration-response normalization. To circumvent this, L9' mutant receptor activation was measured by a fluorescence-based assay using a membrane potential-sensitive dye.

Glutamate activation and IVM activation were first measured individually for GluCl WT channels. Even with this indirect functional assay, different response kinetics

were apparent for the two agonists, resembling the differences observed in their direct electrophysiological response[25]. Specifically, the raw signal (in relative fluorescence units, RFU) induced by glutamate reaches a maximum within 3 min, followed by a decline for nonsaturating concentrations. The IVM-induced signal is slower to rise but remains at maximum for up to 5 min (Figure 3-6A). Both glutamate and IVM generated fluorescent signals for GluCl WT and WT-XFP receptors in a concentration-dependent manner (Figure 3-6B). All L9' mutants, except for L9'F, displayed a much weaker signal for both glutamate and IVM activation (Figure 3-6C). The reduced signal results from elevated baseline fluorescence (Figure 3-6D) which is likely a reflection of the increased background conductance observed for these mutants. Normalization of the raw RFU signal indicates that the L9'F mutation increases receptor sensitivity to both glutamate and IVM compared to WT and WT-XFP receptors (Figure 3-6E). Glutamate activation parameters are comparable to those obtained by electrophysiology (Table 3-3). IVM activation parameters reveal that WT-XFP receptors do not have the same concentration-dependent relationship as WT receptors, and the L9'F mutant receptor displays a biphasic concentration-dependent response.

Homomeric channels were assayed once more for agonist activation using the membrane potential dye. As expected, GluCl α(WT) homomers were not activated by glutamate. GluCl α(WT) homomers were, however, responsive to IVM (Figure 3-7). This was unexpected as previous studies report that no current was obtained from mammalian cells when the α subunit was expressed alone[23,51]. GluCl α-XFP homomers, as well as those containing the L9'F mutation were also responsive, producing much steeper and right-shifted concentration-response curves for IVM (Table 3-4). Removal of the XFP tag

from the L9'F mutant channel did not recover IVM sensitivity. This implies two things: (1) that the XFP insertion is having some functional effect on GluCl activation by IVM that was not apparent with glutamate, and (2) that incorporation of the β subunit is necessary for the increased IVM sensitivity observed with the heteromeric GluCl L9'F mutant. GluCl β(WT) homomers did not respond to glutamate or IVM applications.

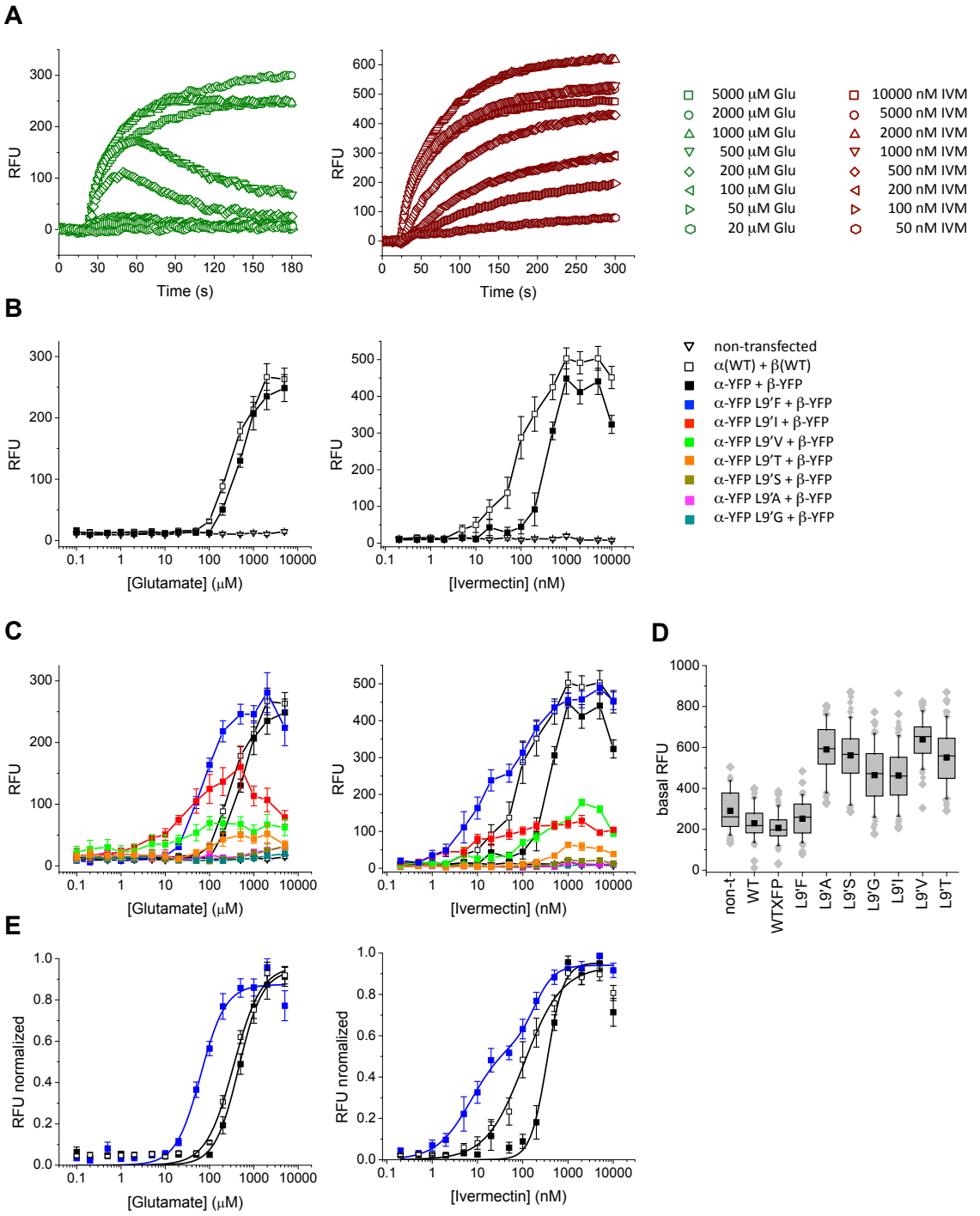

Figure 3-6. Heteromeric GluCl αβ WT, WT-XFP, and L9' mutant receptor activation measured by a fluorescent membrane potential-sensitive dye. *(Left panel: glutamate activation; Right panel: IVM activation) A*. Example of raw RFU signal for GluCl WT (8 of 15 responses shown). *B.* RFU signals for GluCl WT and WT-XFP are concentration-dependent. Nontransfected cells do not respond to agonist. *C & D.* All L9' mutants receptors, except for L9'F, show diminished agonist-induced RFU signals and elevated baseline RFU signals. *E.* Normalized concentration-response curves for GluCl WT, WT-XFP, and L9'F mutant receptors. The concentration-response relation for IVM activation of the L9'F mutant was best fit by the sum of two Hill equations.

	Glu activation		*IVM activation*	
GluCl channel	**EC_{50} (μM)**	**Hill**	**EC_{50} (nM)**	**Hill**
α(WT) + β(WT)	349.00 ± 44.29	1.40 ± 0.18	138.45 ± 9.60	1.04 ± 0.06
α-YFP + β-YFP	455.80 ± 53.14	1.62 ± 0.23	342.64 ± 31.52	2.41 ± 0.39
α-YFP L9'F + β-YFP	63.07 ± 7.12	1.55 ± 0.24	7.27 ± 2.85 *(61%)*	1.14 ± 0.24
			185.35 ± 50.16	1.99 ± 0.82

Table 3-3. Activation parameters acquired with the membrane potential assay for heteromeric GluCl αβ WT, WT-XFP, and L9'F mutant channels. Parameters correspond to concentration-response curves in Figure 3-6E. The EC_{50} and Hill coefficient values represent the mean ± SEM for six measurements. The high sensitivity component of the biphasic L9'F curve corresponds to 61% of the normalized response.

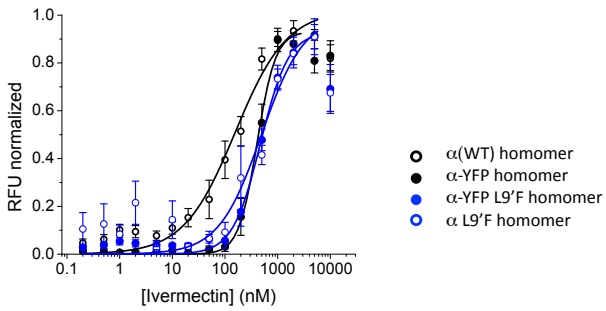

Figure 3-7. Ivermectin activation of homomeric GluCl α WT, WT-XFP, and L9'F mutant channels. Normalized concentration-response curves were fit with the Hill equation.

	IVM activation	
GluCl channel	**EC_{50} (nM)**	**Hill**
α(WT) homomer	285.51 ± 75.17	1.01 ± 0.15
α-YFP homomer	406.88 ± 21.08	2.47 ± 0.24
α-YFP L9'F homomer	472.67 ± 44.23	1.64 ± 0.19
α L9'F homomer	492.99 ± 95.91	1.07 ± 0.20

Table 3-4. Ivermectin activation parameters for homomeric GluCl α WT, WT-XFP, and L9'F mutant channels. Parameters correspond to concentration-response curves in Figure 3-7. The EC_{50} and Hill coefficient values represent the mean ± SEM for six measurements.

Discussion

L9' effects

Mutational effects of L9' have varied across the family of Cys-loop receptors and are dependent on the physical properties of the amino acid being introduced. Even the slightest differences are likely to have big functional consequences in such a critical region of the channel. For GluCl, six of seven L9' mutations significantly increased glutamate sensitivity, and not all of the L9' mutants show increased spontaneous activity. This is the first report of a correlation between pore-lining helix stability and agonist sensitivity. According to the Monod-Wyman-Changeux (MWC) model of allosteric activation[52], channel gating (i.e., events that enable the closed-to-open state transitions) involves global conformational changes within and across subunits. Destabilization of the M2 α-helix by β-branched amino acids may lower the energy barrier for a closed-to-open conformational change making it easier for the channel to open both in the presence (apparent from the left-shifted EC_{50}) and absence (apparent from the increased background conductance) of agonist. However, the L9'A mutant, which should form the most stable pore-lining helix, actually shows the greatest increase in background conductance. It may be that the 9' position requires a large, hydrophobic, non-β-branched side-chain to stabilize the closed state conformation. Whether or not the L9' residue prevents ion flow by physically occluding the channel pore cannot be determined from this study.

Variability from cell-to-cell during the electrophysiology experiments made it difficult to draw conclusions about any L9' mutational effects on receptor desensitization.

In general, it appeared that high sensitivity glutamate responses for all receptors showed more desensitization. This may also be reflected in the raw glutamate-induced signals of the membrane potential assays (Figure 3-6A, left panel). For example, signal responses for low concentrations, which would activate high sensitivity channels, show a decline after the first minute of glutamate application. As higher concentrations are applied low sensitivity channels, which do not desensitize, would become activated so the signal no longer declines over time.

Stoichiometry

There is some evidence for the co-existence of two pharmacologically distinct and physiologically relevant GluCl channels. Invertebrate neuron recordings display glutamate-induced currents comprised of variable fractions of desensitizing and non-desensitizing components, which were blocked differentially by picrotoxin and fipronil sulfone[46-49]. These differential pore-blocking effects may be explained by a subunit specific dependence of blockade[44], suggesting the presence of more than one GluCl stoichiometry.

The biphasic IVM concentration-response curve of the L9'F mutant in the membrane potential assay supports a mixed stoichiometry hypothesis. The glutamate concentration-response relation obtained for this mutant, however, is monophasic. Furthermore, the L9'F mutant was the only receptor that did not show variation in glutamate sensitivity during whole-cell patch-camp recordings. It is possible the 10 cells patched were not representative of the entire transiently transfected cell population.

While patch-clamp experiments directly sample individual cells, sample sets are small and can be biased by cell selection and sealing success of the experimenter. The membrane potential assay, on the other hand, is a population measurement. Any cell-to-cell variability is coalesced into a single composite response.

With expression of GluCl in HEK293 cells, glutamate activated currents are most likely conducted by heteromeric receptors, since β homomers are probably not expressed at the cell surface and α homomers are not directly gated by glutamate. It is conceivable that different receptor stoichiometries do not differ significantly in glutamate sensitivity, resulting in a concentration-dependence that is uninterrupted. The biphasic heteromeric and monophasic homomeric concentration-response curves for the L9'F mutant indicate that incorporation of the β subunit significantly increases IVM sensitivity. The precise stoichiometric ratio of α:β subunits cannot be determined from this functional study. It should also be noted that the number of bound IVM molecules required to gate the channel is unknown. It cannot be ruled out that the number of agonists bound could influence the biphasic concentration response.

Studies employing L9' mutations in all five subunits have shown that the extent of increased agonist sensitivity was dependent on the number of subunits containing L9' substitutions, i.e., the magnitude of EC_{50} shifts were additive[5,6,9,53]. It was consequently inferred that each subunit provides independent and equivalent contributions to channel gating. More detailed analysis of this mutagenesis data found that L9' effects of individual subunits are not identical, rather, the various subunits bearing L9' mutations contribute unequally to channel gating[10,14,18,20,53]. The gain-of-function effect of an L9' mutation appears to be influenced by the structurally asymmetric pore of a heteromeric

channel compared to the perfectly symmetrical pore geometry of homomers. The influence of asymmetry is especially apparent in the present study, as heteromeric channels bear L9' mutations only in the α subunit; the β subunit still contains Leu at this position. A ring of five L9'F mutations as in the α homomer does not increase sensitivity to IVM. Differences in constitutive activity between heteromeric and homomeric receptors have also been reported[20].

FlexStation assay limitations

In the membrane potential assay, the voltage sensitive dye partitions across the cell membrane depending on the resting membrane potential of the cell. Dye quenchers are present in the extracellular solution. Upon stimulus, the dye follows movement of positively charged ions, so membrane depolarization allows the dye to enter the cell where it is dequenched resulting in a positive fluorescent signal. Conversely, during hyperpolarization, dye is requenched as it exits the cell resulting in a negative fluorescent signal. The positive fluorescent signal observed in the present study following induction of Cl^- currents therefore seems counterintuitive. A similar result, however, has been observed and eloquently discussed for HEK293 cells expressing GlyR[54]. In short, as an embryonic cell line, HEK293 cells have a relatively high intracellular chloride concentration compared to other mammalian cells, so channel opening allows efflux, rather than influx, of Cl^- current thereby decreasing the separation of charge and resulting in depolarization of the membrane. Elevated basal levels of fluorescence and negligible agonist-induced responses were observed in a related GlyR study with receptors

containing other M2 domain mutations[55]. The authors propose constitutive activation as a possible explanation. The present study confirms that receptors with increased levels of spontaneous activity do show elevated basal signals and diminished responses to agonist application in a membrane potential assay. An increased background conductance likely affects distribution of the dye during the incubation period. The amount of de-quenched dye that has already entered the cell is high, so the amount of additional dye moving into the cell upon application of agonist is low. Since the assay only measures changes in membrane potential rather than inherent values, a diminished signal is observed.

L9'F as an optimized silencer

We have previously demonstrated that an engineered GluCl channel can be used to selectively silence electrical activity in targeted CNS neurons *in vivo* when activated by IVM. Both α and β subunits were necessary in order to achieve silencing. GluCl α homomers were reportedly not expressed. This study shows that α homomers are indeed expressed and that α-XFP homomers require greater concentrations of IVM for activation. Introduction of an L9'F mutation may promote β subunit incorporation as a method of increasing IVM sensitivity. Unlike other mutants, L9'F substantially increased agonist sensitivity without increasing background conductance, a fundamental requirement as spontaneous openings would be detrimental to the goal of a pharmacologically induced silencer. While all L9' mutants reduced the maximum glutamate response of patch-clamped cells, the fluorescent signal generated by L9'F mutants in the membrane potential assay was not diminished compared to WT receptors.

Nevertheless, HEK293 cells generally produce massive currents, so it is conceivable that the L9'F mutant receptor would conduct sufficient Cl^- current to silence a neuron. Altogether, introduction of an L9'F mutation may enhance the GluCl/IVM silencing tool.

Materials and Methods

Site-Directed Mutagenesis

Previously described plasmid vector pcDNA3.1/V5-His TOPO (Invitrogen #K4800-01) containing the complete optimized coding sequence for either unlabeled or fluorescently tagged *Caenorhabditis elegans* GluCl α and β subunits, namely optGluCl αWT, optGluCl βWT, optGluCl α-YFP, and optGluCl β-YFP[56], were used in this study. Note, 'opt' has been removed from the nomenclature in this text. Enhanced yellow fluorescent protein (YFP) insertions are located within the intracellular M3-M4 loop[24]. Leucine 9' mutations were made using the QuikChange II XL site-directed mutagenesis kit (Agilent Technologies #200522) with PfuTurbo DNA polymerase (Agilent Technologies #600250) using the following forward and reverse primers: 5' – CC CTG GGC GTG ACC ACC CTG xxx AC – 3' and 5' – GC GGA CTG AGC GGT CAT GGT xxx CA – 3', where 'xxx' delineates the mutated Leu9' codon. Leu9' mutations included Ile, Phe, Val, Ser, Thr, Ala, and Gly. All mutations were confirmed by DNA sequencing.

Cell Culture

Human embryonic kidney (HEK) 293 cells were purchased from ATCC (#CRL-1573). Cells were cultured in Dulbecco's modified Eagle's medium (DMEM; Gibco #11965) supplemented with 10% FBS (Gibco #26140), 100 units/ml penicillin, 100 μg/ml streptomycin (Gibco #15140), and 1 mM sodium pyruvate (Gibco #11360), and maintained at 37°C and 5% CO_2 in a humidified incubator. Cells were passaged when

confluent at a subcultivation ratio of 1:5 or 1:10 every 3 to 4 days. For electrophysiology experiments, HEK293 cells were plated at a density of 150,000 cells/dish in 35 mm culture dishes. GluCl receptors were expressed via transient transfection for which 1 µg DNA in 100 µl DMEM was combined with 4 µl ExpressFect (Denville Scientific #E2650) in 100 µl DMEM that was pre-incubated for 20 minutes before adding to culture dishes containing 2 ml fresh culture medium. For FlexStation assays, HEK293 cells were plated at 20,000 cells/well, with a plating volume of 100 µl/well, in a black-sided/clear-bottomed 96-well imaging plate (BD Falcon #353219). For transfection, 16 µg total DNA in 750 µl DMEM was mixed with 30 µl ExpressFect in 750 µl DMEM, pre-incubated for 20 minutes, and then added at 15 µl/well to cells containing 100 µl fresh culture media. For both electrophysiology and FlexStation assays, cells were transfected 24 hours after plating and assayed 48 hours after transfection. Transfection mixes were removed from cultures following a 4–6 hour incubation period at 37°C/5% CO_2 and replaced with fresh culture medium.

Electrophysiology

Whole-cell patch-clamp recordings were obtained using an Axopatch 200A amplifier with a CV201 headstage and Digidata 1200 series interface (Axon Instruments). A Hum Bug device (Quest Scientific) was used to eliminate 50/60 Hz noise. Data was acquired using Clampex 9.2 software (Axon Instruments). Dose-response data was recorded at a sampling frequency of 5 kHz with lowpass filtering at 1 kHz in Gap-free acquisition mode. Voltage ramp data was sampled at 10 kHz with lowpass filtering at 5 kHz in

Episodic Stimulation acquisition mode. External bath recording solution contained (in mM): 140 NaCl, 2.8 KCl, 2 $CaCl_2$, 2 $MgCl_2$, 10 D-glucose, 10 HEPES, 5 NaOH, pH 7.35, 330 mOsm. Internal patch pipette solution contained (in mM): 130 CsCl, 4 $MgCl_2$, 4 Na_2-ATP, 1 EGTA, 10 HEPES, 10 CsOH, pH 7.35, 315 mOsm. Pipettes were made from borosilicate glass with resistances of 4–10 MΩ. Co-transfection of soluble pmaxGFP (Amaxa) was used to identify transfected HEK293 cells. Cells were voltage-clamped with a holding potential of −60 mV. All recordings were performed at ambient temperature.

Glutamate concentration-response experiments were conducted using the Dynaflow Pro II system, a millisecond microperfusion chip (Cellectricon). GluCl-expressing HEK293 cells initially plated in 35 mm plastic culture dishes were washed with bath solution, detached using a cell scraper, and declumped by trituration to produce a 500 µl volume of round cells in suspension. Cells were added 100 µl at a time to 2 ml fresh bath solution intermittently to avoid lengthy pre-exposure to glutamate due to accumulation from the lanes of laminar flow into the cell reservoir. Na^+ glutamate (Sigma #G1626) was dissolved in water as a 100 mM stock and stored as 1 ml aliquots at -20°C. Glutamate concentrations, prepared as serial dilutions in bath solution, were applied in increasing order for 1 second each, alternating with 1 second applications of external bath solution for complete ligand washout.

A continuous voltage ramp protocol was used to measure background conductance in the absence of ligand. Cells were whole-cell voltage-clamped at −60 mV with no capacitive compensation then ramped from −60 mV to +60 mV over 50 ms.

Membrane Potential Measurements

A fluorescence-based assay employing the FLIPR Membrane Potential Assay Kit, BLUE formulation, (Molecular Devices, #R8042) was used to detect voltage changes across the cell membrane. The dye reagent is of proprietary composition[57]. Dye loading buffer was prepared according to package literature. Specifically, the contents of one vial of BLUE reagent was dissolved with 5 ml of 1x Assay Buffer, followed by a wash of the vial with another 5 ml of 1x Assay Buffer, to yield a total volume of 10 ml of dye loading buffer. Unused portions of dye loading buffer were stored at -20°C and used within 5 days. For the functional assay, culture medium was removed from the cells and replaced with 50 µl DMEM. Cells were then loaded with 50 µl of Blue dye loading buffer and incubated for 40 min at 37°C/5% CO_2. The signal was detected using the FlexStation 3 multimode benchtop microplate reader operated by SoftMax Pro Data Acquisition & Analysis Software (Molecular Devices). Excitation and emission wavelengths were set at 530 nm and 565 nm, respectively, with an emission cut-off of 550 nm. Plate reads were performed at ambient temperature with a 'Low PMT' setting. Run times, of which the first 20 s measured basal fluorescence, were 180 s for glutamate-induced signals or 300 s for ivermectin-induced signals. Other FlexStation parameters included a pipette height of 230 µl, an initial well volume of 100 µl, a transfer volume of 50 µl (therefore, drug concentrations were prepared 3x), and a transfer rate setting of 2, corresponding to ~31 µl/sec. Glutamate concentrations were prepared from 100 mM aliquots as 1:10 serial dilutions of 5, 2, and 1 mM dissolved in a 1x commercial stock of Hanks' balanced salt solution (HBSS, without phenol red; Invitrogen #14025) with 20 mM HEPES, pre-adjusted to pH 7.4 with sodium hydroxide. Ivermectin (Sigma #18898) was dissolved in

DMSO as a 10 mM stock and stored as 0.3 mM aliquots at -20°C. Ivermectin concentrations for the FlexStation assay were prepared as 1:10 serial dilutions of 10, 5, and 2 μM using 1x HBSS with 20 mM HEPES at pH 7.4, containing 0.1% DMSO.

Data Analysis

Electrophysiology data was analyzed using Clampfit 9.2 software. Glutamate-induced currents were normalized for each cell individually by the maximal current response for that cell. Concentration-response curves were constructed and fit to the following sigmoid Hill function in Origin 7.0 (OriginLab),

$$y = V_{max}\left(\frac{x^n}{k^n + x^n}\right)$$

which can be rewritten as,

$$\frac{I}{I_{max}} = \frac{1}{1 + \left(\frac{EC_{50}}{[A]}\right)^H}$$

where I is the amount of current induced by a given agonist concentration [A], I_{max} is the maximum current induced, EC_{50} is the concentration required to elicit half the maximal response and H is the Hill coefficient.

For voltage ramp experiments, the total current, I_m, can be broken down as the sum of the capacitive current, I_C, and the resistive current, I_R, across the membrane ($I_m = I_C + I_R$). Background conductance, G, was measured from the slope of the resistive current ramp ($G = dI_R/dV$). Membrane capacitance, C_m, was calculated by measuring the

capacitive current from the offset of the current ramp ($I_C = C_m(dV/dt)$). The background conductance was then normalized by the mean capacitance for each receptor and plotted as mean ± SEM from 12 or more cells. To distinguish a large background conductance from poor sealing of the patch pipette, cells with a seal resistance of < 40 MΩ, corresponding to a chord conductance of > 25 nS (as determined by G = I/V = 1/R), were omitted.

Raw FlexStation signals were exported as '.txt' files from SoftMax Pro 5 and analyzed offline using Microsoft Excel 2008 and Origin 7.0. Relative fluorescent unit signals were zeroed by mean subtraction of the first 5 data points, then smoothed using a 3-point sliding average before determining the maximum data point per well. Six, 15-point concentration-response data sets were obtained from a single 96-well plate, set up as 2 columns of 8 wells including a blank, repeated 5 more times in subsequent columns. Signals of each well were normalized by the maximum signal for that particular 2-column set to compensate for signal run-down over time. Normalized data was then averaged to construct concentration-response curves as described above.

Statistics

Pooled data for each mutation are shown as means ± SEM. Boxplots represent the mean, median, 25^{th}, and 75^{th} percentiles. Statistical significance ($P < 0.05$) was determined by one-way analysis of variance (ANOVA) on ranks using multiple pairwise comparison.

Acknowledgments

Thanks to Herwig Just and Sindhuja Kadambi for point mutation and sequencing primers.

References

1. Hibbs RE, Gouaux E. (2011) Principles of activation and permeation in an anion-selective Cys-loop receptor. *Nature* **474**:54–60.

2. Unwin N. (1993) Nicotinic acetylcholine receptor at 9 Å resolution. *J Mol Biol* **229**:1101–1124.

3. Miyazawa A, Fujiyoshi Y, Unwin N. (2003) Structure and gating mechanism of the acetylcholine receptor pore. *Nature* **423**:949–955.

4. Beckstein O, Sansom MS. (2006) A hydrophobic gate in an ion channel: the closed state of the nicotinic acetylcholine receptor. *Phys Biol* **3**:147–159.

5. Labarca C, Nowak MW, Zhang H, Tang L, Deshpande P, Lester HA. (1995) Channel gating governed symmetrically by conserved leucine residues in the M2 domain of nicotinic receptors. *Nature* **376**:514–516.

6. Filatov GN, White MM. (1995) The role of conserved leucines in the M2 domain of the acetylcholine receptor in channel gating. *Mol Pharmacol* **48**:379–384.

7. Revah F, Bertrand D, Galzi JL, Devillers-Thiery A, Mulle C, Hussy N, Bertrand S, Ballivet M, Changeux JP. (1991) Mutations in the channel domain alter desensitization of a neuronal nicotinic receptor. *Nature* **353**:846–849.

8. Yakel JL, Lagrutta A, Adelman JP, North RA. (1993) Single amino acid substitution affects desensitization of the 5-hydroxytryptamine type 3 receptor expressed in Xenopus oocytes. *Proc Natl Acad Sci U S A* **90**:5030–5033.

9. Chang Y, Weiss DS. (1999) Allosteric activation mechanism of the α1β2γ2 gamma-aminobutyric acid type A receptor revealed by mutation of the conserved M2 leucine. *Biophys J* **77**:2542–2551.

10. Kearney PC, Zhang H, Zhong W, Dougherty DA, Lester HA. (1996) Determinants of nicotinic receptor gating in natural and unnatural side chain structures at the M2 9' position. *Neuron* **17**:1221–1229.

11. Kosolapov AV, Filatov GN, White MM. (2000) Acetylcholine receptor gating is influenced by the polarity of amino acids at position 9' in the M2 domain. *J Membr Biol* **174**:191–197.

12. Thompson SA, Smith MZ, Wingrove PB, Whiting PJ, Wafford KA. (1999) Mutation at the putative GABA(A) ion-channel gate reveals changes in allosteric modulation. *Br J Pharmacol* **127**:1349–1358.

13. Shan Q, Nevin ST, Haddrill JL, Lynch JW. (2003) Asymmetric contribution of α and β subunits to the activation of αβ heteromeric glycine receptors. *J Neurochem* **86**:498–507.

14. Bianchi MT, Macdonald RL. (2001) Mutation of the 9' leucine in the GABA(A) receptor γ2L subunit produces an apparent decrease in desensitization by stabilizing open states without altering desensitized states. *Neuropharmacology* **41**:737–744.

15. Bertrand S, Devillers-Thiery A, Palma E, Buisson B, Edelstein SJ, Corringer PJ, Changeux JP, Bertrand D. (1997) Paradoxical allosteric effects of competitive inhibitors on neuronal α7 nicotinic receptor mutants. *Neuroreport* **8**:3591–3596.

16. Chang Y, Weiss DS. (1998) Substitutions of the highly conserved M2 leucine create spontaneously opening ρ1 gamma-aminobutyric acid receptors. *Mol Pharmacol* **53**:511–523.

17. Pan ZH, Zhang D, Zhang X, Lipton SA. (1997) Agonist-induced closure of constitutively open gamma-aminobutyric acid channels with mutated M2 domains. *Proc Natl Acad Sci U S A* **94**:6490–6495.

18. Gleitsman KR, Shanata JA, Frazier SJ, Lester HA, Dougherty DA. (2009) Long-range coupling in an allosteric receptor revealed by mutant cycle analysis. *Biophys J* **96**:3168–3178.

19. Bertrand D, Devillers-Thiery A, Revah F, Galzi JL, Hussy N, Mulle C, Bertrand S, Ballivet M, Changeux JP. (1992) Unconventional pharmacology of a neuronal nicotinic receptor mutated in the channel domain. *Proc Natl Acad Sci U S A* **89**:1261–1265.

20. Dalziel JE, Cox GB, Gage PW, Birnir B. (2000) Mutating the highly conserved second membrane-spanning region 9' leucine residue in the α(1) or β(1) subunit produces subunit-specific changes in the function of human α(1)β(1) gamma-aminobutyric Acid(A) receptors. *Mol Pharmacol* **57**:875–882.

21. Tierney ML, Birnir B, Pillai NP, Clements JD, Howitt SM, Cox GB, Gage PW. (1996) Effects of mutating leucine to threonine in the M2 segment of α1 and β1 subunits of GABAA α1β1 receptors. *J Membr Biol* **154**:11–21.

22. Haubensak W, Kunwar PS, Cai H, Ciocchi S, Wall NR, Ponnusamy R, Biag J, Dong HW, Deisseroth K, Callaway EM, Fanselow MS, Luthi A, Anderson DJ. (2010) Genetic dissection of an amygdala microcircuit that gates conditioned fear. *Nature* **468**:270–276.

23. Lerchner W, Xiao C, Nashmi R, Slimko EM, van Trigt L, Lester HA, Anderson DJ. (2007) Reversible silencing of neuronal excitability in behaving mice by a genetically targeted, ivermectin-gated Cl- channel. *Neuron* **54**:35–49.

24. Li P, Slimko EM, Lester HA. (2002) Selective elimination of glutamate activation and introduction of fluorescent proteins into a Caenorhabditis elegans chloride channel. *FEBS Lett* **528**:77–82.

25. Cully DF, Vassilatis DK, Liu KK, Paress PS, Van der Ploeg LH, Schaeffer JM, Arena JP. (1994) Cloning of an avermectin-sensitive glutamate-gated chloride channel from Caenorhabditis elegans. *Nature* **371**:707–711.

26. Etter A, Cully DF, Schaeffer JM, Liu KK, Arena JP. (1996) An amino acid substitution in the pore region of a glutamate-gated chloride channel enables the coupling of ligand binding to channel gating. *J Biol Chem* **271**:16035–16039.

27. Leduc-Nadeau A, Lussier Y, Arthus MF, Lonergan M, Martinez-Aguayo A, Riveira-Munoz E, Devuyst O, Bissonnette P, Bichet DG. (2010) New autosomal recessive mutations in aquaporin-2 causing nephrogenic diabetes insipidus through deficient targeting display normal expression in Xenopus oocytes. *J Physiol* **588**:2205–2218.

28. Moeller HB, Fenton RA. (2010) Can one Bad Egg' really spoil the batch? *J Physiol* **588**:2283–2284.

29. Smit LS, Strong TV, Wilkinson DJ, Macek M, Jr., Mansoura MK, Wood DL, Cole JL, Cutting GR, Cohn JA, Dawson DC, et al. (1995) Missense mutation (G480C) in the CFTR gene associated with protein mislocalization but normal chloride channel activity. *Hum Mol Genet* **4**:269–273.

30. Yasui M, Hazama A, Kwon TH, Nielsen S, Guggino WB, Agre P. (1999) Rapid gating and anion permeability of an intracellular aquaporin. *Nature* **402**:184–187.

31. Moroni M, Bermudez I. (2006) Stoichiometry and pharmacology of two human α4β2 nicotinic receptor types. *J Mol Neurosci* **30**:95–96.

32. Nelson ME, Kuryatov A, Choi CH, Zhou Y, Lindstrom J. (2003) Alternate stoichiometries of α4β2 nicotinic acetylcholine receptors. *Mol Pharmacol* **63**:332–341.

33. Zhou Y, Nelson ME, Kuryatov A, Choi C, Cooper J, Lindstrom J. (2003) Human α4β2 acetylcholine receptors formed from linked subunits. *J Neurosci* **23**:9004–9015.

34. ATCC. Cell line authentication test recommendations. in *ATCC: Technical Bulletin No. 8* (2007).

35. Nakamura N, Yamazawa T, Okubo Y, Iino M. (2009) Temporal switching and cell-to-cell variability in Ca2+ release activity in mammalian cells. *Mol Syst Biol* **5**:247.

36. Eisenberg D, Weiss RM, Terwilliger TC. (1984) The hydrophobic moment detects periodicity in protein hydrophobicity. *Proc Natl Acad Sci U S A* **81**:140–144.

37. Miller S, Janin J, Lesk AM, Chothia C. (1987) Interior and surface of monomeric proteins. *J Mol Biol* **196**:641–656.

38. O'Neil KT, DeGrado WF. (1990) A thermodynamic scale for the helix-forming tendencies of the commonly occurring amino acids. *Science* **250**:646–651.

39. Marqusee S, Robbins VH, Baldwin RL. (1989) Unusually stable helix formation in short alanine-based peptides. *Proc Natl Acad Sci U S A* **86**:5286–5290.

40. Pace CN, Scholtz JM. (1998) A helix propensity scale based on experimental studies of peptides and proteins. *Biophys J* **75**:422–427.

41. Creamer TP, Rose GD. (1992) Side-chain entropy opposes alpha-helix formation but rationalizes experimentally determined helix-forming propensities. *Proc Natl Acad Sci U S A* **89**:5937–5941.

42. Dao-Pin S, Baase WA, Matthews BW. (1990) A mutant T4 lysozyme (Val 131→Ala) designed to increase thermostability by the reduction of strain within an alpha-helix. *Proteins* **7**:198–204.

43. Hermans J, Anderson AG, Yun RH. (1992) Differential helix propensity of small apolar side chains studied by molecular dynamics simulations. *Biochemistry* **31**:5646–5653.

44. Etter A, Cully DF, Liu KK, Reiss B, Vassilatis DK, Schaeffer JM, Arena JP. (1999) Picrotoxin blockade of invertebrate glutamate-gated chloride channels: subunit dependence and evidence for binding within the pore. *J Neurochem* **72**:318–326.

45. Ikeda T, Zhao X, Kono Y, Yeh JZ, Narahashi T. (2003) Fipronil modulation of glutamate-induced chloride currents in cockroach thoracic ganglion neurons. *Neurotoxicology* **24**:807–815.

46. Raymond V, Sattelle DB, Lapied B. (2000) Co-existence in DUM neurones of two GluCl channels that differ in their picrotoxin sensitivity. *Neuroreport* **11**:2695–2701.

47. Zhao X, Salgado VL, Yeh JZ, Narahashi T. (2004) Kinetic and pharmacological characterization of desensitizing and non-desensitizing glutamate-gated chloride channels in cockroach neurons. *Neurotoxicology* **25**:967–980.

48. Zhao X, Yeh JZ, Salgado VL, Narahashi T. (2004) Fipronil is a potent open channel blocker of glutamate-activated chloride channels in cockroach neurons. *J Pharmacol Exp Ther* **310**:192–201.

49. Zhao X, Yeh JZ, Salgado VL, Narahashi T. (2005) Sulfone metabolite of fipronil blocks gamma-aminobutyric acid- and glutamate-activated chloride channels in mammalian and insect neurons. *J Pharmacol Exp Ther* **314**:363–373.

50. Schmitt BM, Koepsell H. (2002) An improved method for real-time monitoring of membrane capacitance in Xenopus laevis oocytes. *Biophys J* **82**:1345–1357.

51. Slimko EM, McKinney S, Anderson DJ, Davidson N, Lester HA. (2002) Selective electrical silencing of mammalian neurons in vitro by the use of invertebrate ligand-gated chloride channels. *J Neurosci* **22**:7373–7379.

52. Monod J, Wyman J, Changeux JP. (1965) On the Nature of Allosteric Transitions: A Plausible Model. *J Mol Biol* **12**:88–118.

53. Chang Y, Wang R, Barot S, Weiss DS. (1996) Stoichiometry of a recombinant GABAA receptor. *J Neurosci* **16**:5415–5424.

54. Jensen AA, Kristiansen U. (2004) Functional characterisation of the human α1 glycine receptor in a fluorescence-based membrane potential assay. *Biochem Pharmacol* **67**:1789–1799.

55. Jensen AA, Bergmann ML, Sander T, Balle T. (2010) Ginkgolide X is a potent antagonist of anionic Cys-loop receptors with a unique selectivity profile at glycine receptors. *J Biol Chem* **285**:10141–10153.

56. Slimko EM, Lester HA. (2003) Codon optimization of Caenorhabditis elegans GluCl ion channel genes for mammalian cells dramatically improves expression levels. *J Neurosci Methods* **124**:75–81.

57. Krahn T, Paffhausen W, Schade A, Bechem M, Schmidt D. (2002) US Patent 6,420,183. *Chem Abstr* **128**:59162.

Chapter 4

GluClv2.0: An Improved Tool For Neuronal Silencing

Abstract

A variety of genetically encoded tools have been developed that allow physical manipulation of neuronal excitability in a reversible, cell-specific manner. We previously engineered an invertebrate glutamate-gated chloride channel (GluCl αβ) that enabled pharmacologically induced silencing of electrical activity in targeted CNS neurons *in vivo* by the anthelmintic drug compound ivermectin (IVM). With this receptor, GluCl opt α-CFP + opt β-YFP Y182F, the concentration of IVM necessary to elicit a consistent silencing phenotype was high enough to raise concern about its potential side effects. Variability in the extent of spike suppression was also apparent and correlated with co-expression levels of the fluorescently tagged α and β subunits. To address these issues, mutant receptors were generated via rational protein engineering strategies and subjected to functional screening and fluorescence-based assays. It has since been learned that GluCl α homomers are indeed expressed at the plasma membrane and are responsive to IVM, but incorporation of the β subunit confers greater IVM sensitivity. Introduction of a gain-of-function mutation (L9'F) in the second transmembrane domain of the α subunit appears to facilitate β subunit incorporation and substantially increase heteromeric GluCl αβ sensitivity to IVM without permitting unliganded channel opening. Removal of an arginine-based ER retention motif (RSR mutated to AAA) from the intracellular loop of the β subunit further promotes heteromeric expression at the plasma membrane by preventing ER-associated degradation of the β subunit. Introduction of a monomeric XFP mutation (A206K) complements these effects. The newly engineered GluCl opt α-mXFP L9'F + opt β-mXFP Y182F RSR_AAA receptor significantly increases conductance and

reduces variability in evoked spike generation *in vitro* using a lower concentration of IVM. This receptor, dubbed 'GluClv2.0', is an improved tool for IVM-induced silencing.

Introduction

Neurons are organized into anatomically distinct regions that transmit excitatory or inhibitory information to the regions they project to, following a specific pathway or circuit. Inappropriate activity within such a circuit is thought to be the basis of most psychiatric and neurological disorders. Unraveling the intricate circuitry and functional basis of various neuronal networks will provide a better understanding of complex behavior and help pinpoint the underlying causes of brain related dysfunction.

A number of tools have been developed that allow the physical manipulation of neuronal excitability in a reversible, cell-specific manner. These tools enable mapping of neuronal connectivity and are essential for assigning functional roles to particular cell types and determining their contribution to perception or behavior. One such tool employs a heteromeric glutamate-gated chloride channel (GluCl αβ) from the invertebrate species *Caenorhabditis elegans* and the anthelmintic drug compound ivermectin (IVM). IVM-induced activation of GluCl αβ heterologously expressed in mammalian neurons elicits a chloride conductance that drives the membrane potential toward the Nernst potential of chloride (E_{Cl}) to prevent action potential generation for effective neuronal silencing.

The GluCl/IVM method was the first to show neuronal silencing induced by a systemically administered drug in awake, behaving animals[1]. In this study, proof-of-concept was demonstrated in mice using a robust and reproducible striatal lesion assay known to induce amphetamine-dependent rotational behavior[2,3]. In mice expressing GluCl unilaterally in the striatum via AAV2-mediated infection, systemic administration

of IVM caused unidirectional rotation of the animal, indicating that striatal neurons were silenced (Figure 4-1A). The rotational phenotype was observed within hours of induction and was fully reversed within days, allowing multiple cycles of silencing and recovery to be performed on a single animal.

IVM is a widely used commercial drug that is well tolerated by both animals and humans because GluCl channels do not exist in mammals. Selective and reversible silencing was achieved without measurable toxicity of either the individual neurons or the animal as a whole. However, the dose of IVM required to elicit a consistent silencing phenotype (5–10 mg/kg; Figure 4-1B)[1] was unexpectedly higher than that routinely used to treat mice with parasitic infections (0.2 mg/kg)[4] and high enough to raise concern about potential side effects. Though IVM can successfully cross the BBB, some fraction is presumably being cleared continuously from the brain by the mdr1a P-glycoprotein transporter[5], resulting in a lower effective concentration in the cerebrospinal fluid. Further increasing the dose (20 mg/kg) enters the range of toxicity, visible by paralysis[6]. Toxic effects are likely mediated through off-target agonism, as IVM is known to activate or potentiate other ligand-gated ion channels present in the CNS, though it does so with much lower affinity[7-10].

Silencing experiments with the GluCl/IVM system were also subject to considerable variability. Rotation data from the *in vivo* study displays a bimodal distribution with one group of animals exhibiting a weak but significant phenotype, and the other exhibiting a strong behavioral phenotype. The strength of the behavioral phenotype was correlated with both the extent of viral infection (i.e., the volume of striatum expressing GluCl $\alpha\beta$) and the extent of spike suppression (i.e., individual

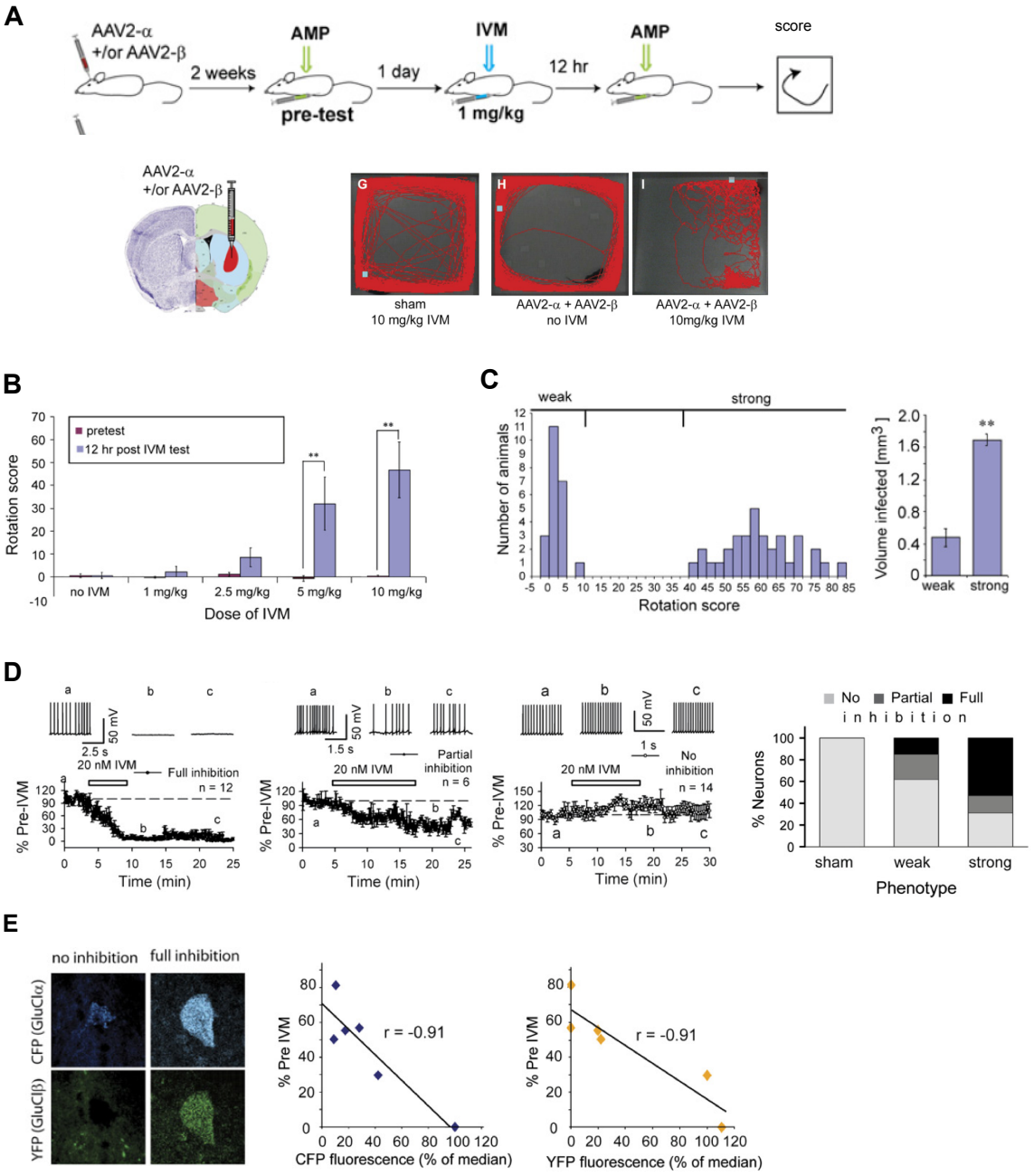

Figure 4-1. Proof-of-concept for GluCl/IVM neuronal silencing *in vivo*. *A*. Experimental design schematic of amphetamine-induced rotation test for silencing striatal neurons. Unilateral striatum was virally infected with GluCl α and β subunits. Control mice move around the chamber perimeter. Mice expressing GluCl and administered IVM display rotational behavior. *B*. Dose-response relation for amphetamine-induced rotation. *C*. Histogram of rotation score shows bimodal distribution. Strength of the phenotype correlates with the volume of the virally infected region. *D*. Neuron firing rates show full, partial and no inhibition. Lowercase letters display sample spike trains before (a) and after (b & c) IVM perfusion. Strength of the phenotype correlates with the extent of spike suppression. *E*. Confocal images show varying subunit expression levels. Extent of spike suppression is correlated with fluorescence intensity of α-CFP and β-YFP Y182F subunits. (Figures adapted from Lerchner et al., 2007.)[1]

neurons showing either full, partial, or no inhibition), which further correlated with co-expression levels of α and β subunits (Figure 4-1C, D, E).

Prior to its implementation as a silencing tool, the GluCl receptor was modified in several ways. First, it was rendered insensitive to its native ligand glutamate by a single point mutation in the β subunit, Y182F (Figure 4-2A)[11]. Insensitivity is necessary since glutamate is an endogenous neurotransmitter present in cerebrospinal fluid and released during synaptic transmission. In addition, the DNA sequence of this invertebrate gene was codon-optimized to achieve greater expression levels in mammalian systems (Figure 4-2B)[12], and tagged with fluorescent proteins YFP and CFP for direct visualization of protein expression (Figure 4-2C)[11]. This GluCl opt α-CFP + opt β-YFP Y182F receptor is referred to throughout this study as 'the original tool'.

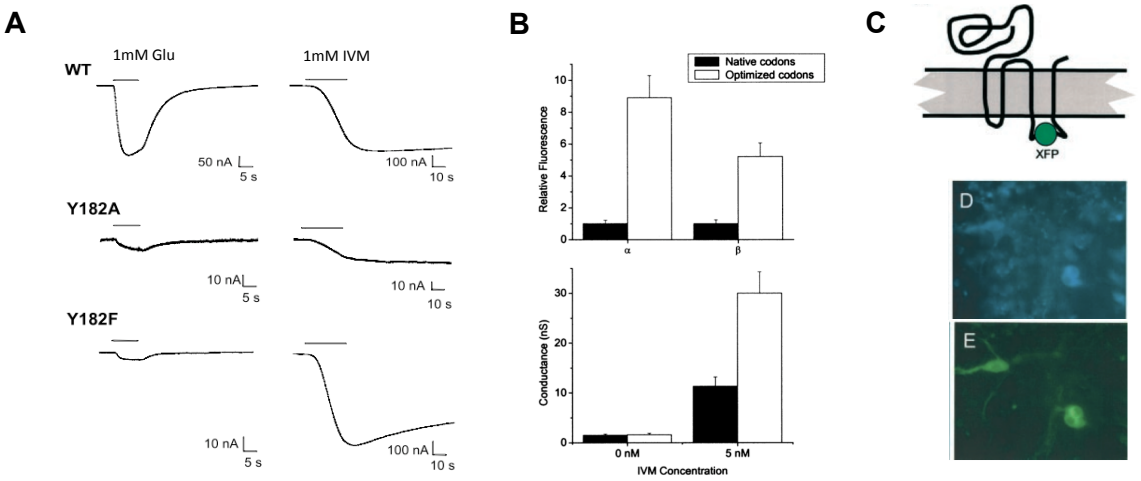

Figure 4-2. Construct modifications generating the original GluCl opt α-CFP + opt β-YFP Y182F silencing tool. *A.* A tyrosine-to-phenylalanine mutation at position 182 of the β subunit abolishes glutamate sensitivity but maintains activation by IVM. *B.* Codon optimization of GluCl subunits increased expression levels in mammalian cells. *C.* Fluorescent labels, CFP and YFP, were inserted into the intracellular M3-M4 loop for direct visualization of subunit expression. (Figures adapted from Li et al., 2002; Slimko et al., 2002; Slimko & Lester, 2003.)[11-13]

The current study aimed to optimize the original GluCl/IVM tool by introducing rational point mutations intended to (1) increase receptor sensitivity to IVM in order to achieve silencing by lower doses and, (2) improve subunit expression at the plasma membrane in order to reduce spike suppression variability. Such optimization would alleviate the concern of off-target side effects and avoid suboptimal spike inhibition. As was the subject of Chapter 3, introduction of an L9'F gain-of-function mutation in the second transmembrane domain of the α subunit appears to facilitate β subunit incorporation and substantially increase heteromeric GluCl αβ sensitivity to IVM without permitting unliganded channel opening. Glutamate insensitivity must be reinstated to this high sensitivity mutant receptor for it to function effectively as a silencing tool. It was also determined that GluCl α homomers are indeed expressed at the plasma membrane of mammalian cells and are responsive to IVM. A mixed presence of heteromeric and homomeric receptors could be responsible for the variability in spike suppression. To address this possibility in the current study, the secretory pathway of membrane receptor trafficking was considered. Rational protein engineering strategies to improve heteromeric GluCl αβ surface expression may be combined with the increased sensitivity mutation to produce an optimized GluCl/IVM silencing tool.

Results

Mutation of a putative ER retention motif enhances IVM sensitivity

In the cell, multimeric receptors destined for the plasma membrane are synthesized, matured, and assembled at the endoplasmic reticulum (ER)[14,15]. The amino acid sequence contains specific signaling motifs that instruct the cellular machinery to either let the protein exit the ER or retain it there. Subunits that have been assembled into complete receptors are prepared for ER export at 'exit sites' where they are packaged into coat protein II (COPII) vesicles that mediate anterograde transport from the ER to the Golgi. In the Golgi, receptors are either subject to posttranslational modifications after which they are trafficked to the plasma membrane, or they undergo retrograde transport (i.e., retrieval) by COPI vesicles back to the ER. This ER retention-retrieval process serves as a quality control mechanism to ensure that only properly assembled receptors are transported to the cell surface. Proteins that are misfolded, unassembled, or improperly assembled are retained in the ER and ultimately targeted for ER-associated degradation[16,17].

Consensus signaling motifs exist for both ER export and ER retention. The best-characterized exit signals include DxE[18,19], LxxL/ME[20], and I/LxM[21]. These ER export motifs are found on the cytosolic loops of a variety of membrane-associated proteins and are recognized by Sec24, the primary cargo-selection protein of the COPII coated vesicles for transport from ER to Golgi. Well-described ER retention signals include the classical C-terminal motifs, KDEL and KKxx[22,23], and the cytosolic arginine-based signal, RxR[24]. The RxR motif has been found in potassium channels[24], G-protein coupled

receptors[25], voltage-dependent Ca^{2+} channels[26], ionotropic glutamate receptors[27-29] and ionotropic Cys-loop receptors[30-32]. Proteins containing an RxR motif are retained in the ER or maintained by COPI retrieval until the signal is masked as a result of heteromultimeric assembly with additional subunits[33-35].

To check for putative ER signaling motifs present in GluCl α and β, the amino acid sequence of the large TM3–TM4 intracellular loop of each subunit was examined (Figure 4-3). The α subunit has one potential ER export motif, LNLLE, immediately following the fluorescent fusion protein insertion (note, XFP tags were originally placed in TM3–TM4 loop at restriction sites[11]). The β subunit has two putative ER export motifs, LEM and DAE, as well as two putative ER retention motifs, RSR and RRR. The presence of these possible signaling motifs correlates with functional expression observed for each of these subunits in mammalian systems. In HEK293 cells, heteromeric GluCl αβ channels are activated by glutamate and IVM; α homomers form functional channels at the plasma membrane responsive to IVM, while no response is observed for β homomers with either glutamate or IVM. It is possible that one or both of the ER retention motifs present in the β subunit prevents its trafficking to the plasma membrane in the absence of α subunits, fitting with the premise that subunits bearing an arginine-based ER retention motif require 'masking' by assembly with other appropriate subunits in order to exit the ER. It also suggests that variability in receptor expression and silencing could be due to ER retention of the β subunit. Thus, removal of ER retention signals may allow more uniform receptor expression and consistent neuronal silencing. To test this hypothesis, the putative ER retention motifs of GluCl β were mutated to

alanine residues: GluCl β-YFP R318A, S319A, R320A for a 'RSR_AAA mutant' and GluCl β-YFP R329A, R330A, R331A for a 'RRR_AAA mutant'.

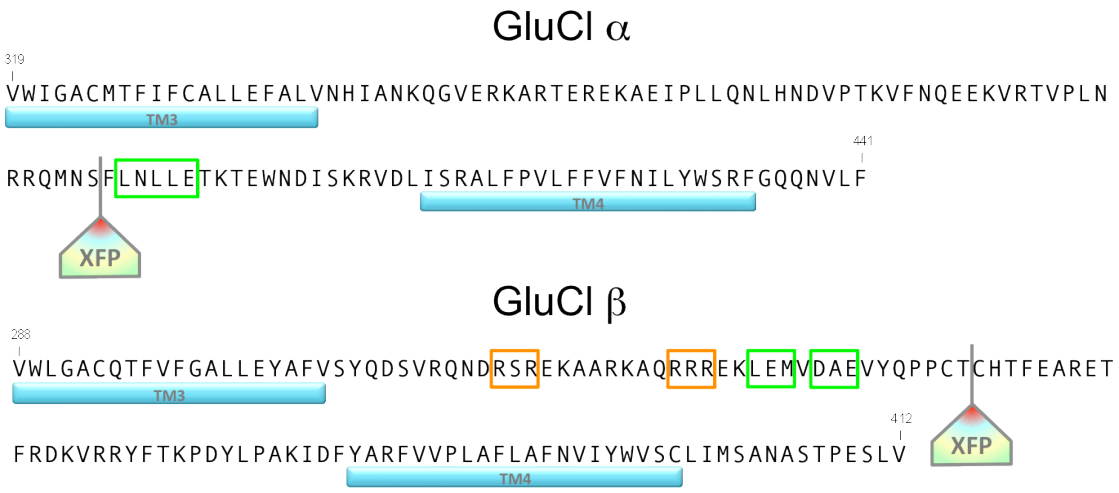

Figure 4-3. Putative ER signaling motifs in GluCl α and β subunits. Amino acid sequence including the intracellular TM3–TM4 loop of GluCl α and GluCl β subunits. The last amino acid of each sequence is the C-terminal residue. Transmembrane spanning helices (TM3 and TM4) are defined by blue rectangles. Position of the fluorescent protein insertion is noted by 'XFP'. ER export motifs are shown in green boxes; ER retention motifs are shown in orange boxes. The α subunit contains a single putative ER export motif (LxxL/ME). The β subunit contains two possible ER export motifs (I/LxM; DxE) and two potential ER retention motifs (RxR).

Mutant β subunits were expressed as heteromeric receptors and tested for IVM activation using a membrane potential assay to ensure that the RSR_AAA and RRR_AAA mutations did not disrupt channel function. The α-YFP + β-YFP RSR_AAA and α-YFP + β-YFP RRR_AAA mutant receptors, and the double mutant receptor, α-YFP + β-YFP RSR_AAA&RRR_AAA, each displayed a concentration-dependent IVM response similar to the WT and WT-XFP receptors (Figure 4-4A, Table 4-1). No

response was observed for any of the mutated β subunits when transfected in the absence of the α subunit, suggesting that removal of these putative retention motifs is not sufficient to allow membrane expression of β homomers. Noticeable differences including a biphasic dependency of the (β)RSR_AAA mutant and increased raw RFU signal (Figure 4-4B) for both the (β)RSR_AAA and (β)RRR_AAA mutants conveyed these mutations were having an effect. Removal of an ER retention motif could either be increasing the total number of receptors expressed at the surface, or shifting the receptor subunit stoichiometry, or both.

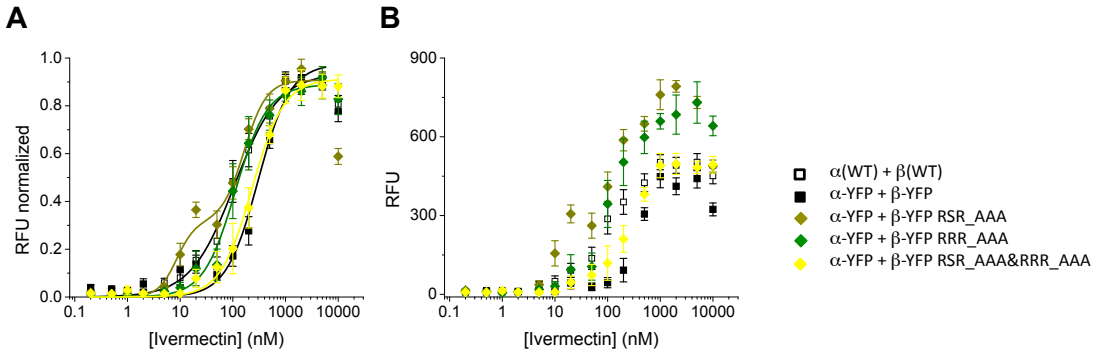

Figure 4-4. Ivermectin concentration-response curves for putative ER retention mutants. IVM activation was assayed using the FlexStation. *A*. Normalized IVM concentration-response curves for the heteromeric (β)RSR_AAA, (β)RRR_AAA, and (β)RSR_AAA&RRR_AAA mutant receptors are similar to WT and WT-XFP. IVM activation parameters are shown in Table 4-1. *B*. The (β)RSR_AAA and (β)RRR_AAA mutants show increased raw RFU signals.

If removal of the putative retention motifs increases the number of receptors trafficked to the plasma membrane, it should result in greater whole-cell currents. Avoiding the issues with IVM electrophysiology as discussed in the previous chapter, glutamate-induced currents of the heteromeric (β)RSR_AAA and (β)RRR_AAA mutant receptors were recorded in whole-cell patch-clamp mode using the Dynaflow microperfusion chip. Pooled concentration-response relations of these mutants were again similar to WT and WT-XFP, but there was no statistically significant increase in maximal current for the number of cells recorded (Figure 4-5A, B). Multiple sensitivities were observed as before (Figure 4-5C; Chapter 3, Figure 3-3) with comparable EC_{50} values and a greater number of cells showing a 'low sensitivity' response to glutamate.

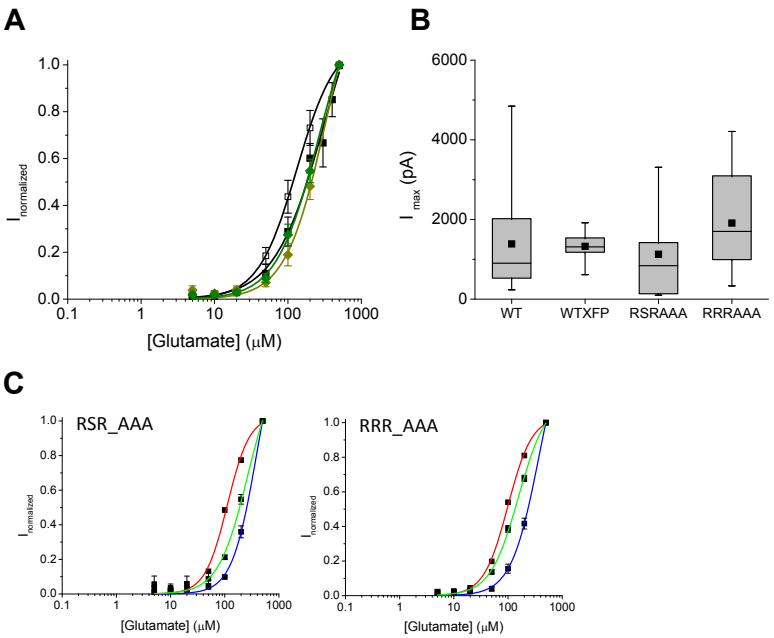

GluCl channel	abbr.	EC_{50} (μM)	Hill	n
α(WT) + β(WT)	WT	314 ± 133*	1.28 ± 0.23	14
α-YFP + β-CFP	WT-XFP	132 ± 5	1.64 ± 0.07	12
α-YFP + β-YFP RSR_AAA	RSR_AAA	331 ± 88	1.57 ± 0.22	8
α-YFP + β-YFP RRR_AAA	RRR_AAA	262 ± 30	1.50 ± 0.11	11

	High Sensitivity			Mixed			Low Sensitivity		
	EC_{50} (μM)	Hill	n	EC_{50} (μM)	Hill	n	EC_{50} (μM)	Hill	n
WT	44.71 ± 0.00	3.05 ± 0.17	1	159.65 ± 0.01	2.03 ± 0.12	9	2564.9 ± 3.98*	1.45 ± 0.15	4
WT-XFP	80.68 ± 0.00	2.22 ± 0.13	6	145.91 ± 0.02	1.49 ± 0.16	3	306.90 ± 0.01*	2.41 ± 0.09	3
RSR_AAA	111.90 ± 6.79	2.11 ± 0.21	1	262.22 ± 78.65	1.61 ± 0.33	3	385.27 ± 123.6	1.92 ± 0.35	4
RRR_AAA	99.56 ± 4.70	1.95 ± 0.14	1	155.62 ± 8.56	1.67 ± 0.09	4	368.23 ± 79.14	1.71 ± 0.19	6

Figure 4-5. Glutamate concentration-response curves for putative ER retention mutants. Glutamate activation was assayed by whole-cell electrophysiology. *A*. Normalized glutamate concentration-response curves for heteromeric (β)RSR_AAA and (β)RRR_AAA mutant receptors are similar to WT and WT-XFP. *B.* Maximal glutamate-induced currents of the mutant receptors are not significantly different from WT and WT-XFP. *C.* Concentration response curves of individual cells could be separated into three categories: high sensitivity (red line), low sensitivity (blue line), and mixed (green line). Glutamate activation parameters for putative ER retention mutants are presented in the corresponding tables. Curves for cell-to-cell variability of WT and WT-XFP are shown in Chapter 3, Figure 3-3. The EC_{50} and Hill coefficient values represent the mean ± SEM for the number of cells (n) recorded. The * indicates concentration-response normalization to a less-than-saturating maximum concentration.

In the previous chapter, introduction of an (α)L9'F mutation yielded a biphasic concentration-dependent relationship with increased sensitivity to IVM (Chapter 3, Figure 3-6). Addition of the (α)L9'F mutation with the putative ER retention mutations produced pronounced two-component relationships for both the (α)L9'F + (β)RSR_AAA and the (α)L9'F + (β)RSR_AAA&RRR_AAA mutant receptors (Figure 4-6A). In particular, the (α)L9'F + (β)RSR_AAA mutant receptor shows a significant increase in activation with low (10 nM) concentrations of IVM (Figure 4-6B).

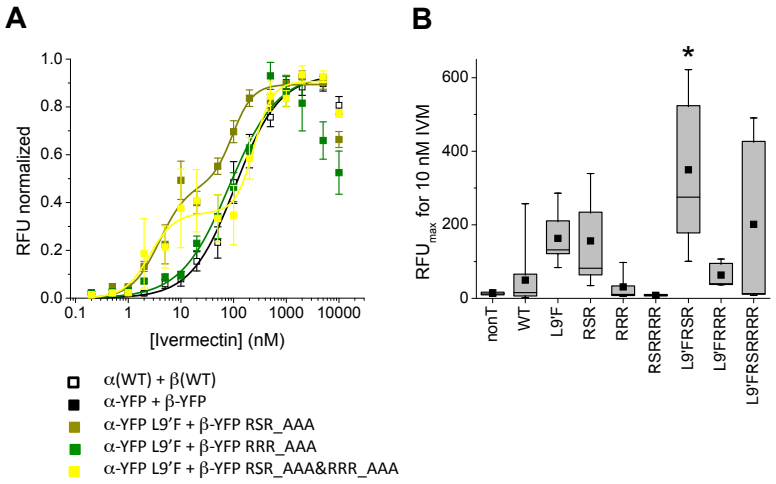

Figure 4-6. IVM concentration-response curves for putative ER retention mutants plus the (α)L9'F mutation. IVM activation was assayed using the FlexStation. *A*. Normalized IVM concentration-response curves for (α)L9'F + (β)RSR_AAA and (α)L9'F + (β)RSR_AAA&RRR_AAA show a pronounced biphasic relationship. IVM activation parameters are shown in Table 4-1. *B*. The (α)L9'F + (β)RSR_AAA mutant receptor is significantly more sensitive to 10 nM IVM than WT.

Glutamate insensitive mutations eliminate increased sensitivity to IVM

The significant increase in IVM sensitivity was encouraging toward the goal of GluCl optimization. The (α)L9'F and β subunit ER retention mutations tested up to this point, however, had been examined using glutamate-sensitive receptors. True optimization of the silencing tool requires glutamate insensitivity, accomplished by the binding site mutation, Y182F, in the β subunit. Astonishingly, reintroduction of the (β)Y182F mutation into the (α)L9'F + (β)RSR_AAA receptor abolished the high IVM sensitivity component of the biphasic concentration-response curve (Figure 4-7A). The same loss of high IVM sensitivity was observed when the glutamate insensitive (β)Y182F mutation was restored to the individual (α)L9'F and (β)RSR_AAA mutant receptors (Figure 4-7B, C).

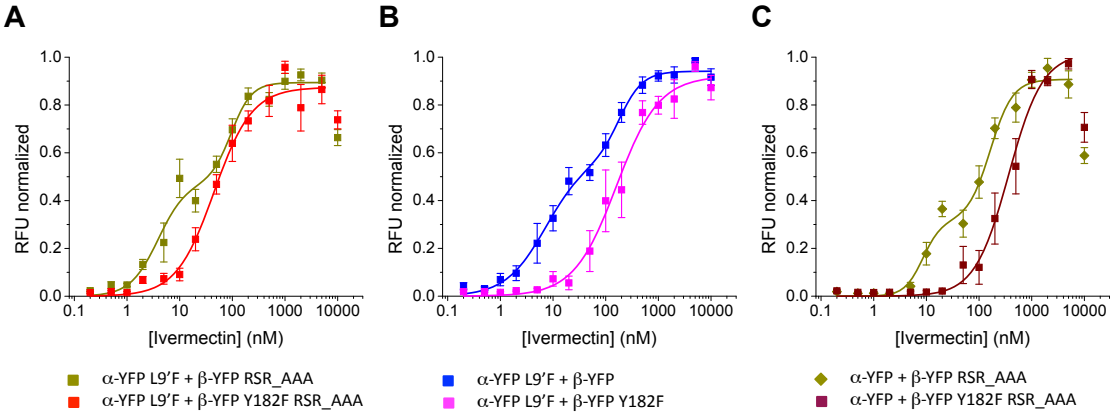

Figure 4-7. Reintroduction of a glutamate insensitive mutation affects IVM sensitivity of proposed optimized receptor. IVM activation was assayed using the FlexStation. Normalized IVM concentration-response curves show presence of a (β)Y182F mutation eliminates the high sensitivity component of the biphasic relationship for the combined (α)L9'F + (β)RSR_AAA mutant receptor (*A)* as well as the individual (α)L9'F and (β)RSR_AAA mutant receptors (*B&C*). IVM activation parameters are shown in Table 4-1.

In spite of these effects, the (β)Y182F mutation alone was confirmed to behave as expected, rendering heteromeric GluCl αβ receptors insensitive to glutamate without affecting IVM sensitivity (Figure 4-8).

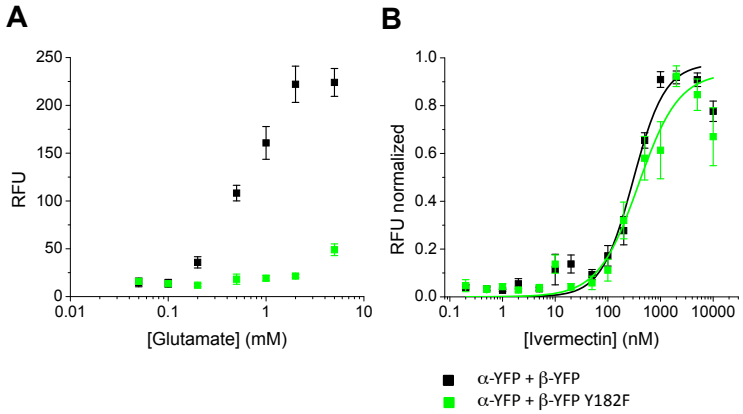

Figure 4-8. Confirmation of the (β)Y182F glutamate insensitive mutation. Glutamate (raw RFU) and IVM (normalized RFU) activation were assayed using the FlexStation. The (β)Y182F mutation renders heteromeric GluCl receptors insensitive to glutamate (*A*) while maintaining sensitivity to IVM (*B*). IVM activation parameters are shown in Table 4-1.

The incompatibility of the (β)Y182F mutation prompted the consideration of alternative mutations to achieve glutamate insensitivity. A recently available crystal structure of GluCl provides the precise molecular interactions of glutamate within the receptor binding site (Figure 4-9A)[36]. Structural coordinates reveal a cation-pi interaction between the electron-rich aromatic ring of a tyrosine residue (Y200 of $GluCl_{cryst}$) and the positively charged amino group of glutamate. This tyrosine residue corresponds to Y261 of the nascent α subunit which aligns with Y232 of the nascent β subunit (note, nascent numbering includes signal peptide residues). Since the resolved structure is comprised of

only α subunits, it is not known which subunit, α or β, provides the principle and complimentary faces of the binding site in the heteromeric receptor. For that reason, the potential cation-pi-forming tyrosine residue of each subunit was mutated to alanine, (α)Y261A and (β)Y232A, and tested individually for glutamate and IVM activation.

The (β)Y232A mutant was successful in abolishing glutamate sensitivity while perfectly maintaining IVM sensitivity (Figure 4-9B, C). The (α)Y261A mutant was also insensitive to glutamate (Figure 4-9E). However, the IVM concentration-response curve for this mutant was right-shifted with a steep Hill coefficient, much like that observed for GluCl α-YFP homomers (Figure 4-9F; see Chapter 3, Figure 3-7). This suggests that the (α)Y261A mutation gives rise to a predominating population of α homomer receptors, which are inherently unresponsive to glutamate binding events. Though not conclusive, these results suggest that β serves as the principle subunit of heteromeric GluCl αβ receptors. To determine if (β)Y232A could function as an alternative glutamate insensitive mutation toward an optimized silencing tool, it was combined with the (α)L9'F mutation. Unfortunately, the high sensitivity component of the biphasic (α)L9'F response was still not maintained (Figure 4-9D).

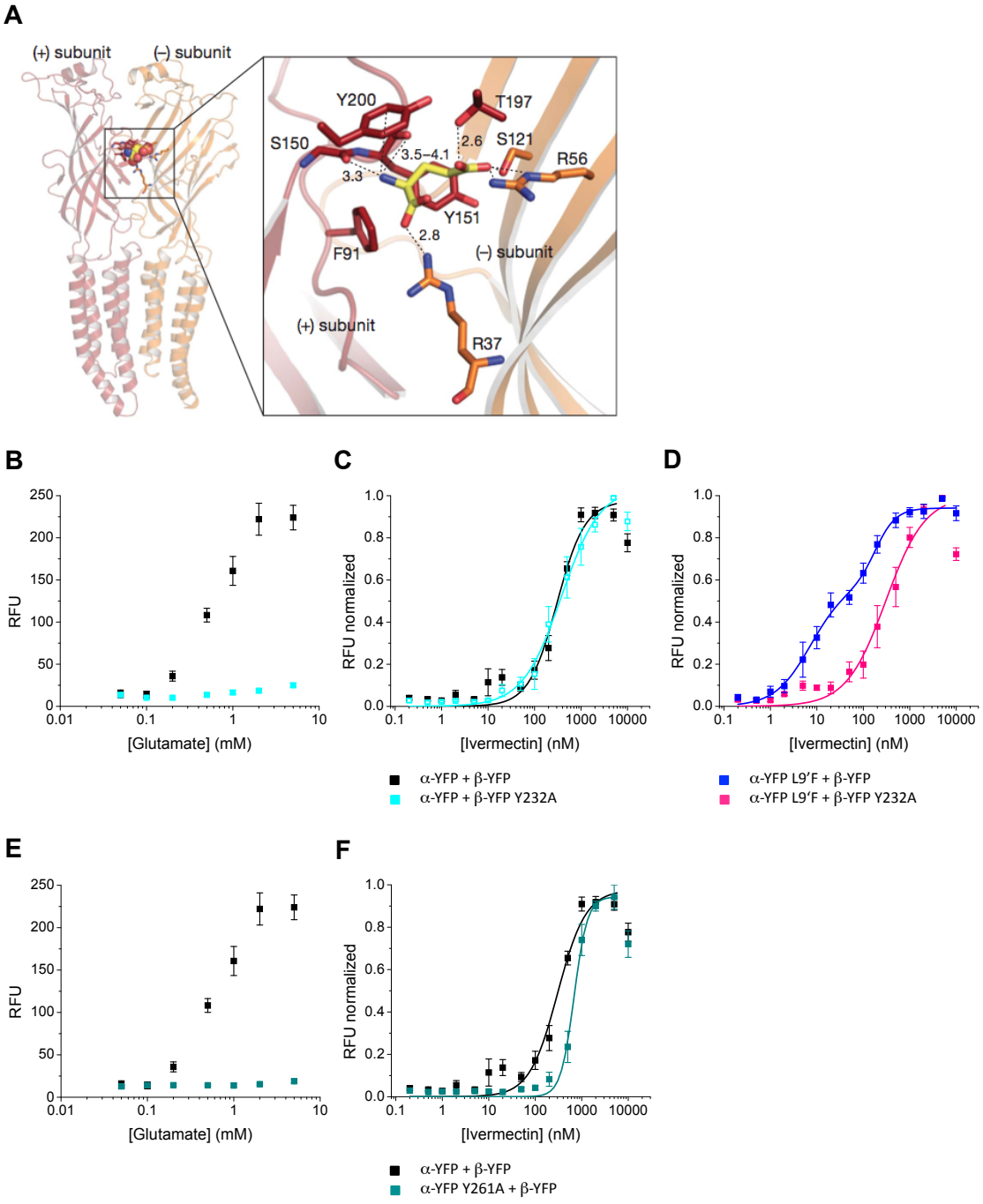

Figure 4-9. An alternative glutamate insensitive mutation still does not maintain high IVM sensitivity. *A.* Glutamate binding interactions with $GluCl_{cryst}$ α homomer. (Figure adapted from Hibbs & Gouaux, 2011.)[36] The Y200 residue forms a cation-pi interaction with the amino group of glutamate. *B–F.* Glutamate (raw RFU) and IVM (normalized RFU) activation were assayed using the FlexStation. *B&C.* The (β)Y232A mutation renders heteromeric receptors insensitive to glutamate while maintaining sensitivity to IVM. *D.* The (β)Y232A mutation still eliminates the high sensitivity component of the (α)L9'F biphasic response. *E&F.* The (α)Y261A mutant receptor is also insensitive to glutamate, but the right-shifted IVM concentration-response curve suggests predominant expression of α homomers which are already insensitive to glutamate. IVM activation parameters are shown in Table 4-1.

XFP tag oligomerization affects IVM sensitivity

Reappearance of the steep, right-shifted IVM concentration-response curve characteristic of the GluCl α-YFP homomers warranted a closer look at the effects of fluorescent protein insertion. A four-way comparison of heteromeric WT-XFP receptors with YFP and CFP tags on either or both subunits shows a right shift from the nontagged WT receptor (Figure 4-10A). Cross-comparison of XFP-tagged and nontagged subunits revealed right-shifted curves only when the fluorescent protein was present in the α subunit (Figure 4-10B). It appears the XFP insertion in the α subunit affects IVM sensitivity of both α homomeric and αβ heteromeric receptors.

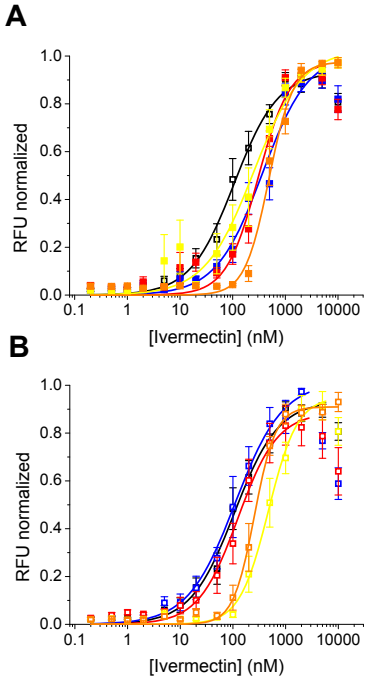

GluCl channel	EC_{50} (μM)	Hill	n
α(WT) + β(WT)	107.14 ± 10.94	1.04 ± 0.09	12
α-YFP + β-CFP	365.20 ± 96.76	0.99 ± 0.16	12
α-YFP + β-YFP	302.08 ± 54.34	1.44 ± 0.27	12
α-CFP + β-YFP	249.59 ± 57.09	0.94 ± 0.15	6
α-CFP + β-CFP	490.25 ± 39.35	1.89 ± 0.24	6
α(WT) + β-CFP	110.26 ± 13.09	0.96 ± 0.08	6
α(WT) + β-YFP	123.85 ± 17.74	1.16 ± 0.15	6
α-YFP + β(WT)	471.85 ± 35.39	1.58 ± 0.14	6
α-CFP + β(WT)	255.72 ± 11.82	2.16 ± 0.17	6

Figure 4-10. The α subunit fluorescent protein (XFP) insertion affects IVM sensitivity. IVM activation was assayed using the FlexStation. *A*. Heteromers with YFP and CFP tags on either or both subunits all show a slight right shift from the nontagged WT receptor. *B*. Heteromers with a YFP or CFP tag on one subunit shows right-shifted curves only when the fluorescent protein is on the α subunit. Ivermectin activation parameters are presented in the corresponding table.

Fluorescent proteins have a tendency to dimerize at high concentrations. A crystal structure of GFP shows a hydrophobic dimer interface comprised of amino acid residues Ala206, Leu221, and Phe223 (Figure 4-11A)[37]. A strictly monomeric form of XFP can be obtained by mutating Ala206 to a Lys residue which introduces a long, positively charged side chain that disrupts the hydrophobic interface[38]. Fluorescent protein dimerization is likely to occur when restricted to two-dimensional space as when fused to membrane proteins[39]. To determine if XFP dimerization was having an effect on channel function or possibly even stoichiometry of GluCl, an A206K mutation was incorporated into the engineered constructs. The IVM concentration-response curve of the wild-type monomeric YFP-tagged (mYFP) receptor was no longer right-shifted compared to the WT receptor, and even revealed a distinctive second component (Figure 4-11B). Incorporation of mYFP into the (α)L9'F receptor produced a more pronounced biphasic relationship than any previously observed. The same extreme biphasic behavior resulted when the L9'F mutation was present in the β subunit or present both α and β subunits (Figure 4-11C). Addition of (β)Y182F to the (α)L9'F mutation with mYFP tags now maintained a high sensitivity component, however the proportion was still reduced (Figure 4-11D).

Due the significant improvement of mYFP, this A206K mutation was combined iteratively with the L9'F mutations, (α)L9'F and/or (β)L9'F, the glutamate insensitive mutations, (β)Y182F or (β)Y232A, and the ER-retention mutation, (β)RSR_AAA, to screen for the greatest increase in IVM sensitivity (Figure 4-12A). This process revealed high sensitivity IVM activation for the initially favored receptor (α-YFP L9'F + β-YFP RSR_AAA) now including a glutamate insensitive mutation and monomeric fluorescent

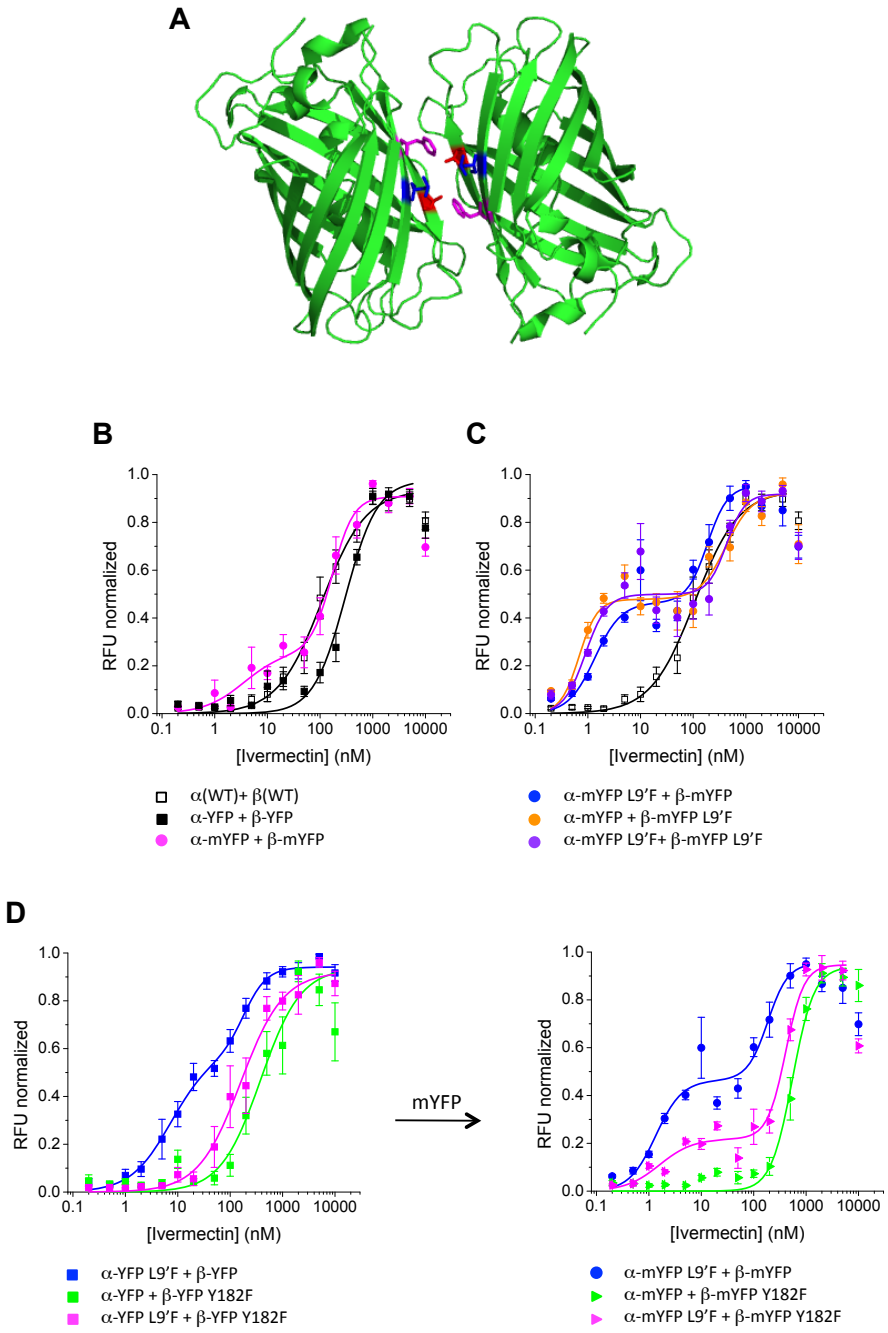

Figure 4-11. Monomeric YFP mutation (A206K) increases high IVM sensitivity component. *A.* Crystal structure of GFP dimer (1GFL.pdb) indicates a hydrophobic interface composed of residues Ala206, Leu221, and Phe223. *B.* Receptors with mYFP tags on both α and β subunits are no longer right-shifted from the nontagged WT receptor. *C.* The incorporation of mYFP enhances the high IVM sensitivity component of the (α)L9'F biphasic curve. An L9'F mutation in the β subunit or in both α and β subunits gives similar results. *D.* The mYFP mutation maintains a high IVM sensitivity component upon addition of the (β)Y182F mutation to (α)L9'F. IVM activation was assayed using the FlexStation. IVM activation parameters are shown in Table 4-1.

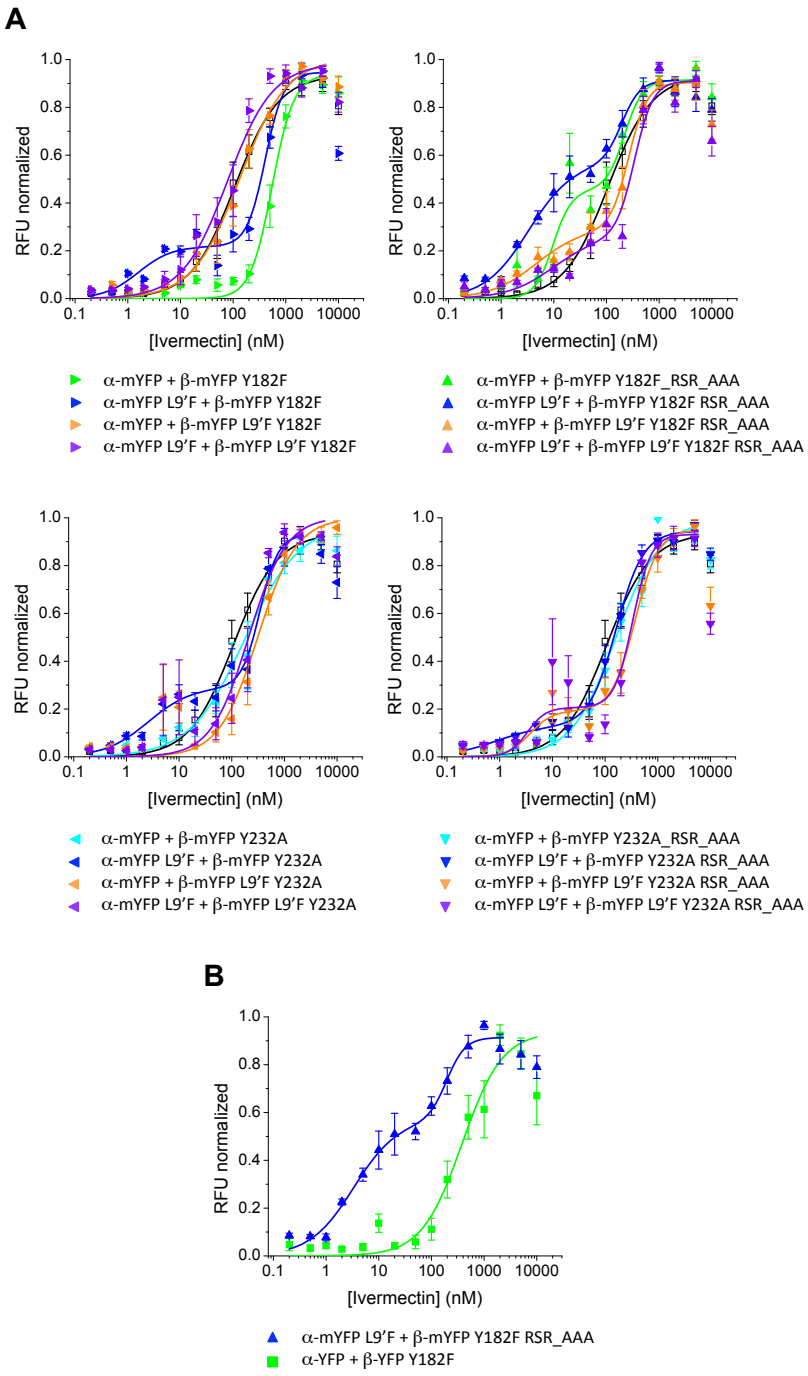

Figure 4-12. Identification of an optimally engineered receptor. IVM activation was assayed using the FlexStation. *A.* Normalized IVM concentration-response curves of mutant receptor combinations including mYFP tags (*all panels*) with the (α)L9'F and/or (β)L9'F mutations (*all panels*), the glutamate insensitive mutations (β)Y182F (*top panels*) and (β)Y232A (*bottom panels*), and the ER-retention mutation (β)RSR_AAA (*right panels*). *B.* GluCl α-mYFP L9'F + β-mYFP Y182F RSR_AAA has the greatest increase in IVM sensitivity compared to the original silencing tool. IVM activation parameters are shown in Table 4-1.

GluCl channel		1st comp	EC_{50} (nM)	Hill	EC_{50} (nM)	Hill	n
α(WT) + β(WT)	□				107.14 ± 10.94	1.04 ± 0.09	12
α-YFP + β-YFP	■				302.08 ± 54.34	1.44 ± 0.27	12
α-YFP + β-YFP RSR_AAA	◆	0.35	8.55 ± 3.16	2.5 ± 1.67	163.15 ± 38.31	2.04 ± 0.84	6
α-YFP + β-YFP RRR_AAA	◆				111.88 ± 9.98	1.44 ± 0.16	6
α-YFP + β-YFP RSR_AAA&RRR_AAA	◆				233.06 ± 17.71	1.44 ± 0.13	6
α-YFP L9'F + β-YFP	■	0.61	7.27 ± 2.85	1.14 ± 0.24	185.35 ± 50.16	1.99 ± 0.82	6
α-YFP L9'F + β-YFP RSR_AAA	■	0.53	3.91 ± 1.69	1.64 ± 0.69	95.28 ± 30.91	2.24 ± 1.27	12
α-YFP L9'F + β-YFP RRR_AAA	■				83.31 ± 21.70	0.94 ± 0.17	6
α-YFP L9'F + β-YFP RSR_AAA&RRR_AAA	■	0.39	2.52 ± 0.83	1.81 ± 0.83	243.71 ± 44.61	2.50 ± 0.98	6
α-YFP + β-YFP Y182F	■				380.41 ± 105.68	1.14 ± 0.24	6
α-YFP L9'F + β-YFP Y182F	■				159.81 ± 20.71	1.07 ± 0.12	6
α-YFP + β-YFP Y182F RSR_AAA	■				365.49 ± 48.35	1.35 ± 0.17	6
α-YFP L9'F + β-YFP Y182F RSR_AAA	■				45.08 ± 5.37	1.21 ± 0.14	6
α-YFP + β-YFP Y232A	■				377.56 ± 44.80	1.04 ± 0.08	6
α-YFP L9'F + β-YFP Y232A	■				304.01 ± 31.67	1.03 ± 0.10	6
α-YFP Y261A + β-YFP	■				682.81 ± 34.37	3.04 ± 0.38	6
α-mYFP + β-mYFP	●	0.29	3.58 ± 3.66	1.16 ± 0.80	170.46 ± 32.61	2.16 ± 0.79	6
α-mYFP L9'F + β-mYFP	●	0.49	1.35 ± 0.47	1.36 ± 0.85	185.58 ± 62.75	2.24 ± 1.65	6
α-mYFP + β-mYFP L9'F	●	0.48	0.68 ± 0.15	2.5 ± 1.25	418.17 ± 165.12	1.75 ± 1.00	6
α-mYFP L9'F + β-mYFP L9'F	●	0.54	0.90 ± 0.24	2.13 ± 1.15	429.33 ± 156.96	2.5 ± 2.00	6
α-mYFP + β-mYFP Y182F	▶				549.07 ± 50.34	2.11 ± 0.35	6
α-mYFP L9'F + β-mYFP Y182F	▶	0.23	1.59 ± 0.85	1.36 ± 0.85	408.08 ± 49.78	2.5 ± 0.65	6
α-mYFP + β-mYFP L9'F Y182F	▶				134.27 ± 19.92	0.97 ± 0.11	6
α-mYFP L9'F + β-mYFP L9'F Y182F	▶				78.38 ± 14.54	1.01 ± 0.15	6
α-mYFP + β-mYFP Y182F RSR_AAA	▲	0.50	9.73 ± 3.98	2.50 ± 2.04	218.57 ± 91.48	2.5 ± 2.47	6
α-mYFP L9'F + β-mYFP Y182F RSR_AAA	▲	0.63	3.35 ± 1.36	1.04 ± 0.27	196.26 ± 49.81	2.5 ± 1.64	6
α-mYFP + β-mYFP L9'F Y182F RSR_AAA	▲	0.33	4.70 ± 2.98	1.00 ± 0.39	265.91 ± 32.59	2.5 ± 0.61	6
α-mYFP L9'F + β-mYFP L9'F Y182F RSR_AAA	▲	0.29	9.92 ± 20.71	1.00 ± 1.12	340.09 ± 103.09	2.5 ± 1.41	6
α-mYFP + β-mYFP Y232A	◀				174.49 ± 38.29	0.83 ± 0.10	6
α-mYFP L9'F + β-mYFP Y232A	◀	0.31	2.61 ± 1.51	1.07 ± 0.48	343.17 ± 52.89	2.5 ± 0.75	6
α-mYFP + β-mYFP L9'F Y232A	◀				311.27 ± 85.60	1.18 ± 0.29	6
α-mYFP L9'F + β-mYFP L9'F Y232A	◀				209.70 ± 69.82	1.22 ± 0.38	6
α-mYFP + β-mYFP Y232A RSR_AAA	▼	0.27	1.81 ± 4.53	1.08 ± 1.88	141.98 ± 69.99	1.73 ± 1.27	6
α-mYFP L9'F + β-mYFP Y232A RSR_AAA	▼	0.36	21.58 ± 53.57	1.00 ± 0.89	277.64 ± 85.65	2.30 ± 1.31	6
α-mYFP + β-mYFP L9'F Y232A RSR_AAA	▼	0.20	3.72 ± 2.11	2.04 ± 1.76	371.81 ± 60.99	1.99 ± 0.54	6
α-mYFP L9'F + β-mYFP L9'F Y232A RSR_AAA	▼	0.22	3.35 ± 3.06	2.5 ± 4.08	333.88 ± 96.74	2.50 ± 1.34	6

Table 4-1. Ivermectin activation parameters for various GluCl mutant receptors. Parameters correspond to concentration-response curves in Figures 4-4A, 4-6A, 4-7A,B,C, 4-8B, 4-9C,D,F, 4-11B,C,D, 4-12A,B. The EC_{50} and Hill coefficient values represent the mean ± SEM for the number of measurements (n) obtained.

protein tags. Thus, the mYFP mutation restored the high IVM sensitivity component previously lost upon addition of (β)Y182F. The optimized GluCl α-mYFP L9'F + β-mYFP Y182F RSR_AAA receptor is more sensitive to IVM than the original receptor silencing tool by ~2 orders of magnitude (Figure 4-12B, Table 4-1).

Biphasic response is not due to potentiation

Every instance of increased IVM sensitivity transpired as part of a biphasic response. The persistent low sensitivity component and the deleterious effect of including a glutamate insensitive mutation on the high sensitivity component were perplexing. With regard to the latter issue, it is conceivable that low (nM) glutamate present in the extracellular fluid could contribute to the high sensitivity component of the IVM response, since the (α)L9'F mutation has increased sensitivity for glutamate in addition to IVM (Chapter 3, Figure 3-6). Furthermore, examples of IVM potentiation of the glutamate response, as well as, glutamate potentiation of the IVM response have both been reported for GluCl[40-42]. If the high sensitivity component of the (α)L9'F biphasic response is due to potentiation by low levels of extracellular glutamate, then a glutamate insensitive mutation would withdraw the effect.

To test this possibility, a complex FlexStation assay was conducted. A large concentration range of glutamate (from 1 nM to 5 mM) was sampled in the presence of 10 nM IVM. This concentration of IVM was chosen to represent high sensitivity activation, and an additional '10 nM IVM only' dose was included for response normalization. This approach probed the possibility of potentiation in both directions, identifying (1) whether low concentrations of glutamate potentiate the 10 nM IVM response, and (2) if the presence of 10 nM IVM potentiates the glutamate response, both at nonactivating and activating concentrations of glutamate.

Using the mYFP-tagged constructs, the WT, (α)L9'F, (β)Y182F, and the combined (α)L9'F + (β)Y182F receptors were assayed. The mean '10 nM IVM only'

response was as expected; the (α)L9'F mutation increases IVM sensitivity and addition of the (β)Y182F mutation abolishes this effect (Figure 4-13A). For each receptor, low glutamate (1 nM to 20 μM) does not potentiate the 10 nM IVM response, as normalization results in a value of 1 (Figure 4-13B). For the (α)L9'F receptor in particular, higher concentrations of glutamate do not increase the magnitude more than that already induced by 10 nM IVM, confirming that extracellular glutamate levels do not influence the high sensitivity component of the biphasic response. Furthermore, a plot of the raw concentration-response relationship of glutamate in the presence of 10 nM IVM is essentially the same as that of glutamate alone (Figure 4-13C). A ratio of the responses at 1 mM glutamate reveals, if anything, that the presence of IVM might slightly recover some glutamate sensitivity of the (β)Y182F mutant receptor, but it does not potentiate the glutamate response of the (α)L9'F mutant receptor (Figure 4-13D).

Biphasic response is due to stoichiometry

A second possible explanation for the biphasic response, discussed in Chapter 3, is a shift in receptor stoichiometry, i.e., a shift in the ratio of α:β subunits in the assembled pentamer. The presence of multiple stoichiometric populations with differing agonist sensitivities can result in a multicomponent concentration-response curve. In FlexStation assays, the expression of GluCl α homomers consistently produces a monophasic curve, while co-expression of α with the β subunit has yielded biphasic concentration-response curves for several receptors, most prominently in the case of individual (α)L9'F and (β)RSR_AAA mutant receptors. For a simple test to determine if stoichiometry could be

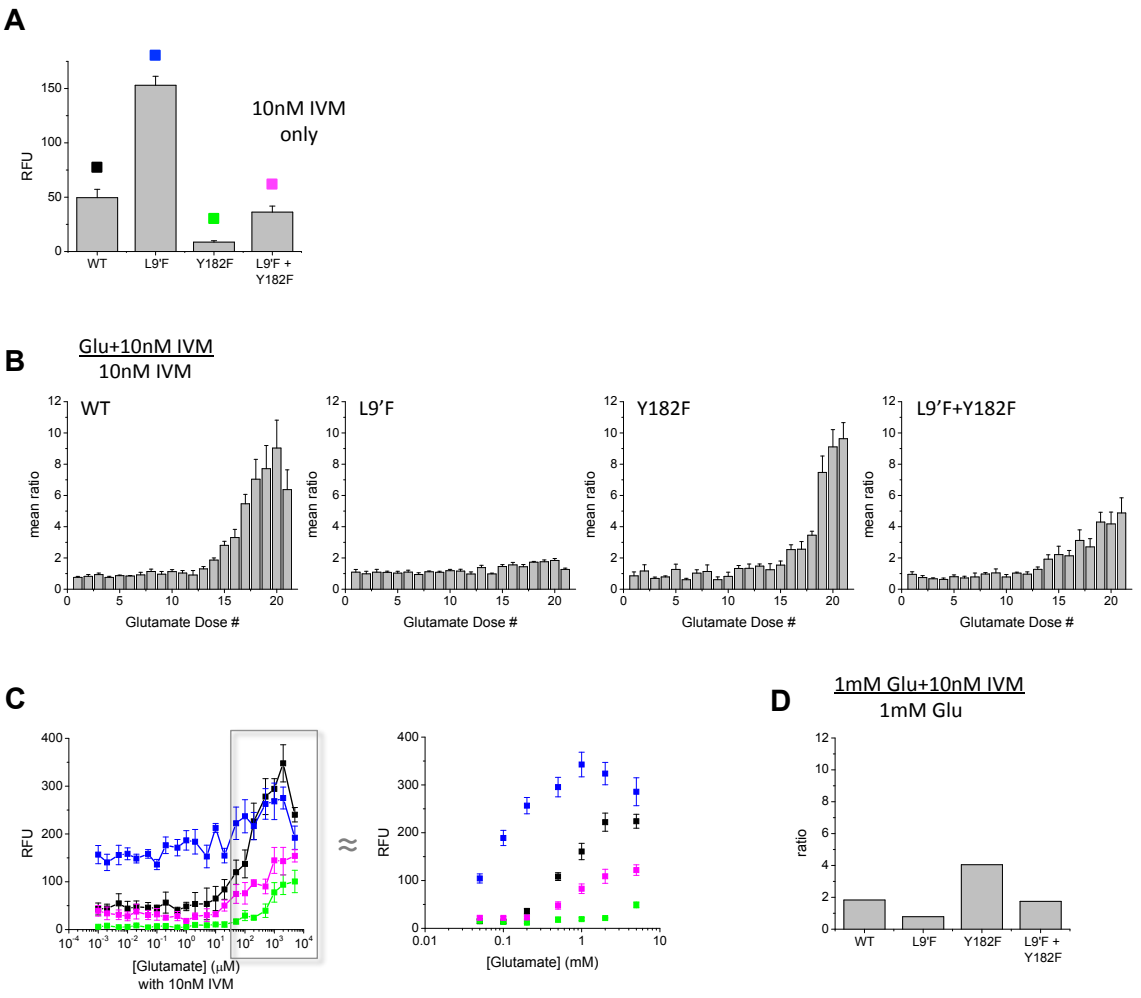

Figure 4-13. Potentiation does not explain the biphasic response of (α)L9'F mutant receptors. IVM activation was assayed using the FlexStation. *A.* Mean response of WT, (α)L9'F, (β)Y182F, and (α)L9'F + (β)Y182F receptors to a '10 nM IVM only' application (for normalization). *B.* Signals of twenty-one increasing concentrations of glutamate in the presence of 10 nM IVM normalized by the '10 nM IVM only' response. Low concentrations of glutamate (1 nM to 20 μM) do not potentiate the 10 nM IVM response. *C.* Raw RFU signal for activating concentrations of glutamate in the presence of 10 nM IVM (last 7 doses) is comparable to that of glutamate alone. *D.* Response ratio for 1 mM glutamate shows 10 nM IVM does not potentiate the glutamate response of (α)L9'F mutant receptors.

responsible for the biphasic response of these two mutant receptors (tagged with mYFP), different ratios of α and β DNA (1:1, 4:1, and 1:4) were transfected into HEK293 cells and assayed on the FlexStation. As previously observed for both cases, a 1:1 ratio

produced a two-component concentration-dependent relationship. Biasing for β (1:4), in general, showed no further increase in IVM sensitivity, while biasing for α (4:1) indeed showed a decrease in IVM sensitivity (Figure 4-14). Therefore, incorporation of the β subunit confers increased sensitivity to IVM, but requires unbiased co-expression with the α subunit for the maximum effect. This confirms multiple receptor populations are contributing to the biphasic concentration-response curve but the stoichiometric identities remain to be determined.

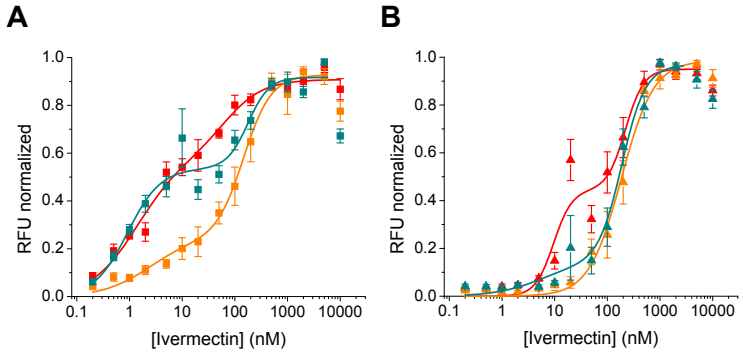

		1st comp	EC_{50} (μM)	Hill	EC_{50} (μM)	Hill	n
■	α-mYFP L9'F + β-mYFP 1:1	0.64	1.37 ± 1.16	1.00 ± 0.40	65.16 ± 70.35	1.17 ± 0.86	6
■	α-mYFP L9'F + β-mYFP 4:1	0.26	2.38 ± 2.64	1.00 ± 0.61	147.24 ± 27.16	1.66 ± 0.42	6
■	α-mYFP L9'F + β-mYFP 1:4	0.58	0.92 ± 0.29	1.39 ± 0.56	178.36 ± 61.16	2.17 ± 1.51	6
▲	α-mYFP + β-mYFP RSR_AAA 1:1	0.47	9.56 ± 3.60	2.50 ± 1.90	220.21 ± 76.06	2.50 ± 2.03	6
▲	α-mYFP + β-mYFP RSR_AAA 4:1				184.22 ± 16.99	1.42 ± 0.15	6
▲	α-mYFP + β-mYFP RSR_AAA 1:4	0.15	5.58 ± 20.08	1.00 ± 1.64	188.88 ± 42.35	1.95 ± 0.78	6

Figure 4-14. Multiple receptor stoichiometries explain the biphasic response. IVM activation was assayed using the FlexStation. *A.* Different ratios of α and β DNA (1:1, 4:1, and 1:4) were transfected into HEK293 cells. The 1:1 ratio (*red*) produced the expected two-component concentration-dependent relationship for (α)L9'F (*panel A.*) and (β)RSR_AAA (*panel B.*) mutant receptors. Biasing for β (1:4, *aqua*) does not further enhance IVM sensitivity. Biasing for α (4:1, *orange*) decreases in IVM sensitivity. Ivermectin activation parameters are presented in the corresponding table.

Retention mutations are not sufficient for β homomer surface expression

The fluorescent protein insertions allow direct visualization and localization of GluCl receptors expressed in a cell. TIRF images of HEK293 cells show GluCl α homomers and αβ heteromers are expressed at the plasma membrane; GluCl β homomers are not (Figure 4-15). Specifically, the α-mYFP subunit shows plasma membrane fluorescence when transfected alone or cotransfected with β(WT). Plasma membrane fluorescence is also observed when the β-mYFP subunit is cotransfected with α(WT). Transfection of the β-mYFP subunit alone, however, displays exclusive ER retention, as indicated by a reticulated pattern of fluorescence and a lack of hair-like filopodia at the periphery. GluCl β-mYFP subunits bearing either the individual RSR_AAA or RRR_AAA mutations, or the double RSR_AAA&RSR_AAA mutation, display a similar fluorescence pattern as seen for the β-mYFP homomer (Figure 4-16). Thus, mutation of the putative ER retention motifs in the β subunit is not sufficient to allow plasma membrane expression of β homomers.

Western blot analysis was performed to determine if the putative ER retention mutations were increasing heteromeric incorporation of the β subunit at the plasma membrane. Receptors composed of untagged α and the different mYFP-tagged β subunits were expressed in HEK293 cells and probed for only β subunit expression using a GFP antibody. Whole-cell lysate analyses suggest slightly increased protein expression levels for mutated β subunits, despite a similar trend in nonspecific staining (Figure 4-17A). Biotinylation of surface exposed receptors indicates no difference in the number of β subunits assembled into pentamers at the plasma membrane (Figure 4-17B). It should

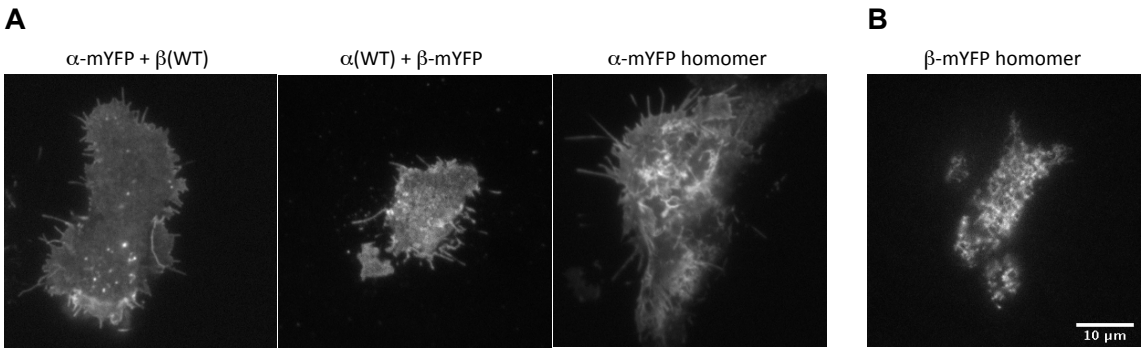

Figure 4-15. GluCl subunit expression in HEK293 cells. *A*. TIRF images show GluCl αβ heteromers and α homomers are expressed at the plasma membrane. The α-mYFP subunit shows plasma membrane fluorescence when transfected alone or cotransfected with β(WT). Plasma membrane fluorescence is also observed when the β-mYFP subunit is cotransfected with α(WT). *B*. GluCl β homomers are not expressed at the plasma membrane. Transfected alone, the β-mYFP subunit displays a reticulated pattern of fluorescence indicative of ER retention and a lack of hair-like filopodia at the periphery.

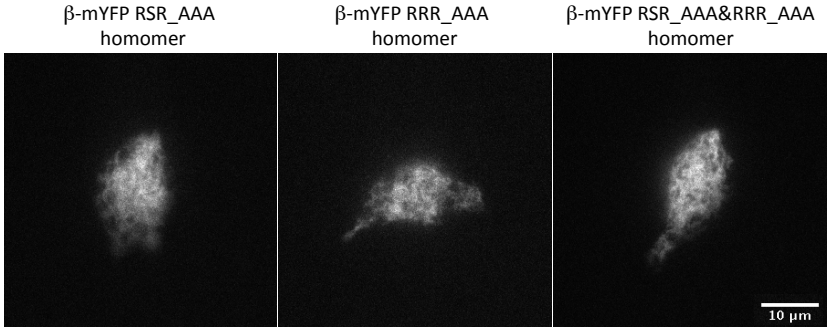

Figure 4-16. GluCl β homomers containing putative ER retention motif mutations still do not exit the ER. TIRF images of HEK293 cells transfected with β-mYFP subunits bearing either the individual putative ER retention motif mutations (RSR_AAA or RRR_AAA) or the double mutation (RSR_AAA&RRR_AAA) show a fluorescence pattern similar to β-mYFP homomers.

be noted that protein bands in these Western blot experiments were visualized by enhanced chemiluminescence with horseradish peroxidase and exposed on radiography film. This method has a limited linear dynamic range so quantification in these instances may be unreliable.

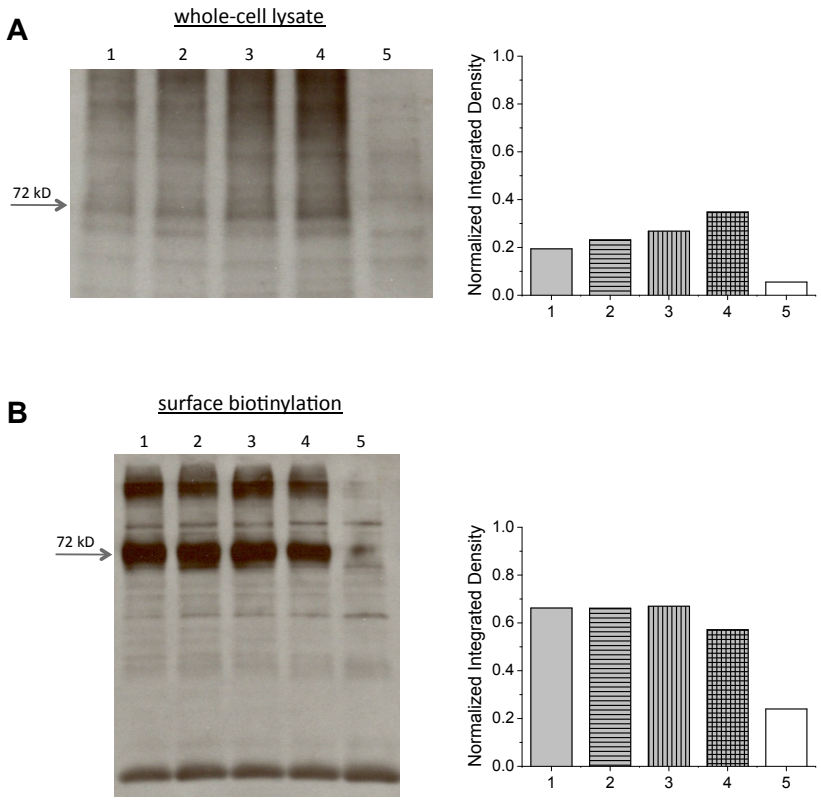

Figure 4-17. Western blot analysis of GluCl β-mYFP subunit expression in HEK293 cells. Quantification of mutated β-mYFP subunits obtained (*A*.) from whole-cell lysate preparations for total protein expression and (*B*.) using a surface biotinylation assay for plasma membrane expression. Protein bands of transferred gels were detected using rabbit anti-GFP primary antibody and goat anti-rabbit HRP secondary antibody. Cells were transfected with the following subunits:

1. α(WT) + β-mYFP
2. α(WT) + β-mYFP RSR_AAA
3. α(WT) + β-mYFP RRR_AAA
4. α(WT) + β-mYFP RSR_AAA&RRR_AAA
5. nontransfected control

RSR mutation increases β subunit expression

HEK293 cells are a convenient system for studying receptor function. However, it is possible that receptor trafficking events in HEK293 cells could be different from that of neurons, especially with respect to stoichiometric preference. Primary neuronal cultures provide a more appropriate environment for *in vitro* experiments. To detect differences in the neuronal expression of GluCl, fluorescently tagged subunits were transfected into embryonic rat hippocampal neurons. Preliminary confocal images in Figure 4-18 illustrate a deficient expression pattern for GluCl β homomers with minimal extension into the processes and comparatively few fluorescent neurons per imaging dish. GluCl α homomers, and various αβ heteromers, on the other hand, exhibit extensive fluorescent projections with no discernable differences. Fluorescence intensity of transfected neurons varies greatly from cell-to-cell within an imaging dish, so direct measure of integrated density is often uninformative. Since neurons have ER compartments throughout much of the length of their processes, it can be difficult to distinguish between receptors retained in the ER and those expressed at the plasma membrane without the use of colocalization markers.

To target only receptors expressed at the plasma membrane, a live cell immunofluorescent surface staining protocol was devised. A V5 epitope tag was added to the C-terminus of both α and β subunits (Figure 4-19A). To ensure that addition of the V5-tags did not disrupt protein folding and pentameric assembly, tagged subunits were assayed for channel function in HEK293 cells using the FlexStation. The V5-tagged constructs formed functional channels similar to WT-mYFP when the V5 tag was present on either α or β subunits. Receptors with V5 tags on both α and β subunits did not show

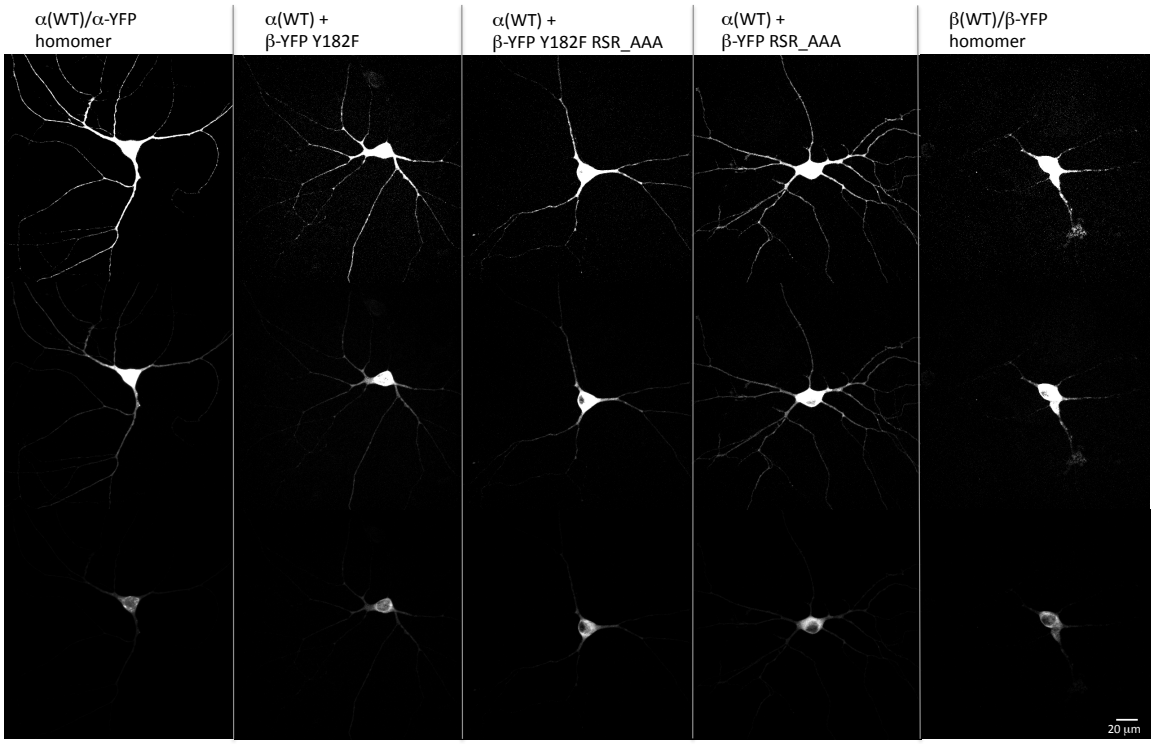

Figure 4-18. Confocal images of transfected rat hippocampal neurons with fluorescent GluCl receptors. Image brightness and contrast was adjusted to compare neuronal processes and soma separately. Extensive fluorescent projections are apparent for GluCl α homomers and various αβ heteromers. A deficient expression pattern is observed for GluCl β homomers with minimal extension into the processes.

a biphasic response, suggesting a slight interference of heteromeric receptor assembly or function with five tagged subunits (Figure 4-19B). Even though inclusion of these penta-tagged receptors would not be critical for data interpretation in the following experiment, they were sampled for the sake of completeness.

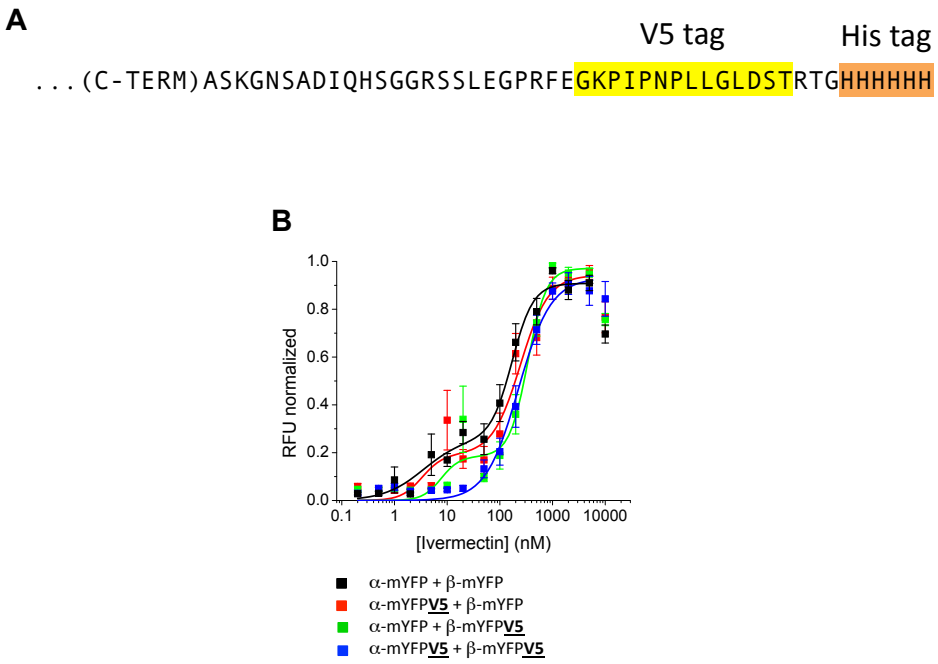

Figure 4-19. Addition of a C-terminal V5 epitope tag does not disrupt pentameric assembly and function. *A*. The V5 epitope tag (also including a 24-residue linker and a 6-His tag; see Materials and Methods) was added to the C-terminus of both α and β subunits. *B*. Fluorescently labeled heteromeric receptors with V5 tags present on either α or β (*red and green*) show a normalized IVM concentration-response curve similar to WT-mYFP. Receptors with V5 tags on both α and β subunits (*blue*) did not show the same two-component response, but had comparable functionality. IVM activation was assayed using the FlexStation.

Rat hippocampal cultures were transfected with α-mYFP and β-mYFP bearing a V5 tag on either or both subunits for three heteromeric receptor conditions: GluCl α-mYFPV5 + β-mYFP, GluCl α-mYFP + β-mYFPV5, and GluCl α-mYFPV5 + β-mYFPV5. Surface exposed receptors were labeled with anti-V5 primary and fluorescent Alexa 555-conjugated secondary antibodies for confocal imaging. Yellow fluorescence contributed by both subunits (mYFP) represented total protein expression, including receptors remaining in subcellular compartments and expressed at the plasma membrane. Red fluorescence from live cell immunostaining (Alexa 555) labeled only subunits

expressed at the cell surface. Red and yellow fluorescent images were acquired as z-stacks and examined for colocalization on a pixel-by-pixel basis. The intensity correlation between a pair of pixels was scored by calculating the normalized mean deviation product (nMDP, see Methods) and visualized on a color scale. Values range from −1 to 1, with values less than zero representing exclusion in cold colors, and values greater than zero signifying colocalization in hot colors (Figure 4-20A). Thus, for a given pixel, a perfect nMDP value of 1 indicates that maximum intensity yellow fluorescence is colocalized with maximum intensity red fluorescence. An nMDP value of −1 results when a pair of pixels contains maximum fluorescence intensity of one color and zero fluorescence intensity for the other color. An nMDP value of zero denotes black background. All pixels including and deviating from these extremes can be represented by a histogram (Figure 4-20B). Colocalization is evidenced by all positive nMDP values ($0< x \leq 1$) and occurs only for receptors expressed at the surface. Hence, greater nMDP values indicate a greater amount of GluCl expression at the plasma membrane.

The average of all positive nMDP values represents total surface expression levels of receptor (note, surface expression levels are not well represented by the sum of all positive nMDP values as the sum is distorted by the size and number of cells imaged). Heteromeric receptors show the same level of surface expression regardless of whether the V5 tag was on the α or β subunit (Figure 4-21A). Lower values were observed when V5 tags were on both subunits, suggesting either lower expression levels or inefficient labeling of all subunits. Transfection of individual V5-tagged subunits corroborated the previous HEK293 cell observations that α homomers are expressed at the plasma membrane of neurons at levels comparable to αβ heteromers, but that β homomers are

not. Heteromeric receptors bearing putative ER retention mutations were assayed in the same format (Figure 4-21B). Incorporation of the (β)RRR_AAA or the double (β)RSR_AAA&RRR_AAA mutations resulted in lower surface expression levels but in a similar manner as WT-mYFP (i.e., less expression when V5 tags are on both α and β subunits). Receptors with the (β)RSR_AAA mutation had the same surface expression levels as WT-mYFP receptors, but in this case, levels were not reduced when V5 tags were on both α and β subunits.

A comparison of the average number of nMDP = 1 values shows that a greater number of maximally correlated pixels occur with V5-tagged α than V5-tagged β when WT and the (β)RRR_AAA and (β)RSR_AAA&RRR_AAA mutant receptors are expressed as heteromers (Figure 4-21C). The average number of nMDP = 1 values is again low when the V5 tag is present on both subunits for these receptors. The (β)RSR_AAA heteromeric receptors, on the other hand, show the opposite result. Maximal colocalization occurs more often for V5-tagged β than V5-tagged α, and the average number of nMDP = 1 values is high when the V5 tag is present on both subunits. Altogether, immunofluorescent results suggest that mutation of the putative β subunit RSR ER retention motif does not increase the total number of receptors trafficked to the plasma membrane, but it may increase the number of β subunits incorporated into the pentamer, shifting the stoichiometric ratio of assembled receptors.

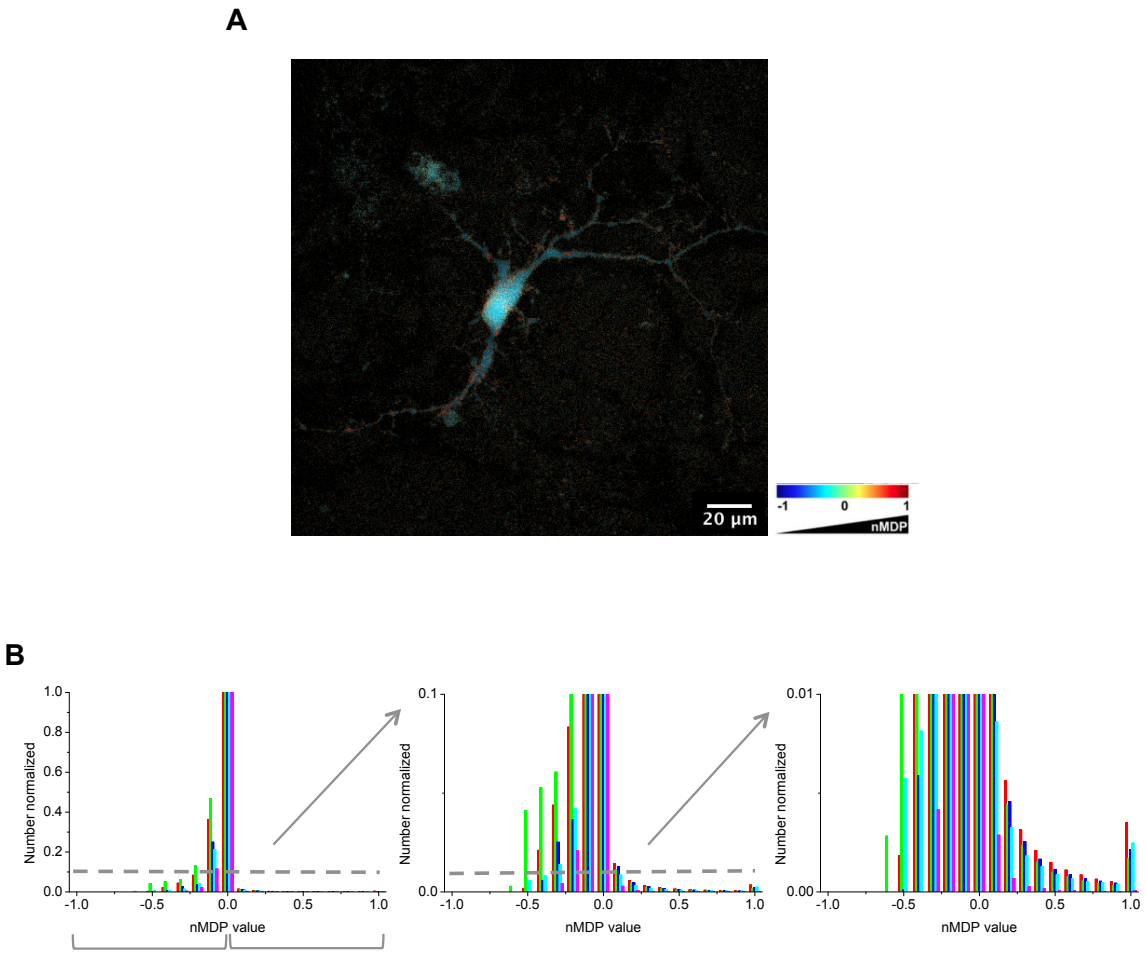

Figure 4-20. Colocalization of immunofluorescent surface staining and intrinsic mYFP fluorescence of GluCl. *A*. Confocal image of GluCl α-mYFPV5 + β-mYFP viewed with the colocalization color scale. (All subunits are fluorescently labeled; only the α subunits expressed at the surface are immunostained.) An nMDP correlation value is calculated for each pixel based on fluorescence intensity. Values range from −1 to 1. Colocalization is shown in hot colors (nMDP > 0); Exclusion is shown in cold colors (nMDP < 0). *B.* Sample histogram of nMDP values. The y-axis is zoomed in for each panel. All positive nMDP values (representing colocalization) indicate expression levels at the surface. Colored bars reflect constructs in Figure 4-21.

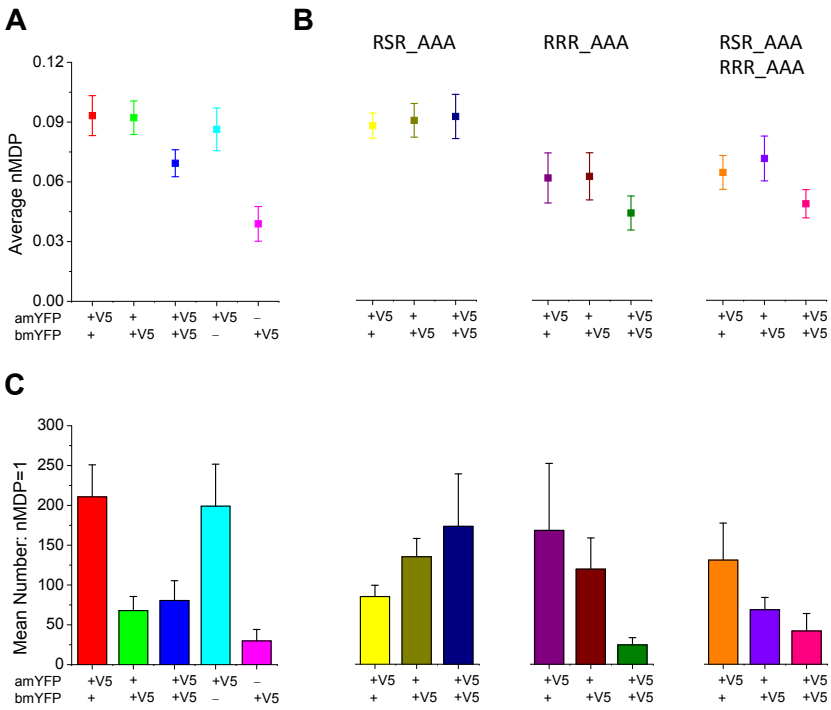

D

	GluCl channel	n cells
■	α-mYFP**V5** + β-mYFP	41
■	α-mYFP + β-mYFP**V5**	49
■	α-mYFP**V5** + β-mYFP**V5**	47
■	α-mYFP**V5** homomer	31
■	β-mYFP**V5** homomer	11
■	α-mYFP**V5** + β-mYFP RSR_AAA	73
■	α-mYFP + β-mYFP RSR_AAA**V5**	50
■	α-mYFP**V5** + β-mYFP RSR_AAA**V5**	34
■	α-mYFP**V5** + β-mYFP RRR_AAA	21
■	α-mYFP + β-mYFP RRR_AAA**V5**	20
■	α-mYFP**V5** + β-mYFP RRR_AAA**V5**	12
■	α-mYFP**V5** + β-mYFP RSRRRR_AAA	21
■	α-mYFP + β-mYFP RSRRRR_AAA**V5**	15
■	α-mYFP**V5** + β-mYFP RSRRRR_AAA**V5**	19

Figure 4-21. The RSR_AAA mutation increases β subunit surface expression but not total receptor surface expression. Confocal colocalization analysis of surface labeled receptors. *A*. Average of all positive nMDP values represents total surface expression levels. GluCl α homomers are expressed at the plasma membrane, β homomers are not. The same level of heteromer surface expression was obtained regardless of whether the V5 tag was on the α or β subunit. Lower expression was observed when V5 tags were on both subunits. *B*. Receptors bearing putative ER retention motif mutations do not increase total receptor surface expression compared to V5-tagged WT (*panel A*.). *C*. Average number of nMDP = 1 values indicates more maximally correlated pixels occur with V5-tagged α than V5-tagged β when WT, RRR_AAA, and RSR_AAA&RRR_AAA receptors are expressed as heteromers. The RSR_AAA mutant receptor shows more maximal colocalization with V5-tagged β subunit than V5-tagged α, suggesting a shift in stoichiometry. *D*. Legend of constructs indicated by color and the number of cells sampled for each.

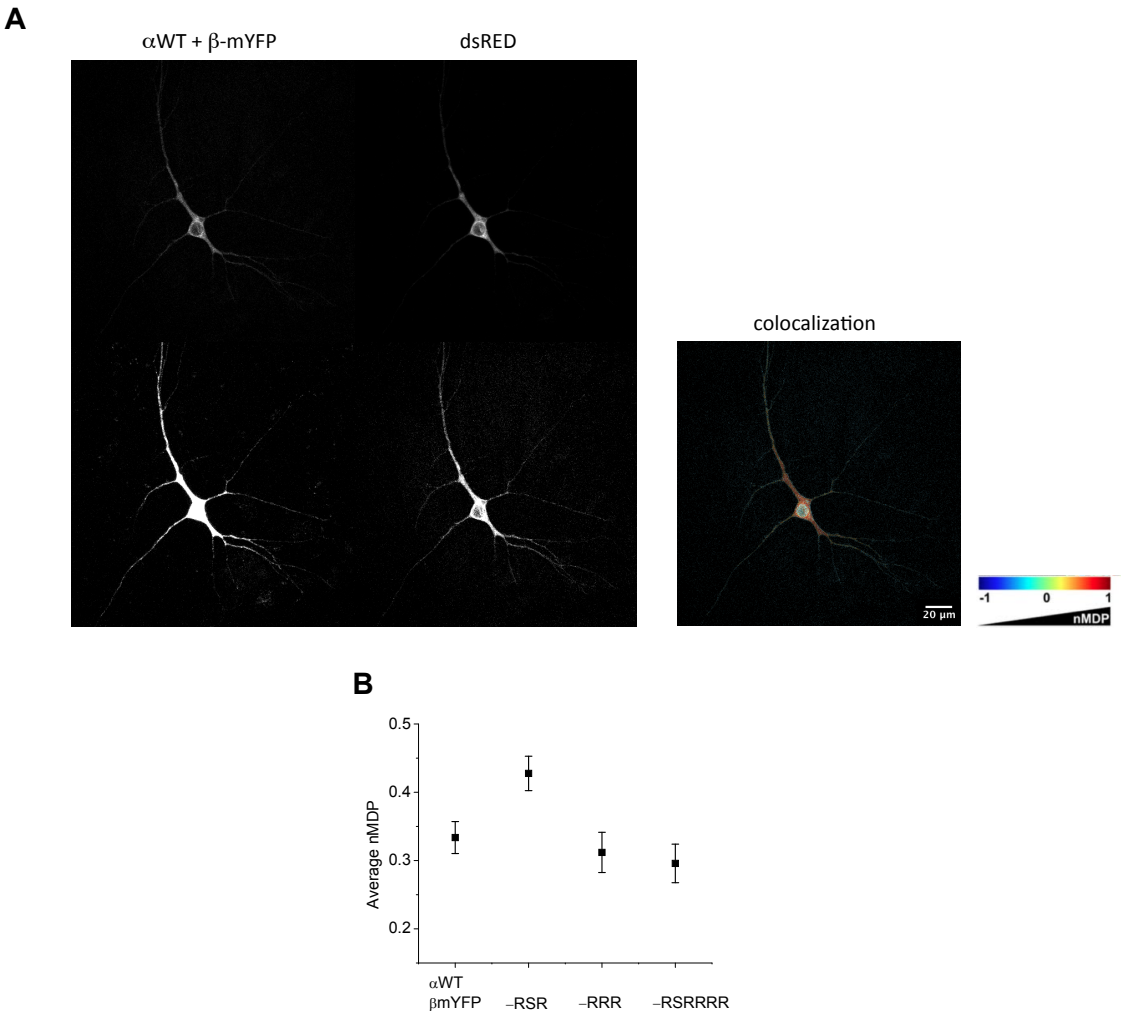

Figure 4-22. The RSR_AAA mutation increases the amount of β subunit in the ER. *A*. Confocal images of GluCl α(WT) + β-mYFP and dsRED (ER marker) viewed independently and with colocalization color scale. Image brightness and contrast was adjusted to compare neuronal processes and soma separately. *B*. Average of all positive nMDP values represents the extent of β subunit localization in the ER. Mutation of the (β)RSR motif probably prevents ER-associated degradation of the β subunit.

Newly synthesized, improperly folded, or unassembled Cys-loop subunits remaining in the ER are degraded rapidly[43-47]. Mutation of an ER retention motif may influence subunit degradation. To determine the relative amounts of WT and mutated β subunits remaining in the ER, a similar pixel-by-pixel colocalization analysis was used.

Rat hippocampal neurons were cotransfected with α(WT) and various β-mYFP subunits along with the fluorescent ER marker, dsRED. Once again, the (β)RSR_AAA mutant was significantly different from WT, (β)RRR_AAA and (β)RSR_AAA&RRR_AAA receptors, showing increased colocalization with ER marker (Figure 4-22). This suggests that the β-mYFP RSR_AAA subunit is not being degraded at the same rate as β-mYFP, leaving more available for heteromeric assembly with α subunits.

An optimized neuronal silencing tool

Mutational screening in HEK293 cells lead to an engineered receptor with increased sensitivity to IVM. Functional data implied that the (β)RSR_AAA mutation increases β subunit incorporation in HEK293 cells and imaging experiments confirmed this mutational effect in neurons. To determine if the newly engineered GluCl α-mXFP L9'F + β-mXFP Y182F RSR_AAA receptor is indeed an improved silencing tool over the original α-XFP + β-XFP Y182F receptor, *in vitro* recordings of IVM-induced spike inhibition were obtained from rat hippocampal neurons. Initially, gap-free recordings were acquired in current clamp mode with bath perfusion of IVM. Continuous recordings were interrupted by two current-injection step protocols, (-100 to 250 pA, 25 pA increments), one following two minutes of bath solution (baseline) and the other after 5 min of 5 nM IVM perfusion. Spontaneous spiking varied from zero to high frequency bursts for transfected and nontransfected neurons. A decrease in spike frequency was not always observed within the duration of IVM application, but greater current injection was often required for spike generation following IVM perfusion (Figure 4-23A).

Several concerns were associated with the bath perfusion protocol including inherent spike variability and run-down effects from internal solution exchange. It also required large solution volumes and the ability to maintain seal resistance for an extended period of time (~10 minutes). Furthermore, variations in real-time silencing may not accurately depict improved sensitivity since it may require up to 15 minutes to achieve full spike inhibition by IVM[1]. For that reason, an alternative pre-incubation procedure was used to ensure adequate time for IVM activation and to avoid submitting patched neurons to lengthy perfusions. Cultured neurons were incubated with 0, 1, or 20 nM IVM for 15 minutes at 37°C/5% CO_2, washed and then recorded for a V-I relationship using the current-injection step protocol (Figure 4-23B and 4-24A). Nontransfected neurons were not influenced by the presence of IVM and construct expression itself had no effect on resting membrane potential (Figure 4-24C). The newly engineered GluCl α-mYFP L9'F + β-mYFP Y182F RSR_AAA receptor shows a significant increase in conductance (as determined by the inverse slope, Figure 4-24D) and a lower mean spike count (Figure 4-24B) for both 1 nM and 20 nM IVM compared to the original α-YFP + β-YFP Y182F silencing tool. Thus, GluCl α-mXFP L9'F + β-mXFP Y182F RSR_AAA, is an optimized construct for IVM-induced spike inhibition.

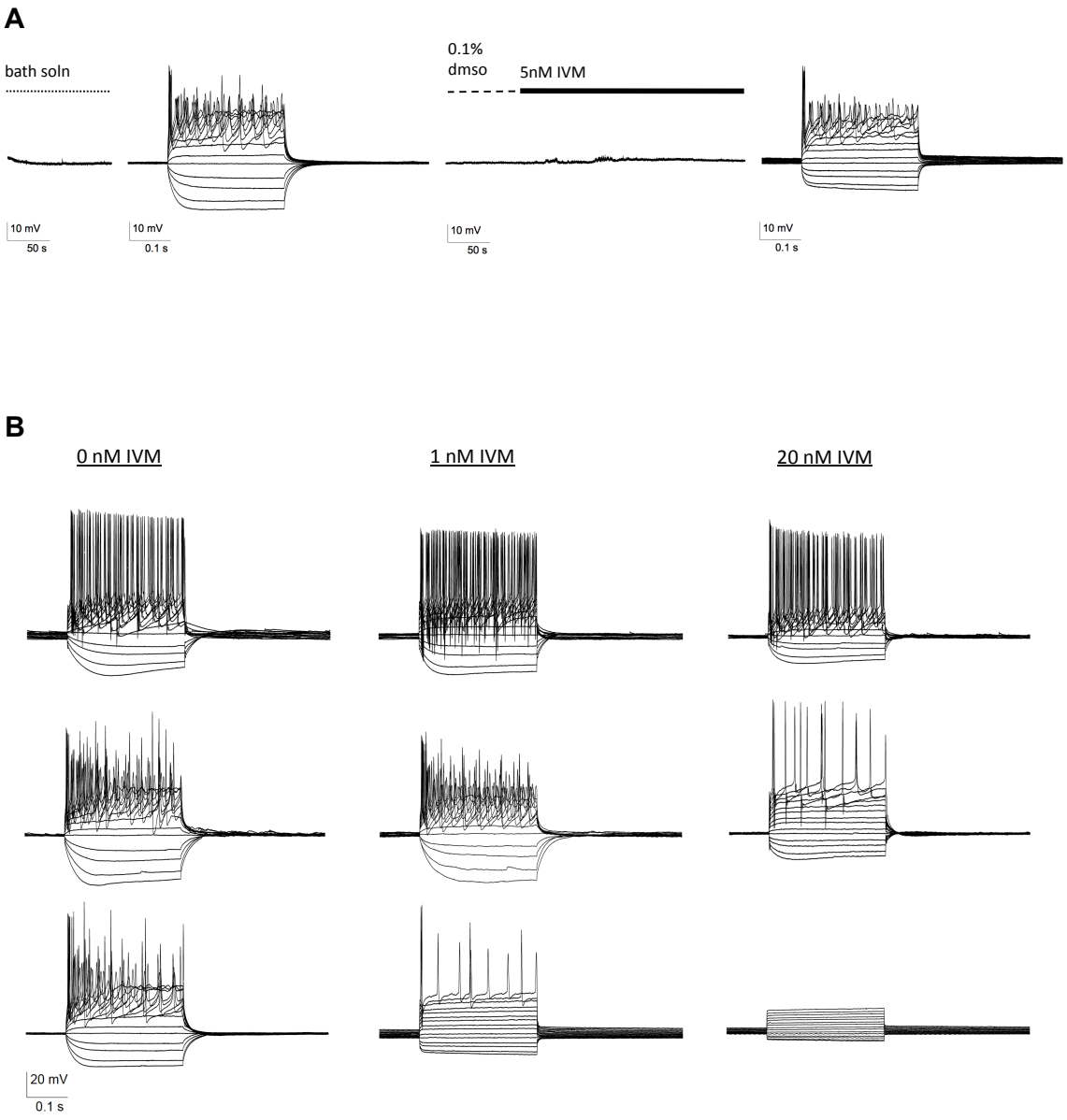

Figure 4-23. Protocols for neuronal silencing by GluCl/IVM *in vitro*. Current clamp recordings of rat hippocampal neuron firing were obtained in response to depolarizing current pulses (-100 to 250 pA, 25 pA increments). *A*. Continuous recording with IVM bath perfusion was a suboptimal method for comparative silencing effects. The neuron depicted was expressing the original silencing tool. (This neuron did not exhibit spontaneous firing.) *B*. A 15-minute pre-incubation of 0, 1, or 20 nM IVM better elucidated a concentration-dependent silencing effect. The optimized construct (α-mYFP L9'F + β-mYFP Y182F RSR_AAA; *bottom panel*), is more sensitive to IVM than the original silencing tool (α-YFP + β-YFP Y182F; *middle panel*), and nontransfected control neurons (*top panel*).

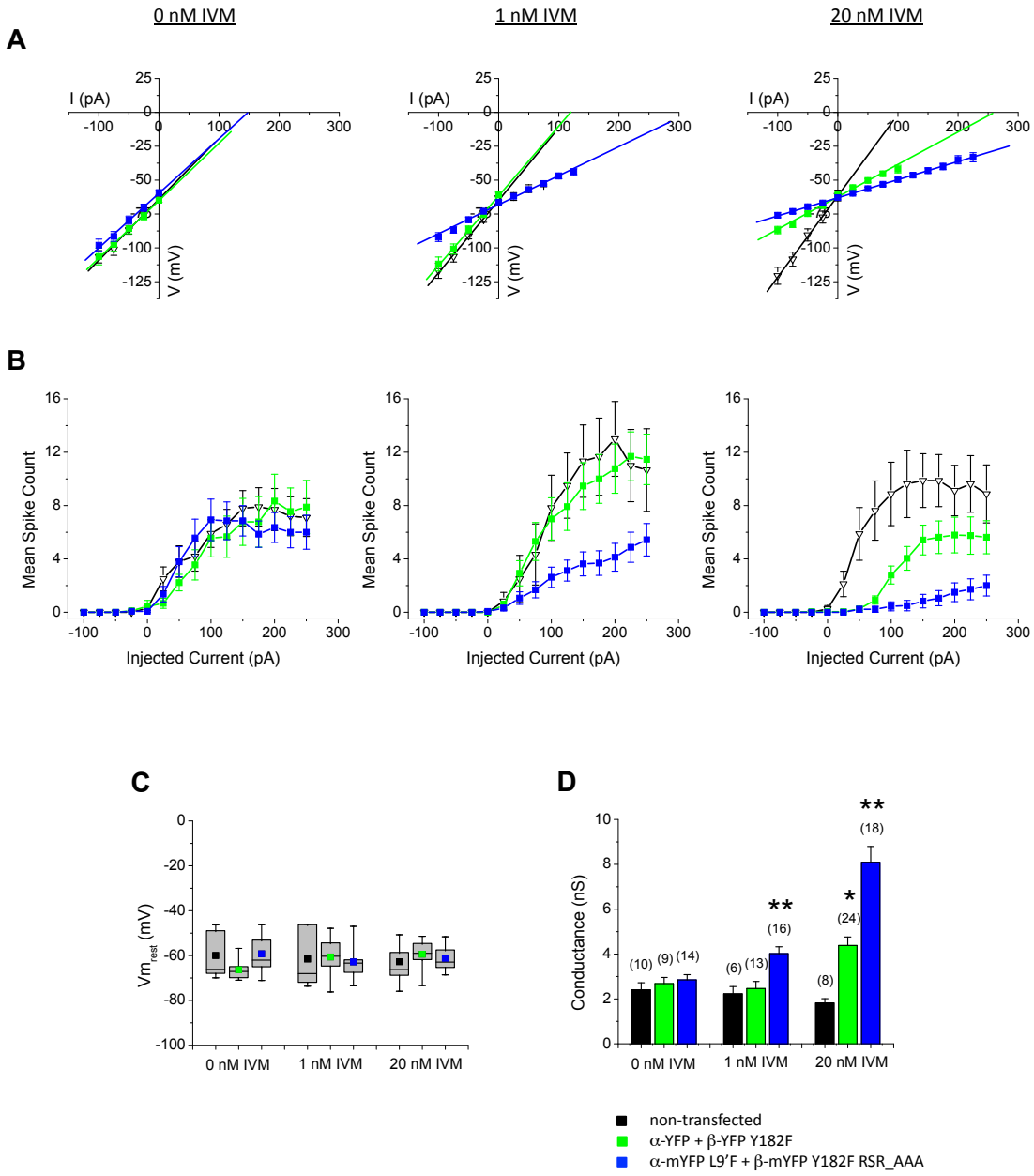

Figure 4-24. An optimized neuronal silencing tool. Current clamp recordings of rat hippocampal neuron firing in response to depolarizing current pulses (-100 to 250 pA, 25 pA increments) were obtained following a 15-min pre-incubation of 0, 1, or 20 nM IVM. *A*. V-I plots from neuronal cultures transfected with the optimized construct (α-mYFP L9'F + β-mYFP Y182F RSR_AAA) were compared to the original construct (α-YFP + β-YFP Y182F) and nontransfected neurons. The optimized receptor exhibits lower slope resistance at 1 and 20 nM IVM. *B*. The optimized receptor also reduced mean evoked spike counts at 1 and 20 nM IVM. *C*. Neither construct expression or the presence of IVM alone significantly altered the resting membrane potential. *D*. The optimized receptor induces a significant increase in conductance (determined by the inverse slope) at both 1 and 20 nM IVM compared to the original silencing tool.

Discussion

Previous reports state that both α and β subunits are required for neuronal silencing by IVM *in vitro* and *in vivo*[1,13]. Variability in GluCl channel expression levels, particularly with the β subunit, appeared responsible for whether or not an individual neuron was inhibited by IVM. It turns out that functional IVM-sensitive α homomers are also expressed at the plasma membrane and that enhanced β subunit incorporation can increase IVM sensitivity. A mixed presence of heteromeric and homomeric receptors within individual neurons may account for the observed variations in spike suppression.

The original GluCl silencing tool has been re-engineered, introducing three new amino acid modifications: the (α)L9'F and (β)RSR_AAA mutations increase IVM sensitivity, probably by altering receptor stoichiometry; the monomeric XFP mutation helps maintain the increased IVM sensitivity upon reintroduction of a glutamate insensitive mutation by relieving the adverse effects of fluorescent protein oligomerization on receptor stoichiometry and function.

Mechanisms of the optimized receptor

In Chapter 2, experiments involving (α)L9'F homomers and heteromers show incorporation of the β subunit significantly increases sensitivity to IVM. The transfection ratio experiment of the current study not only substantiates this claim, but also implies that the (α)L9'F mutation prefers or possibly promotes β subunit incorporation. Biasing for α subunit expression with a 4α:1β ratio still yields a two-component IVM

concentration-response curve for this mutant. Even the low sensitivity component of this curve (EC_{50} = 150 nM) is more sensitive than that of (α)L9'F homomers (EC_{50} = 450 nM). According to one theory of Cys-loop receptor assembly, subunits initially dimerize then two dimers subsequently incorporate a fifth subunit to form an assembled pentamer (reviewed in[48]). The (α)L9'F mutation may either promote α-β dimerization or hinder α-α dimerization by means of intermolecular forces or steric preferences, resulting in a predominantly heteromeric αβ receptor population including more β subunits per assembled receptor.

The fluorescent fusion proteins YFP and CFP are interchangeable between α and β subunits. However, presence of an XFP insertion in the α subunit reduced the IVM sensitivity of both α homomers and αβ heteromers compared to nontagged receptors, suggesting an interference with receptor function. Introduction of an A206K mutation for monomeric XFP alleviated this reduction. The mXFP tag also introduced a modest high IVM sensitivity component for the heteromeric nonmutant receptor and further enhanced the high sensitivity component of the heteromeric (α)L9'F mutant receptor, implying XFP oligomerization affected stoichiometry as well.

The β subunit requires masking of an arginine-based ER retention motif by co-assembly with the α subunit to exit the ER; β homomers are not trafficked to the plasma membrane. In the presence of α, the (β)RSR_AAA retention mutation increases the amount of β at the plasma membrane. The (β)RSR_AAA mutation also elevates β subunit levels in the ER, indicating that it does not simply enhance β subunit surface expression by reducing ER retention. Mutation of putative ER retention motifs alone

were not sufficient to allow surface expression of β homomers, suggesting an additional unknown quality control motif is likely involved in the retention mechanism. Instead, the (β)RSR_AAA mutation probably impedes ER-associated degradation of the β subunit, either directly, by preventing targeted degradation thereby prolonging its availability for α-β dimerization, or indirectly, by facilitating stable α-β dimer formation consequently preventing its degradation. Either way, the (β)RSR_AAA mutation promotes heteromeric receptor assembly evident by the biphasic IVM concentration-response curve. Though it is clear that α homomers are capable of forming functional channels at the plasma membrane, it is unknown to what extent their presence is maintained when β subunits are available. Limiting β subunit degradation may keep α homomer expression to a minimum. A reduced level of α subunit surface expression was confirmed with the (β)RSR_AAA mutation, however, it cannot be determined if the prevalence of α homomer expression was reduced or if the stoichiometry of αβ heteromeric expression was simply shifted to include fewer α subunits per assembled receptor.

Contrary to initial functional assays on the FlexStation, the (β)RSR_AAA mutation does not increase total surface expression. The magnitude of RFU signal from the FlexStation can be influenced by a number of variables, including cell density in the well, transfection efficiency, receptor expression levels, and changes in receptor efficacy and should therefore be interpreted with caution. Like the (α)L9'F mutation, the (β)RSR_AAA mutation gives rise to a biphasic IVM concentration-response, but a monophasic glutamate concentration-response. Though the (α)L9'F and (β)RSR_AAA mutations may not provide a homogeneous receptor population, the populations present have significantly increased IVM sensitivity compared to that of the original silencing

tool, likely eliminating a major contributing factor of suboptimal firing inhibition. During *in vitro* recordings, variability in spike suppression was observed from cell-to-cell with both the original and optimized receptor tools, but was comparable to the variable number of evoked spikes observed from a nontransfected cell. Smaller error bars in the mean spike counts suggest reduced variability in spike suppression with the optimized receptor.

Biphasic curves are due to shifts in stoichiometry

As mentioned, the biphasic concentration-response curve observed with heterologous expression of the optimized GluCl receptor in HEK293 cells is probably the result of multiple receptor populations. Other subunits of the Cys-loop receptor family are known to exist in multiple stoichiometries. For example, α4β2 nicotinic acetylcholine receptors (nAChRs) form two stoichiometric populations with subunit ratios of 2α:3β and 3α:2β constituting high and low sensitivity receptors, respectively[49-51]. The glycine receptor (GlyR), which is the closest mammalian homolog to GluCl, forms functional channels as α homomers and αβ heteromers in mammalian expression systems[52]. The α homomers predominate during embryonic and neonatal development while heteromeric αβ GlyRs exist in the adult[53], though the precise heteromeric stoichiometry, 3α:2β[54] or 2α:3β[55], has been debated.

It is not clear if the stoichiometric GluCl populations present in HEK293 cells coincide with those present in neurons. IVM concentrations required for GluCl activation in HEK293 cells are higher than that required for silencing in neurons. According to the

FlexStation assays of the current study, the IVM EC_{50} for αβ WT GluCl in HEK293 cells is around 100 nM. In neurons, the EC_{50} for IVM-induced conductance measurements of αβ WT GluCl was reportedly 1.3 nM[12]. The time allowed for IVM activation and the method of detection certainly influences these measurements. For example, this ~1 nM IVM EC_{50} can be achieved in HEK293 cells for the WT receptor following lengthy (1 hour) pre-incubation with low concentrations of IVM (see Chapter 5, Figure 5-3). The ~1 nM EC_{50} also corresponds with the high sensitivity component of optimized receptor activation in HEK293 cells, observed as an increasingly robust signal within seconds to minutes. Discrepancies in IVM EC_{50} could be dependent on cell-type with different preferences for receptor stoichiometry or different posttranslational modifications that alter receptor activation. For example, homogeneous receptor populations can often be obtained by biasing transfection ratios in *Xenopus* oocytes[49]. Attempts to bias GluCl subunit expression in HEK293 cells did alter the shape of the IVM concentration-response but did not produce a monophasic high sensitivity curve. Mammalian cells likely possess cell-specific machinery for more regulated receptor trafficking compared to *Xenopus* oocytes. Similarly, neurons may possess alternative posttranslational processing and regulatory mechanisms than standard mammalian cell lines.

Implications of the glutamate insensitive mutation

The (α)L9'F gain-of-function mutation facilitates β subunit incorporation to substantially increase heteromeric GluCl αβ sensitivity to IVM. Reintroduction of a glutamate insensitive mutation, either (β)Y182F or (β)Y232A, to the (α)L9'F mutant eliminated the

increase in IVM sensitivity. Whether this attenuation was an actual defect of structure-function or a consequence of altered stoichiometry is unclear. Mutation of the L9' residue is known to directly impact channel gating. The glutamate insensitive mutations are located within the glutamate binding site of the extracellular domain, some 60 Å away from the (α)L9'F mutation at the channel pore. Some residues at or near the binding site serve as gating pathway residues, engaging in long-range functional coupling to transmit binding events to the channel gate. Mutation of such a residue in combination with an L9' mutation can produce a nonmultiplicative EC_{50}, indicating the distant residues are functionally coupled[56]. Evaluation of the glutamate insensitive mutations by mutant cycle analysis in this case is complicated by the biphasic IVM concentration-dependence (i.e., two EC_{50} values) of the (α)L9'F mutation. Alternatively, mutations at or near the glutamate binding site which is positioned at subunit interfaces, could conceivably affect heteromeric subunit assembly. In this instance, the (β)Y182F or (β)Y232A mutations would be preventing efficient incorporation of the β subunit to eliminate the high IVM sensitivity component of the (α)L9'F mutant. The (α)Y261A mutation, which resulted in a predominantly α homomer population, supports the notion that mutations in this region can affect heteromeric receptor formation. Restoration of the high IVM sensitivity component by the mYFP mutation further supports that an altered subunit stoichiometry is responsible for the counteracting effects of the glutamate insensitive and (α)L9'F mutations.

Combining the (α)L9'F mutation with the (β)Y182F glutamate insensitive mutation did recover some glutamate sensitivity in the concentration range tested, generating concern that this could allow constitutive silencing. Baseline concentrations of

extracellular glutamate *in vivo* are in the nanomolar range[57] as glutamate transient decay is dependent on diffusion and uptake by membrane-bound transporters[58]. In the synaptic cleft of glutamatergic synapses, glutamate can reportedly reach as high as 1 mM[59,60], though this concentration has been contested[61], arguing the amount of transmitter released is highly variable and often nonsaturating[62,63]. Thus, it is not certain that this level of glutamate sensitivity will be detrimental to *in vivo* silencing applications. Punctate immunostaining patterns are suggestive of a synaptic localization for exogenously expressed GluCl receptors. Similar inhibitory receptors such as GlyR and $GABA_A$ are known to be clustered at synapses by binding of the anchor protein gephrin, which recognizes an 18-amino acid binding motif in the intracellular loop of the respective β subunit[64]. Sequence alignments indicate that neither GluCl α nor β subunits possess a gephrin binding motif, discounting the likelihood of clustering by this mechanism. Synaptic localization could be easily confirmed or denied by colocalization experiments with a postsynaptic density marker. If necessary, additional protein engineering strategies may be applied to the optimized GluCl tool to relieve synaptic receptor clustering.

Application of GluClv2.0

Since the initial proof-of concept study, the original GluCl/IVM tool has been used in conjunction with Channelrhodopsin-2-mediated activation to define an inhibitory microcircuit within the amygdala involved in mouse fear conditioning[65] and to identify a hypothalamic locus responsible for male mouse aggression and its close neuroanatomical

relationship to mating circuits[66]. An intersectional approach was used in former study to restrict GluCl expression to PKC-δ-containing GABAergic neurons of the central amygdala. This was achieved by transgenic expression GluCl α-CFP in all PKC-δ^+ neurons followed by stereotaxic injection of an AAV vector encoding GluCl β-YFP Y182F. While GluCl/IVM-induced silencing of PKC-δ^+ neurons yielded a statistically significant enhancement of conditional freezing, this behavioral result was confounded by a bimodal phenotype. Quantitative histological analysis again revealed considerable variation in expression of the virally injected β subunit among individual animals, reminiscent of the striatal proof-of-concept studies. Control animals transgenically expressing α alone or wild-type animals injected with β alone were not affected by treatment with 10 mg/kg IVM. While the present study confirms that α homomers are indeed trafficked to the plasma membrane, it raises the question of whether α homomer activation elicits sufficient chloride current to achieve neuronal silencing. For example, current responses recorded from GluCl α homomers expressed in *Xenopus* oocytes are 10-fold smaller than the αβ heteromeric responses[11,40]. A type of small slow-activating IVM-induced current has also been recorded from HEK293 cells which may result from α homomer expression, though this has not yet been confirmed (see Chapter 5, Figure 5.2). Additional *in vitro* neuronal silencing experiments should be conducted to compare the spike suppression capability of α homomers to αβ heteromers. Nevertheless, an intersectional approach is apparently still practical.

The optimized GluCl receptor, α-mXFP L9'F + β-mXFP Y182F RSR_AAA, dubbed 'GluCl version 2.0' or simply 'GluClv2.0', maintains the requirement for both α and β subunits. The new sequence modifications significantly improve receptor

sensitivity and subunit expression by preventing degradation of the β subunit and promoting its dimerization with the α subunit, in addition to relieving both subunits from the adverse effects of XFP oligomerization. The kinetic properties of the silencing tool have not been altered. An alternative orthogonal pharmacological silencing tool capable of activating and inactivating on shorter time scales has recently been constructed[67]. This tool employs chimeric nAChR-GlyR receptors of mammalian origins. The cognate synthetic nicotinic agonist has demonstrated weak to moderate binding of other endogenous nAChRs and the lack of co-assembly of chimeric subunits with endogenous nAChR subunits has not been verified. Even faster time-resolved neuronal silencing can be achieved using optogenetic techniques[68,69]. This method, however, is invasive and requires implantation of optical fibers that do not allow for manipulation of diffuse signaling networks. The duration of light-induced manipulation is also limited by heat generation which may alter neuronal activity or be damaging to cell health[70]. A separate attempt at improving IVM-induced silencing has also been made by modification of GlyR[71]. A single point mutation increased IVM sensitivity of GlyR by 100-fold, allowing activation in the nM range (i.e., similar to the original GluCl tool), while a separate point mutation eliminated glycine sensitivity. This modified GlyR tool has not been implemented *in vivo*. Future circuitry studies with this tool would be dependent on the assumption that endogenous GlyR expression is confined to spinal cord and brainstem neurons[72]. Experimental evidence, in fact, suggests a more widespread distribution of GlyR expression including higher brain regions such as the hippocampus, thalamus, amygdala, caudate-putamen and cerebral cortex[73-79]. Modified GlyRs would likely co-assemble with endogenous subunits yielding obscure results. GluCl receptors, on the

other hand, do not exist in mammalian neurons and GluClv2.0 manifests even greater sensitivity to IVM. We therefore believe the GluCl/IVM tool remains relevant and fills a niche for behavioral assays necessitating long-term neuronal inhibition (e.g., learning paradigms) and for assessing modulatory as opposed to regulatory roles in circuitry.

The aim of this project was to produce an optimized GluCl silencing tool via rational protein engineering strategies. Throughout this pursuit, a great deal has been learned about structure-function relationships and subunit expression patterns of GluCl. While the system is still not perfectly understood, the success of GluClv2.0 as an improved silencing tool has been demonstrated *in vitro*. The increased sensitivity and improved subunit expression of GluClv2.0 should allow lower doses of IVM to be administered for *in vivo* silencing, thereby alleviating concerns of off-target side effects and reducing the occurrence of suboptimal inhibition.

Materials and Methods

Site-Directed Mutagenesis

Codon optimized sequences of the *Caenorhabditis elegans* GluCl channel cloned into plasmid vector pcDNA3.1/V5-His TOPO (Invitrogen #K4800-01), including optGluCl αWT, optGluCl βWT, optGluCl α-XFP, and optGluCl β-XFP[12], were used in this study. Fluorescent protein insertions (XFP) include enhanced yellow (YFP) and cyan (CFP) variants and are located in the TM3-TM4 loop[11]. All constructs originate from the optimized codon sequences. For convenience, the 'opt' nomenclature has been omitted throughout most of this text. Point mutations were made using the QuikChange II XL site-directed mutagenesis kit (Agilent Technologies #200522) with PfuTurbo DNA polymerase (Agilent Technologies #600250). Forward and reverse primers for the (α)L9'F mutation are listed in Chapter 3. Mutant subunits in the current study were generated with the following forward and reverse primers (new codon is italicized in the forward primer): 5' – GGC GTG ACC ACC CTG *TTC* ACC ATG ACC ACC ATG – 3' and 5' – CAT GGT GGT CAT GGT GAA CAG GGT GGT CAC GCC – 3' for the (β)L9'F mutation; 5' – AC TTC GAC CTG GTG TCC *TTC* GCC CAC ACC – 3' and 5' – GGT GTG GGC GAA GGA CAC CAG GTC GAA GT – 3' for the (β)Y182F mutation; 5' – C AAC ACT GGC TCG *GCC* GGC TGC CTG CGC – 3' and 5' – GCG CAG GCA GCC GGC CGA GCC AGT GTT G – 3' for the (β)Y232A mutation; 5' – ACC AAC ACC GGC ATC *GCC* AGC TGC CTG AGG AC – 3' and 5' – GT CCT CAG GCA GCT GGC GAT GCC GGT GTT GGT – 3' for the (α)Y261A mutation; 5' – TAC CTG AGC TAC CAG TCC *AAG* CTG AGC AAA GAC CCC AAC – 3' and 5' –

GTT GGG GTC TTT GCT CAG CTT GGA CTG GTA GCT CAG GTA – 3' for the monomeric YFP A206K mutation; 5' – TG CGC CAG AAC GAC *GCC GCC GCC* GAG AAG GCG GCC C – 3' and 5' – G GGC CGC CTT CTC GGC GGC GGC GTC GTT CTG GCG CA – 3' for the (β)RSR_AAA mutation; 5' – CG GCC CGC AAG GCC CAG *GCA GCC GCC* GAG AAG CTG GAG ATG G –3' and 5'– C CAT CTC CAG CTT CTC GGC GGC TGC CTG GGC CTT GCG GGC CG – 3' for the (β)RRR_AAA mutation. The C-terminal tags V5 and 6-His are included in the plasmid vector and were added to the α and β subunits by point mutation of the stop codon with the following primers: 5' – G CAG AAC GTT CTG TTC *GGA* GCT AGC AAG GGC AA – 3' and 5' – TT GCC CTT GCT AGC TCC GAA CAG AAC GTT CTG C – 3' for the α subunit; 5' – CC GAG TCC CTG GTG *TTG* GCT AGC AAG G – 3' and 5' – C CTT GCT AGC CAA CAC CAG GGA CTC GG – 3' for the β subunit. All mutations were confirmed by DNA sequencing.

Cell culture

HEK293 cells were cultured, plated and transfected for electrophysiology and FlexStation assays as described in Chapter 3. For TIRF imaging experiments, HEK293 cells were plated on 35 mm glass bottom culture dishes (MatTEK #P35G-1.5-10-C) at 50,000 cells/dish and transfected following the same protocol used for the electrophysiology experiments described in Chapter 3. For Western blot analyses, HEK293 cells were plated in 10 cm dishes at 4×10^6 cells/dish and transfected with 16 μg DNA in 500 μl DMEM combined with 30 μl ExpressFect (Denville Scientific #E2650) in

500 µl DMEM that was preincubated for 20 minutes before adding to culture dishes containing 5 ml fresh culture medium. The transfection mix was removed after 4–6 hours and replaced with 10 ml of fresh culture medium. For all experiments, HEK293 cells were transfected 24 hours after plating and assayed 48 hours after transfection.

Hippocampal neurons were extracted from day 18 Wistar rat embryos[80] and plated at a density of 40,000 cells per dish on 35 mm glass bottom culture dishes coated with poly-DL-lysine (Sigma #P9011). Neurons were cultured in Neurobasal medium (Gibco #21103-049) containing 2% B27 (Gibco #17504-044), and 0.5 mM Glutamax (Gibco #35050). Medium was supplemented with 5% equine serum (Hyclone #SH30074) during plating. Cultures were maintained at 37°C and 5% CO_2 in a humidified incubator, with a 50% media exchange once per week. For imaging experiments, neurons were treated with 1 µM cytosine arabinoside (AraC; Sigma #C1768) on culture day 10 with a 100% media change the following day. Cultures used for electrophysiological experiments were not treated with AraC. Neurons were transiently transfected after 13-14 days in culture and assayed 24 hours later. Transfections were prepared per dish using 4 µg of plasmid DNA with 20 µg Nupherin-neuron (BIOMOL #SE-225) and 10 µl of Lipofectamine 2000 (Invitrogen #11668-019) diluted separately in 400 µl of Neurobasal without phenol red (Gibco #12348-017). Dilutions were individually incubated at room temperature for 15 minutes, then combined and incubated for another 45 minutes. An 800 µl volume of conditioned media was then removed from the neuronal culture dish and replaced with the 800 µl transfection mix. After incubating cultures for 1 hour at 37°C/5% CO_2, an 800 µl volume was removed from the dish and replaced with the original 800 µl of conditioned media.

Membrane Potential Measurements

Membrane Potential assays were performed on the FlexStation 3 multimode benchtop microplate reader using the BLUE formulation kit (Molecular Devices, #R8042) with the same dye preparation and data acquisition parameters described in Chapter 3. Glutamate and IVM drug preparation and dose-response data analysis is also described in Chapter 3.

Electrophysiology

Voltage-clamped HEK293 cells were recorded as described in Chapter 3. Neurons were whole-cell current-clamped using an Axopatch 200A amplifier with a CV201 headstage and Digidata 1200 series interface operated by Clampex 9.2 software (Axon Instruments). Spontaneous neuronal firing was recorded in Gap-free acquisition mode. Episodic Stimulation acquisition mode was used for executing stepwise current injections (-100 to 250 pA, 25 pA increments) to record evoked spike firing. Data was sampled at 50 kHz and lowpass filtered at 5 kHz. Neurons were perfused or incubated with artificial cerebrospinal fluid (ACSF) composed of (in mM): 110 NaCl, 5.4 KCl, 1.8 $CaCl_2$, 0.8 $MgCl_2$, 10 D-glucose, 10 HEPES, pH 7.4, 230 mOsm. Patch pipettes were made from borosilicate glass with resistances of 7–12 MΩ when filled with the following internal solution (in mM): 100 K-gluconate, 0.1 $CaCl_2$, 5 $MgCl_2$, 1.1 EGTA, 10 HEPES, 3 Mg-ATP, 0.3 GTP, 3 phosphocreatine, pH 7.2, 215 mOsm. IVM was dissolved in ACSF containing 0.1% DMSO and applied to cultures by bath perfusion or pre-incubation at 37°C/5% CO_2 for 15 minutes. All recordings were performed at ambient temperature.

Data was analyzed using Clampfit 9.2 software. Resting membrane potential was measured in the absence of any injected current and corrected for the liquid junction potential. Cells with a resting membrane potential of > −45 mV or with a seal resistance of < 100 MΩ or were omitted from analysis. The steady-state voltage response was plotted against the amount of current injected for a voltage-current (V-I) relationship. Input resistance of the cell was determined from the slope, according to Ohm's law, V = IR. Conductance was calculated as the inverse of resistance (G = 1/R = I/V). Induced spikes were counted manually and plotted against injected current.

Immunofluorescent labeling

Live, nonpermeabilized neurons were immunolabeled according to the protocol described in Glynn & McAllister, 2006[81]. A V5 epitope tag (GKPIPNPLLGLDST) followed by a 6-His tag (HHHHHH) already encoded in the pcDNA3.1 vector was added to the C-terminus of GluCl α and β subunits (including a 24-residue linker sequence, see Figure 4-19A) by mutation of the stop codon (see Site-Directed Mutagenesis). The 6-His tag was not utilized in these experiments. Surface receptors were labeled with primary mouse monoclonal anti-V5 antibody (1:200; Invitrogen #R960-25) followed by a conjugated secondary Alexa Fluor 555 donkey anti-mouse antibody (1:400; Invitrogen #A-31570). Antibodies were diluted into warm ACSF and applied sequentially, incubating each for 30 min at 37°C/5% CO_2 with appropriate wash steps. Live immunostained cultures were imaged immediately.

Western Blot Analysis

Whole-cell lysates were obtained from transiently transfected HEK293 cells using ice cold extraction buffer containing (in mM): 50 Tris, 50 NaCl, 1 EDTA, 1 EGTA, pH 7.4 and 1% NP40 supplemented with 1% protease inhibitor cocktail (Thermo Scientific #78410). The cell surface receptors were biotinylated and isolated for Western blot analysis using the Pierce Cell Surface Protein Isolation Kit (Thermo Scientific #89881). Cell samples (30 µl) were separated on 'Any kD' Mini-PROTEAN TGX Precast gels (Bio-Rad #456-9033) in Tris/Glycine/SDS running buffer (Bio-Rad #161-0732) at 200 V for 35 minutes. Gel bands were transferred onto presoaked Protran nitrocellulose membranes (Whatman #10485376) in buffer containing 20% methanol and 10% Tris-glycine SDS at 15 V for 20 minutes. Nitrocellulose membranes were initially blocked in 10% milk in TBST (TBS + 0.1% Tween-20; Bio-Rad #170-6435, Sigma #P1379) and then incubated with rabbit anti-GFP antibody (1:1000; Invitrogen #A11122) in 5% BSA in TBST with 10% NaN_3 overnight to probe for GluCl β-mYFP subunit expression. Protein bands were detected by enhanced chemiluminescence (Western Lightning Plus-ECL; PerkinElmer #NEL103001EA) using goat anti-rabbit horseradish peroxidase (1:5000; Promega #W4011) in 5% BSA in TBST and developed on film (Amersham Hyperfilm ECL). The ~72 kDa molecular weight band was identified using the SeeBlue Plus2 prestained protein standard (Invitrogen #LC5925). ImageJ software (National Institutes of Health; http://rsb.info.nih.gov/ij/) was used for quantification of band intensity.

Imaging

All cultured neurons and HEK293 cells and were imaged live at 37°C in a stage-mounted culture dish incubator (Warner Instruments). Transiently transfected HEK293 cells were imaged by Total Internal Reflection Fluorescence (TIRF) microscopy, which enabled visualization of fluorescent receptors expressed in the plasma membrane and nearby intracellular vesicles within 200 nm of the cell-coverslip interface. Prior to imaging, cell culture medium was replaced with phenol red-free CO_2-independent Leibovitz L-15 medium (Gibco #21083-027). TIRF images were obtained using an inverted microscope (Olympus IX81) with a 100x/1.45 NA Plan Apochromat oil objective. A T-cube stepper motor (Thorlabs) was used to control the position of the fiber optic and TIRF evanescent field illumination. A 488 nm laser was used to excite monomeric YFP fluorescence. Images were acquired with MetaMorph Premier software (Molecular Devices) at 16-bit resolution over 512×512 pixels and captured using a back-illuminated EMCCD camera (iXON DU-897) supported by ANDOR iQ2 software (Andor Technology).

Transiently transfected hippocampal neuron cultures were imaged using a laser-scanning confocal microscope (Nikon Eclipse C1si) with a 63x/1.4 NA VC Plan Apochromat oil objective. Monomeric YFP fluorescence was acquired with 514 nm laser excitation. Alexa 555 and pDsRED2 (Clontech #632409) fluorescence was acquired with 561 nm laser excitation. Images were collected as z-stacks at a step size of 1.0 μm with 16-bit resolution over 512×512 pixels and a dwell time of 6.72 μs.

For confocal image analysis, the two different fluorescent signal intensities were correlated on a pixel-by-pixel basis using the Colocalization Colormap ImageJ plug-in

(Adam Gorlewicz, http://sites.google.com/site/colocalizationcolormap/home) based on the algorithm by Jaskolski et al., 2005[82]. The correlation of a pair of pixels was calculated as follows:

$$nMDP_{x,y} = \frac{(Ia - \overline{Ia})(Ib - \overline{Ib})}{(Ia_{max} - \overline{Ia})(Ib_{max} - \overline{Ib})}$$

Ia	intensity for the given pixel in image a
$\overline{Ia}$	average intensity of image a
Ia_{max}	the highest pixel intensity in image a
Ib	intensity for the given pixel in image b
$\overline{Ib}$	average intensity of image b
Ib_{max}	the highest pixel intensity in image b

The normalized mean deviation product (nMDP) values for each pixel range from −1 to 1 and can be visualized on a color scale. Values < 0 are represented by cold colors for exclusion and values > 0 are shown in hot colors for colocalization. Zero values indicate black background. For the experimental conditions of the current study, the average of all positive (colocalized) nMDP values corresponds to total receptor surface expression, while the average number of perfectly correlated pixels (i.e., where nMDP = 1) indicates the relative amounts of each receptor subunit.

Statistics

Pooled data are shown as means ± SEM. Boxplots represent the mean, median, 25^{th}, and 75^{th} percentiles. Statistical significance ($P < 0.05$) was determined by one-way analysis of variance (ANOVA) on ranks using multiple pairwise comparison.

Acknowledgements

Thanks to Sheri McKinney for providing hippocampal neuron cultures.

References

1. Lerchner W, Xiao C, Nashmi R, Slimko EM, van Trigt L, Lester HA, Anderson DJ. (2007) Reversible silencing of neuronal excitability in behaving mice by a genetically targeted, ivermectin-gated Cl- channel. *Neuron* **54**:35–49.

2. Anden NE, Hfuxe K, Hamberger B, Hokfelt T. (1966) A quantitative study on the nigro-neostriatal dopamine neuron system in the rat. *Acta Physiol Scand* **67**:306–312.

3. Schwarcz R, Fuxe K, Agnati LF, Hokfelt T, Coyle JT. (1979) Rotational behaviour in rats with unilateral striatal kainic acid lesions: a behavioural model for studies on intact dopamine receptors. *Brain Res* **170**:485–495.

4. Burdett EC, Heckmann RA, Ochoa R. (1997) Evaluation of five treatment regimens and five diagnostic methods for murine mites (Myocoptes musculinus and Myobia musculi). *Contemp Top Lab Anim Sci* **36**:73–76.

5. Schinkel AH, Smit JJ, van Tellingen O, Beijnen JH, Wagenaar E, van Deemter L, Mol CA, van der Valk MA, Robanus-Maandag EC, te Riele HP, et al. (1994) Disruption of the mouse mdr1a P-glycoprotein gene leads to a deficiency in the blood-brain barrier and to increased sensitivity to drugs. *Cell* **77**:491–502.

6. Roder JD, Stair EL. (1998) An overview of ivermectin toxicosis. *Vet Hum Toxicol* **40**:369–370.

7. Adelsberger H, Lepier A, Dudel J. (2000) Activation of rat recombinant α(1)β(2)γ(2S) GABA(A) receptor by the insecticide ivermectin. *Eur J Pharmacol* **394**:163–170.

8. Khakh BS, Proctor WR, Dunwiddie TV, Labarca C, Lester HA. (1999) Allosteric control of gating and kinetics at P2X(4) receptor channels. *J Neurosci* **19**:7289–7299.

9. Krause RM, Buisson B, Bertrand S, Corringer PJ, Galzi JL, Changeux JP, Bertrand D. (1998) Ivermectin: a positive allosteric effector of the α7 neuronal nicotinic acetylcholine receptor. *Mol Pharmacol* **53**:283–294.

10. Shan Q, Haddrill JL, Lynch JW. (2001) Ivermectin, an unconventional agonist of the glycine receptor chloride channel. *J Biol Chem* **276**:12556–12564.

11. Li P, Slimko EM, Lester HA. (2002) Selective elimination of glutamate activation and introduction of fluorescent proteins into a Caenorhabditis elegans chloride channel. *FEBS Lett* **528**:77–82.

12. Slimko EM, Lester HA. (2003) Codon optimization of Caenorhabditis elegans GluCl ion channel genes for mammalian cells dramatically improves expression levels. *J Neurosci Methods* **124**:75–81.

13. Slimko EM, McKinney S, Anderson DJ, Davidson N, Lester HA. (2002) Selective electrical silencing of mammalian neurons in vitro by the use of invertebrate ligand-gated chloride channels. *J Neurosci* **22**:7373–7379.

14. Ellgaard L, Helenius A. (2003) Quality control in the endoplasmic reticulum. *Nat Rev Mol Cell Biol* **4**:181–191.

15. Teasdale RD, Jackson MR. (1996) Signal-mediated sorting of membrane proteins between the endoplasmic reticulum and the golgi apparatus. *Annu Rev Cell Dev Biol* **12**:27–54.

16. Hurtley SM, Helenius A. (1989) Protein oligomerization in the endoplasmic reticulum. *Annu Rev Cell Biol* **5**:277–307.

17. Klausner RD, Sitia R. (1990) Protein degradation in the endoplasmic reticulum. *Cell* **62**:611–614.

18. Nishimura N, Balch WE. (1997) A di-acidic signal required for selective export from the endoplasmic reticulum. *Science* **277**:556–558.

19. Nishimura N, Bannykh S, Slabough S, Matteson J, Altschuler Y, Hahn K, Balch WE. (1999) A di-acidic (DXE) code directs concentration of cargo during export from the endoplasmic reticulum. *J Biol Chem* **274**:15937–15946.

20. Mossessova E, Bickford LC, Goldberg J. (2003) SNARE selectivity of the COPII coat. *Cell* **114**:483–495.

21. Mancias JD, Goldberg J. (2008) Structural basis of cargo membrane protein discrimination by the human COPII coat machinery. *EMBO J* **27**:2918–2928.

22. Jackson MR, Nilsson T, Peterson PA. (1990) Identification of a consensus motif for retention of transmembrane proteins in the endoplasmic reticulum. *EMBO J* **9**:3153–3162.

23. Munro S, Pelham HR. (1987) A C-terminal signal prevents secretion of luminal ER proteins. *Cell* **48**:899–907.

24. Zerangue N, Schwappach B, Jan YN, Jan LY. (1999) A new ER trafficking signal regulates the subunit stoichiometry of plasma membrane K(ATP) channels. *Neuron* **22**:537–548.

25. Margeta-Mitrovic M, Jan YN, Jan LY. (2000) A trafficking checkpoint controls GABA(B) receptor heterodimerization. *Neuron* **27**:97–106.

26. Bichet D, Cornet V, Geib S, Carlier E, Volsen S, Hoshi T, Mori Y, De Waard M. (2000) The I-II loop of the Ca2+ channel α1 subunit contains an endoplasmic reticulum retention signal antagonized by the β subunit. *Neuron* **25**:177–190.

27. Scott DB, Blanpied TA, Swanson GT, Zhang C, Ehlers MD. (2001) An NMDA receptor ER retention signal regulated by phosphorylation and alternative splicing. *J Neurosci* **21**:3063–3072.

28. Standley S, Roche KW, McCallum J, Sans N, Wenthold RJ. (2000) PDZ domain suppression of an ER retention signal in NMDA receptor NR1 splice variants. *Neuron* **28**:887–898.

29. Xia H, Hornby ZD, Malenka RC. (2001) An ER retention signal explains differences in surface expression of NMDA and AMPA receptor subunits. *Neuropharmacology* **41**:714–723.

30. Boyd GW, Doward AI, Kirkness EF, Millar NS, Connolly CN. (2003) Cell surface expression of 5-hydroxytryptamine type 3 receptors is controlled by an endoplasmic reticulum retention signal. *J Biol Chem* **278**:27681–27687.

31. Sadtler S, Laube B, Lashub A, Nicke A, Betz H, Schmalzing G. (2003) A basic cluster determines topology of the cytoplasmic M3-M4 loop of the glycine receptor α1 subunit. *J Biol Chem* **278**:16782–16790.

32. Srinivasan R, Pantoja R, Moss FJ, Mackey ED, Son CD, Miwa J, Lester HA. (2011) Nicotine up-regulates α4β2 nicotinic receptors and ER exit sites via stoichiometry-dependent chaperoning. *J Gen Physiol* **137**:59–79.

33. Brock C, Boudier L, Maurel D, Blahos J, Pin JP. (2005) Assembly-dependent surface targeting of the heterodimeric GABAB Receptor is controlled by COPI but not 14-3-3. *Mol Biol Cell* **16**:5572–5578.

34. Michelsen K, Yuan H, Schwappach B. (2005) Hide and run. Arginine-based endoplasmic-reticulum-sorting motifs in the assembly of heteromultimeric membrane proteins. *EMBO Rep* **6**:717–722.

35. Yuan H, Michelsen K, Schwappach B. (2003) 14-3-3 dimers probe the assembly status of multimeric membrane proteins. *Curr Biol* **13**:638–646.

36. Hibbs RE, Gouaux E. (2011) Principles of activation and permeation in an anion-selective Cys-loop receptor. *Nature* **474**:54–60.

37. Yang F, Moss LG, Phillips GN, Jr. (1996) The molecular structure of green fluorescent protein. *Nat Biotechnol* **14**:1246–1251.

38. Zacharias DA, Violin JD, Newton AC, Tsien RY. (2002) Partitioning of lipid-modified monomeric GFPs into membrane microdomains of live cells. *Science* **296**:913–916.

39. Zacharias DA. (2002) Sticky caveats in an otherwise glowing report: oligomerizing fluorescent proteins and their use in cell biology. *Sci STKE* **2002**:pe23.

40. Cully DF, Vassilatis DK, Liu KK, Paress PS, Van der Ploeg LH, Schaeffer JM, Arena JP. (1994) Cloning of an avermectin-sensitive glutamate-gated chloride channel from Caenorhabditis elegans. *Nature* **371**:707–711.

41. Forrester SG, Beech RN, Prichard RK. (2004) Agonist enhacement of macrocyclic lactone activity at a glutamate-gated chloride channel subunit from Haemonchus contortus. *Biochem Pharmacol* **67**:1019–1024.

42. Forrester SG, Prichard RK, Beech RN. (2002) A glutamate-gated chloride channel subunit from Haemonchus contortus: expression in a mammalian cell line, ligand binding, and modulation of anthelmintic binding by glutamate. *Biochem Pharmacol* **63**:1061–1068.

43. Bonifacino JS, Cosson P, Shah N, Klausner RD. (1991) Role of potentially charged transmembrane residues in targeting proteins for retention and degradation within the endoplasmic reticulum. *EMBO J* **10**:2783–2793.

44. Bonifacino JS, Lippincott-Schwartz J. (1991) Degradation of proteins within the endoplasmic reticulum. *Curr Opin Cell Biol* **3**:592–600.

45. Gorrie GH, Vallis Y, Stephenson A, Whitfield J, Browning B, Smart TG, Moss SJ. (1997) Assembly of GABAA receptors composed of α1 and β2 subunits in both cultured neurons and fibroblasts. *J Neurosci* **17**:6587–6596.

46. Merlie JP, Lindstrom J. (1983) Assembly in vivo of mouse muscle acetylcholine receptor: identification of an α subunit species that may be an assembly intermediate. *Cell* **34**:747–757.

47. Blount P, Merlie JP. (1990) Mutational analysis of muscle nicotinic acetylcholine receptor subunit assembly. *J Cell Biol* **111**:2613–2622.

48. Green WN. (1999) Ion channel assembly: creating structures that function. *J Gen Physiol* **113**:163–170.

49. Moroni M, Bermudez I. (2006) Stoichiometry and pharmacology of two human α4β2 nicotinic receptor types. *J Mol Neurosci* **30**:95–96.

50. Nelson ME, Kuryatov A, Choi CH, Zhou Y, Lindstrom J. (2003) Alternate stoichiometries of α4β2 nicotinic acetylcholine receptors. *Mol Pharmacol* **63**:332–341.

51. Zhou Y, Nelson ME, Kuryatov A, Choi C, Cooper J, Lindstrom J. (2003) Human α4β2 acetylcholine receptors formed from linked subunits. *J Neurosci* **23**:9004–9015.

52. Bormann J, Rundstrom N, Betz H, Langosch D. (1993) Residues within transmembrane segment M2 determine chloride conductance of glycine receptor homo- and hetero-oligomers. *EMBO J* **12**:3729–3737.

53. Becker CM, Hoch W, Betz H. (1988) Glycine receptor heterogeneity in rat spinal cord during postnatal development. *EMBO J* **7**:3717–3726.

54. Langosch D, Thomas L, Betz H. (1988) Conserved quaternary structure of ligand-gated ion channels: the postsynaptic glycine receptor is a pentamer. *Proc Natl Acad Sci U S A* **85**:7394–7398.

55. Grudzinska J, Schemm R, Haeger S, Nicke A, Schmalzing G, Betz H, Laube B. (2005) The beta subunit determines the ligand binding properties of synaptic glycine receptors. *Neuron* **45**:727–739.

56. Gleitsman KR, Shanata JA, Frazier SJ, Lester HA, Dougherty DA. (2009) Long-range coupling in an allosteric receptor revealed by mutant cycle analysis. *Biophys J* **96**:3168–3178.

57. Herman MA, Jahr CE. (2007) Extracellular glutamate concentration in hippocampal slice. *J Neurosci* **27**:9736–9741.

58. Diamond JS, Jahr CE. (1997) Transporters buffer synaptically released glutamate on a submillisecond time scale. *J Neurosci* **17**:4672–4687.

59. Clements JD. (1996) Transmitter timecourse in the synaptic cleft: its role in central synaptic function. *Trends Neurosci* **19**:163–171.

60. Clements JD, Lester RA, Tong G, Jahr CE, Westbrook GL. (1992) The time course of glutamate in the synaptic cleft. *Science* **258**:1498–1501.

61. Bergles DE, Diamond JS, Jahr CE. (1999) Clearance of glutamate inside the synapse and beyond. *Curr Opin Neurobiol* **9**:293–298.

62. Frerking M, Wilson M. (1996) Saturation of postsynaptic receptors at central synapses? *Curr Opin Neurobiol* **6**:395–403.

63. McAllister AK, Stevens CF. (2000) Nonsaturation of AMPA and NMDA receptors at hippocampal synapses. *Proc Natl Acad Sci U S A* **97**:6173–6178.

64. Meyer G, Kirsch J, Betz H, Langosch D. (1995) Identification of a gephyrin binding motif on the glycine receptor beta subunit. *Neuron* **15**:563–572.

65. Haubensak W, Kunwar PS, Cai H, Ciocchi S, Wall NR, Ponnusamy R, Biag J, Dong HW, Deisseroth K, Callaway EM, Fanselow MS, Luthi A, Anderson DJ. (2010) Genetic dissection of an amygdala microcircuit that gates conditioned fear. *Nature* **468**:270–276.

66. Lin D, Boyle MP, Dollar P, Lee H, Lein ES, Perona P, Anderson DJ. (2011) Functional identification of an aggression locus in the mouse hypothalamus. *Nature* **470**:221–226.

67. Magnus CJ, Lee PH, Atasoy D, Su HH, Looger LL, Sternson SM. (2011) Chemical and genetic engineering of selective ion channel-ligand interactions. *Science* **333**:1292–1296.

68. Gradinaru V, Thompson KR, Deisseroth K. (2008) eNpHR: a Natronomonas halorhodopsin enhanced for optogenetic applications. *Brain Cell Biol* **36**:129–139.

69. Zhang F, Wang LP, Brauner M, Liewald JF, Kay K, Watzke N, Wood PG, Bamberg E, Nagel G, Gottschalk A, Deisseroth K. (2007) Multimodal fast optical interrogation of neural circuitry. *Nature* **446**:633–639.

70. Tye KM, Deisseroth K. (2012) Optogenetic investigation of neural circuits underlying brain disease in animal models. *Nat Rev Neurosci* **13**:251–266.

71. Lynagh T, Lynch JW. (2010) An improved ivermectin-activated chloride channel receptor for inhibiting electrical activity in defined neuronal populations. *J Biol Chem* **285**:14890–14897.

72. Rajendra S, Lynch JW, Schofield PR. (1997) The glycine receptor. *Pharmacol Ther* **73**:121–146.

73. Betz H. (1991) Glycine receptors: heterogeneous and widespread in the mammalian brain. *Trends Neurosci* **14**:458–461.

74. Danober L, Pape HC. (1998) Strychnine-sensitive glycine responses in neurons of the lateral amygdala: an electrophysiological and immunocytochemical characterization. *Neuroscience* **85**:427–441.

75. Darstein M, Landwehrmeyer GB, Kling C, Becker CM, Feuerstein TJ. (2000) Strychnine-sensitive glycine receptors in rat caudatoputamen are expressed by cholinergic interneurons. *Neuroscience* **96**:33–39.

76. Malosio ML, Marqueze-Pouey B, Kuhse J, Betz H. (1991) Widespread expression of glycine receptor subunit mRNAs in the adult and developing rat brain. *EMBO J* **10**:2401–2409.

77. McCool BA, Farroni JS. (2001) Subunit composition of strychnine-sensitive glycine receptors expressed by adult rat basolateral amygdala neurons. *Eur J Neurosci* **14**:1082–1090.

78. Naas E, Zilles K, Gnahn H, Betz H, Becker CM, Schroder H. (1991) Glycine receptor immunoreactivity in rat and human cerebral cortex. *Brain Res* **561**:139–146.

79. Rampon C, Luppi PH, Fort P, Peyron C, Jouvet M. (1996) Distribution of glycine-immunoreactive cell bodies and fibers in the rat brain. *Neuroscience* **75**:737–755.

80. Li YX, Zhang Y, Lester HA, Schuman EM, Davidson N. (1998) Enhancement of neurotransmitter release induced by brain-derived neurotrophic factor in cultured hippocampal neurons. *J Neurosci* **18**:10231–10240.

81. Glynn MW, McAllister AK. (2006) Immunocytochemistry and quantification of protein colocalization in cultured neurons. *Nat Protoc* **1**:1287–1296.

82. Jaskolski F, Mulle C, Manzoni OJ. (2005) An automated method to quantify and visualize colocalized fluorescent signals. *J Neurosci Methods* **146**:42–49.

Chapter 5

Addendum

The present study utilized mammalian HEK293 cells as a model expression system for screening mutational effects of the GluCl receptor. As discussed in Chapter 3, much cell-to-cell variability was observed during electrophysiology experiments on L9' mutants. Additional functional assays performed for silencing tool optimization, supplemental to those presented in Chapter 4, also displayed a great deal of variability and are the subject of this addendum.

Prior to introducing the monomeric YFP mutation, negative effects on IVM sensitivity imparted by the fluorescent protein insertion in the α subunit were first investigated by simple extraction of the YFP tag. Removal of YFP from the α subunit of (α)L9'F, (β)Y182F, and (β)RSR_AAA mutant receptors yielded ambiguous results (Figure 5-1A, B, C). Individually, the removal of YFP from α increased the high sensitivity component of the (α)L9'F mutant but eliminated the high sensitivity component from the (β)RSR_AAA mutant, while the (β)Y182F mutant remained unchanged. Assorted combinations of these mutations were equally puzzling (Figure 5-1D).

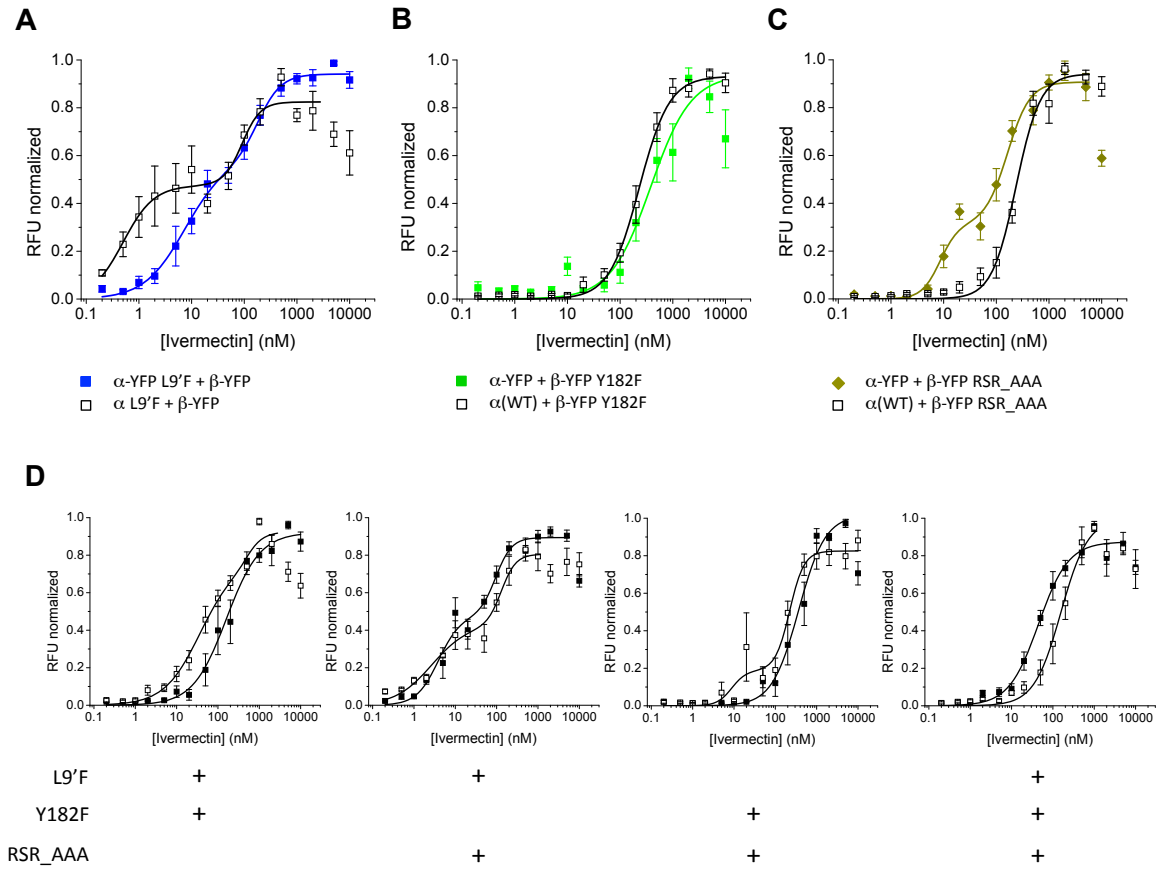

Figure 5-1. Removal of YFP from the α subunit affects IVM sensitivity. IVM activation was assayed using the FlexStation. Normalized IVM concentration-response curves showing removal of the YFP tag from the α subunit increased the high sensitivity component of the (α)L9'F mutant (*panel A.*) but eliminated the high sensitivity component from the (β)RSR_AAA mutant (*panel C.*) while IVM sensitivity of the (β)Y182F mutant (*panel B.*) was unchanged. *D.* Normalized IVM concentration-response curves of assorted mutant combinations with (filled symbol) and without (open symbol) YFP on the α subunit did not reveal a consistent effect.

In retrospect, oligomerization of the fluorescent fusion proteins presumably affected receptor stoichiometry in these experiments. The contradicting effects on the biphasic response of (α)L9'F and (β)RSR_AAA receptors, are in accordance with the proposed mutational implications. For example, in the ER, YFP oligomerization of α-α dimers, α-β dimers and β-β dimers presumably occur with the same prevalence. Removal

of YFP from the α subunit may boost its availability for the preferred α-β dimerization effect of the (α)L9'F mutation. This inadvertently reduces α-α dimerization while further promoting β subunit incorporation, visible by the enhanced high sensitivity component of the IVM concentration-response curve. The (β)RSR_AAA mutation, on the other hand, probably prevents β subunit degradation, but it does not have the heterodimer promotional effect of (α)L9'F. Because YFP tags of the β subunit were left intact, β-β dimers likely predominate, thereby sequestering the β subunit, resulting in primarily α homomer expression and a monophasic response.

The biphasic IVM response of (α)L9'F mutant receptors (with YFP removed from α) exhibited the largest high sensitivity component observed at the time. The IVM-induced currents associated with the two components of this mutant were examined by electrophysiology and compared to WT and (β)Y182F receptors (also with YFP removed from α). Whole-cell currents were recorded from transfected HEK293 cells in voltage-clamp with bath perfusion of 1, 5, and 50 nM IVM. The kinetic response was highly variable, yet two modes of activation were observed: a "slow" mode requiring minutes to peak current with some evidence of recovery (Figure 5-2A, black lines) and a "slower" mode which did not peak within the 5-minute application of IVM, rather, it continued to increase even upon removal of IVM from the bath (Figure 5-2A, red lines). The current magnitude of "slower" mode responses often resembled the steady-state current of the "slow" mode response. Nevertheless, pooled data still indicate a significant increase in mean peak current for the (α)L9'F mutant at 1 nM IVM (Figure 5-2B) and normalization of the mean response reveals a significant increase in IVM sensitivity at both 1 and 5 nM IVM for (α)L9'F (Figure 5-2C). Interestingly, no "slower" responses were observed for

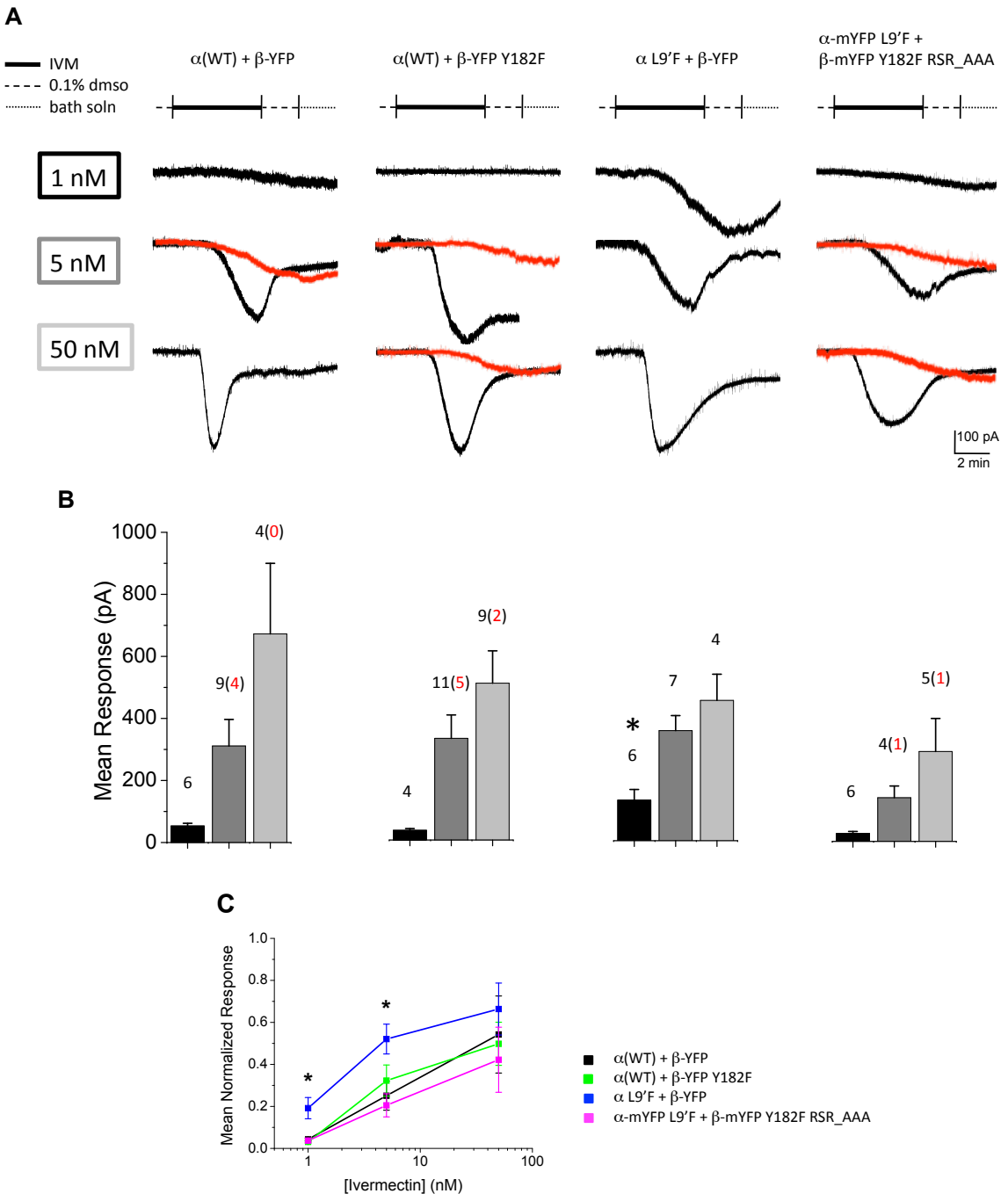

Figure 5-2. Electrophysiology with IVM. *A*. Whole-cell IVM-induced currents recorded from HEK293 cells in voltage-clamp. IVM concentrations of 1, 5, and 50 nM were applied for 5 minutes by bath perfusion. Two modes of activation were observed: 'slow' (*black traces*) and 'slower' (*red traces*). *B*. The (α)L9'F mutant shows a significant increase in mean peak current compared to WT at 1 nM IVM. The total number of cells recorded (*black numbers*) and the number of cells exhibiting 'slower' responses (*red numbers*) are indicated. *C*. Response normalization shows a significant increase in IVM sensitivity at both 1 and 5 nM IVM for (α)L9'F mutant.

the (α)L9'F mutant. At a much later date, similar recordings were obtained for the optimized receptor, α-mYFP L9'F + β-mYFP Y182F RSR_AAA. This receptor displayed both "slow" and "slower" type currents and did not appear to be significantly different from WT. These results were quite discouraging as they took place before neuronal silencing experiments.

The variability observed in the electrophysiological recordings of GluCl in HEK293 cells with IVM may be related to the high and low sensitivity responses observed in electrophysiological recordings with glutamate (Chapter 3), but it is difficult to speculate on the cause. Whether the "slower" IVM-induced currents contribute significantly to the population-based concentration-response curves obtained on the FlexStation seems unlikely as the magnitude of the response is minimal even after 5 minutes. It may be that "slower" currents are conducted by α homomers from cells that did not incorporate both α and β plasmid vectors during transfection. Since HEK293 cells were also cotransfected with soluble GFP to select cells for recording, cells that may have been expressing only the α subunit with no YFP tag would still have been included. Such variability caused by transfection, however, seems improbable since HEK293 cells are typically transfected with high efficiency. Nonetheless, recording from HEK293 cells intentionally transfected with only the α subunit would easily determine if "slower" currents are in fact conducted by α homomers.

Taking into account the slow activation kinetics of IVM and possible long-term accumulation of steady-state currents, mutants were incubated for 1 hour with varying concentrations of low IVM, and then assayed on the FlexStation using a single polarizing concentration of KCl to magnify the response. The EC_{50} concentration of 25 mM KCl

(Figure 5-3A, B) was used for the most sensitive detection of differential activation by low IVM and to avoid a saturating change in membrane potential. During the assay, addition of 25 mM KCl produced a negative signal (Figure 5-3C). This implies that long-term application of low IVM depolarizes cells to such an extent, that addition of an otherwise depolarizing amount of KCl induces repolarization of the membrane. The range of repolarization produced by a single dose of KCl reveals that long-term application of low IVM induces depolarization in concentration-dependent manner (Figure 5-3D). As expected, the (α)L9'F mutation increased sensitivity to IVM. Addition of the (β)Y182F mutation still reduced the (α)L9'F effect, but this double mutant maintained a significant increase in IVM sensitivity compared to the original tool used for silencing.

The A206K monomeric YFP mutation was essential toward the development of an optimized receptor. Even so, monomerization of YFP tags did not resolve the variability issues observed with GluCl in HEK293 cells. In the initial trial, the optimized GluCl α-mYFP L9'F + β-mYFP Y182F RSR_AAA receptor showed ~2 orders of magnitude greater sensitivity to IVM than the original tool used for silencing (Chapter 4, Figure 4-12). Both the optimized and original receptors were then assayed two additional times to ensure repeatability, and on average, the sensitivity improvement was maintained (Figure 5-4A). Examination of individual experiments, however, revealed the fraction of the high sensitivity component of the optimized receptor varied from day-to-day (Figure 5-4B).

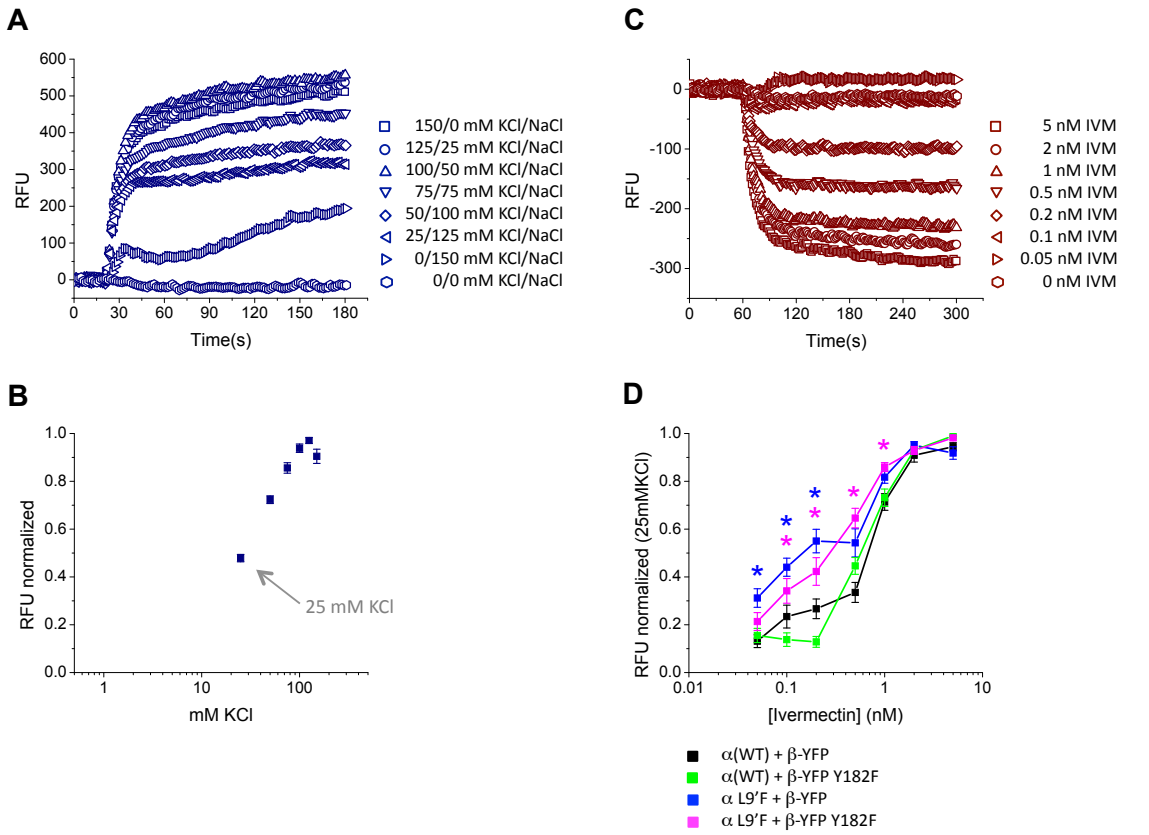

Figure 5-3. Preincubation with low IVM induces a concentration-dependent response. *A&B*. KCl-induced depolarization of nontransfected HEK293 cells reveals an EC_{50} of 25 mM. *C*. Transfected HEK293 cells were incubated for 1 hr with varying concentrations of low IVM, then assayed on the FlexStation with 25 mM KCl. Application of 25 mM KCl induced repolarizing (negative-going) signals in an IVM concentration-dependent manner. *D*. Response normalization reveals significantly increased IVM sensitivity for (α)L9'F and (α)L9'F+(β)Y182F mutant receptors compared to the original silencing tool, (**β**)Y182F.

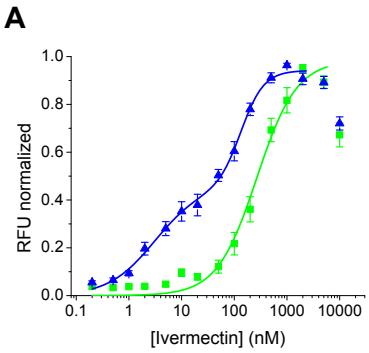

		1st comp	EC_{50} (μM)	Hill	EC_{50} (μM)	Hill	n
▲	α-mYFP L9'F + β-mYFP Y182F RSR_AAA	0.48	3.04 ± 1.41	1.00 ± 0.24	134.49 ± 21.03	2.01 ± 0.56	18
■	α-YFP+ β-YFP Y182F				267.32 ± 43.36	1.15 ± 0.15	18

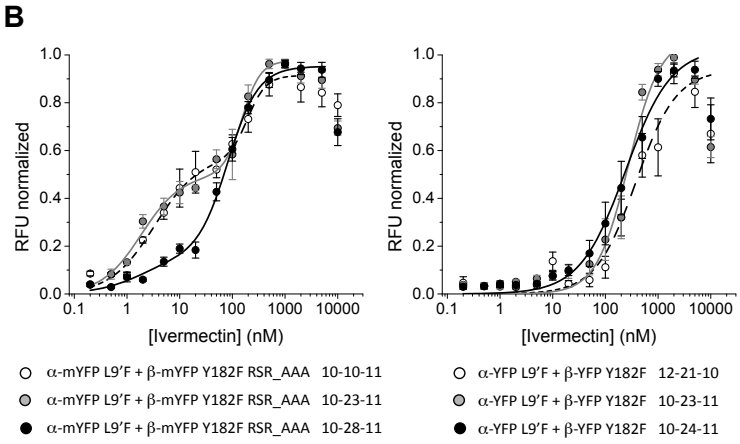

Figure 5-4. Functional assay repeatability of the optimized vs. original receptor silencing tools. IVM activation was assayed using the FlexStation. *A*. Optimized receptor maintains increased IVM sensitivity following triplicate measurements. Ivermectin activation parameters are presented in the corresponding table. *B*. Individual experiments reveal the high sensitivity component fraction of the optimized receptor varies from day-to-day. The consistent concentration-response of the original receptor ensures repeatability of the functional assay.

A host of additional experiments were subsequently performed in attempt to determine the source of this variability. Possible contributing factors tested included cell density, fresh culture media, fresh transfection reagent, the time posttransfection, and the passage number of the cells. All conditions produced a two-component curve with high sensitivity component fractions that varied remarkably (Figure 5-5A). Averaging all ten concentration-response curves of the optimized receptor still showed an improvement over the original silencing tool (Figure 5-5B, C). Time-dependent signal run-down was certainly a contributing factor, but it had been observed even with the WT receptor (Figure 5-6). Thus, the source of high IVM sensitivity variability remains to be determined.

Despite the many issues with variability, FlexStation assays of GluCl mutant receptors in HEK293 cells still served as a successful screening method for generating an optimized neuronal silencing tool. Though the original α-XFP + β-XFP Y182F receptor was effective in silencing neurons, the optimized α-mXFP L9'F + β-mXFP Y182F RSR_AAA receptor is significantly improved. Functional experimentation throughout the optimization process has provided a better understanding of structure-function relationships and subunit expression patterns of the GluCl receptor.

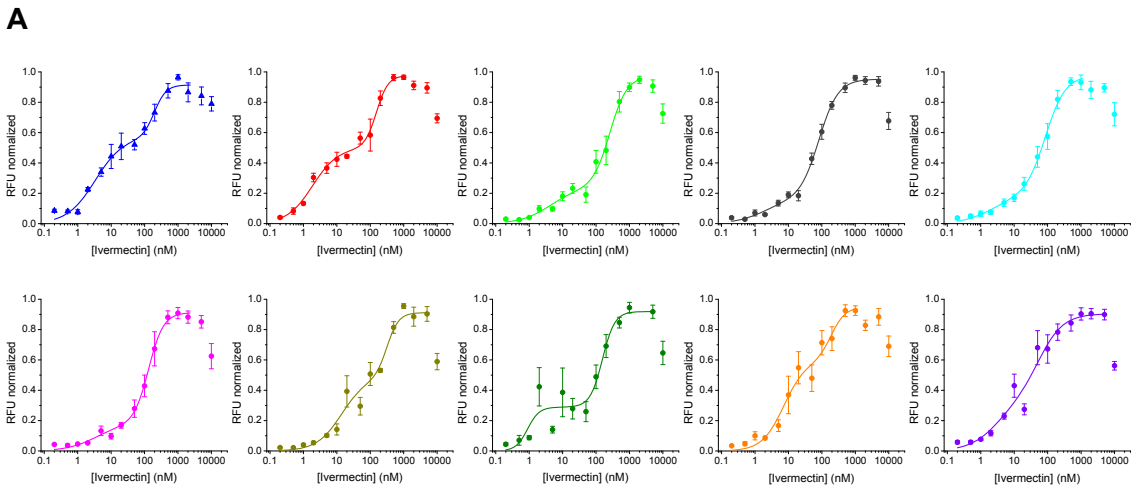

			1st comp	EC_{50} (μM)	Hill	EC_{50} (μM)	Hill	NOTES
●	α-mYFP L9′F + β-mYFP Y182F RSR_AAA	10-10-11 Plate2	0.37	3.35 ± 1.36	1.04 ± 0.27	196.26 ± 49.81	2.50 ± 1.64	P6 (N1)
●	α-mYFP L9′F + β-mYFP Y182F RSR_AAA	10-23-11 Plate1	0.51	1.88 ± 0.53	1.15 ± 0.28	153.28 ± 22.41	2.50 ± 0.86	P10 (N2)
●	α-mYFP L9′F + β-mYFP Y182F RSR_AAA	10-24-11 Plate2	0.24	4.17 ± 5.46	1.00 ± 0.68	260.68 ± 53.17	1.70 ± 0.55	P10 (N3)
●	α-mYFP L9′F + β-mYFP Y182F RSR_AAA	10-28-11 Plate1	0.17	1.92 ± 3.30	1.00 ± 0.86	82.33 ± 13.96	1.51 ± 0.28	P11 (N3)
●	α-mYFP L9′F + β-mYFP Y182F RSR_AAA	11-04-11 Plate1	0.18	2.06 ± 3.76	1.00 ± 0.85	86.37 ± 17.10	1.45 ± 0.37	P13; 18,000 cells/well
●	α-mYFP L9′F + β-mYFP Y182F RSR_AAA	11-04-11 Plate2	0.20	3.52 ± 4.93	1.00 ± 0.68	133.10 ± 16.40	1.96 ± 0.41	P13; 17,000 cells/well
●	α-mYFP L9′F + β-mYFP Y182F RSR_AAA	11-25-11 Plate1	0.53	13.98 ± 12.40	1.17 ± 0.64	317.79 ± 130.56	2.50 ± 1.79	P18; new media; new expressfect
●	α-mYFP L9′F + β-mYFP Y182F RSR_AAA	11-25-11 Plate2	0.31	0.89 ± 0.44	2.50 ± 2.81	155.28 ± 41.67	2.36 ± 1.36	P18; new media
●	α-mYFP L9′F + β-mYFP Y182F RSR_AAA	11-28-11 Plate1	0.63	7.26 ± 4.95	1.33 ± 0.63	191.35 ± 114.68	2.06 ± 2.82	P19; 24 hrs
●	α-mYFP L9′F + β-mYFP Y182F RSR_AAA	11-29-11 Plate1	0.37	3.09 ± 15.78	1.18 ± 1.28	55.98 ± 114.63	1.00 ± 1.52	P19; 48 hrs

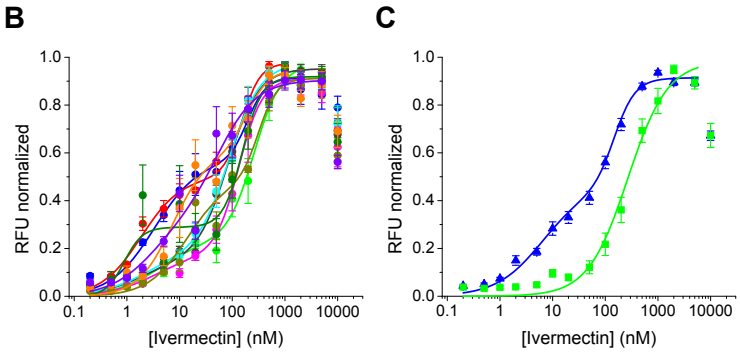

Figure 5-5. The high IVM sensitivity component of the optimized receptor is remarkably variable in HEK293 cells. IVM activation was assayed using the FlexStation. *A*. Additional assays of the optimized receptor considered the influence of cell density, fresh culture media, fresh transfection reagent, the time posttransfection, and the passage number of the cells. All conditions produced a two-component curve with varying fractions of high IVM sensitivity. Ivermectin activation parameters are presented in the corresponding table. The source of variability was not determined. *B&C*. Averaging all ten concentration-response curves of the optimized receptor still shows increased sensitivity compared to the original silencing tool.

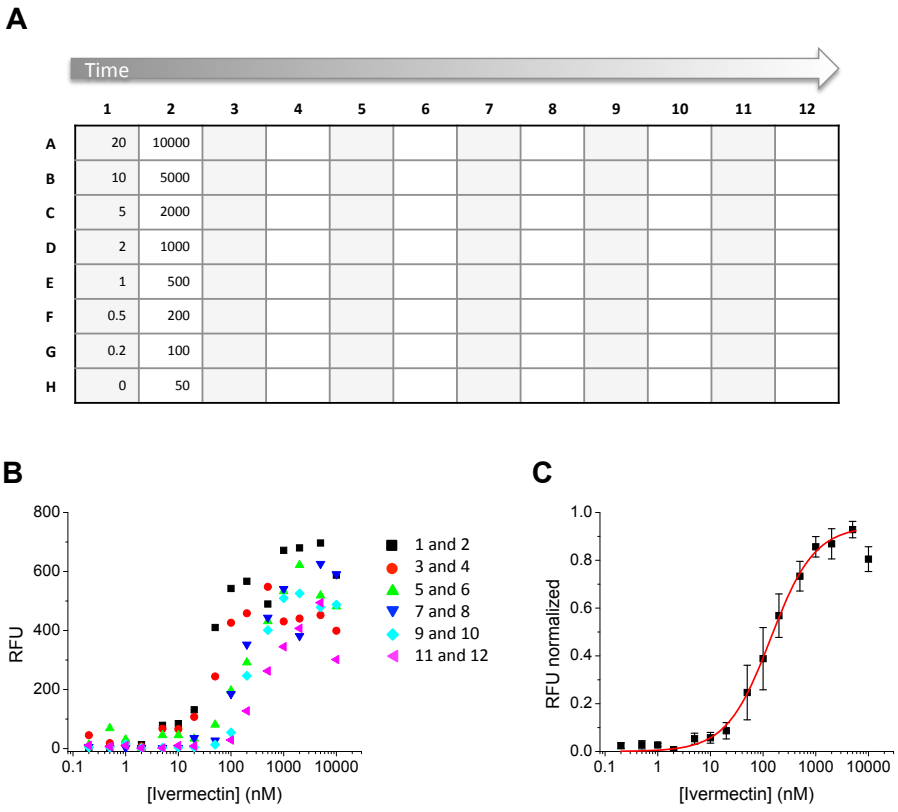

Figure 5-6. Time-dependent run-down of RFU signal. IVM activation was assayed using the FlexStation. *A*. FlexStation experimental design. Different concentrations of IVM are applied to each well. The IVM-induced signal of column 1 is detected for five minutes before moving on to column 2. The time lag between IVM application and signal detection remains constant. One 96-well plate assay takes one hour to complete. *B*. Two columns are combined for a single 15-point concentration response curve. Over time, from columns 1 and 2 (*black*) to columns 11 and 12 (*magenta*), raw signals are reduced in magnitude and concentration dependence is right-shifted. *C*. Despite signal run-down, an exemplary normalized concentration-response relationship is well fit to the Hill equation. Chi^2 per degrees of freedom = 0.00036. R^2 = 0.99772.

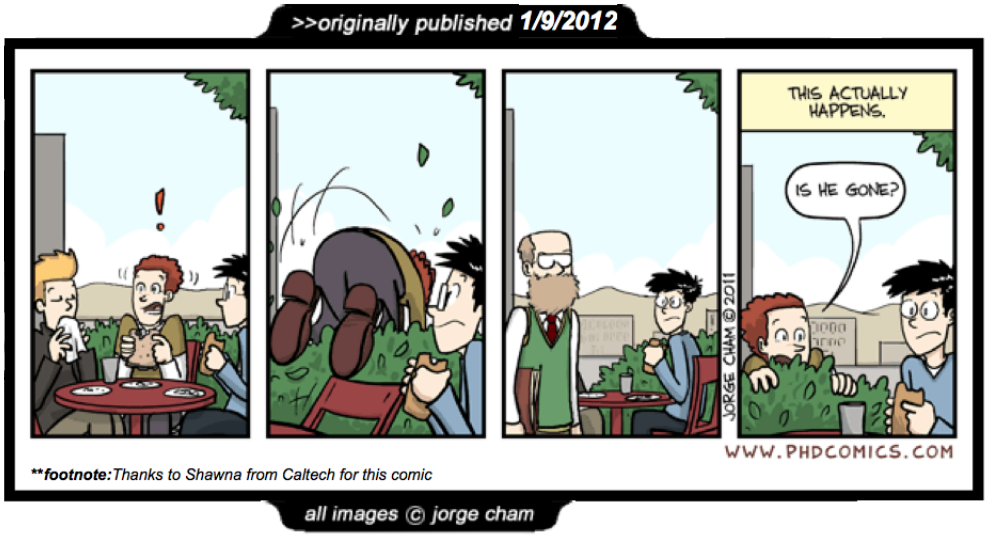
>>originally published 1/9/2012
!
THIS ACTUALLY HAPPENS.
IS HE GONE?
JORGE CHAM © 2011
WWW.PHDCOMICS.COM
**footnote: Thanks to Shawna from Caltech for this comic
all images © jorge cham